Crystallisation in emulsion and microemulsion systems

Catherine Emma Nicholson

Crystallisation in Emulsion and Microemulsion Systems

Catherine Emma Nicholson

A thesis submitted for the degree of Doctor of Philosophy at the University of Durham

December 2006

For my family and friends, and all those who have believed in me.
Your love, support, and kindness will never be forgotten.

Acknowledgements

Many thanks go to my supervisor Dr. Sharon J Cooper, for her guidance, support and many discussions. I also thank her for giving me the space to develop this project into a work of my own.

Thanks go to my mam, for reading all the gibberish I write, and reminding me of the existence of the comma. The English language is very grateful too.

My gratitude goes also to Mr. W. Doug Carswell, for running a few thousand DSC's for me, and for being my best friend.

I would also like to thank the many people, who have helped me during my time here at Durham. You have kept me right, and kept me sane, and I couldn't have done it without you.

Collaborative Work

The author would like to acknowledge the collaboration of group members past and present for their contribution to work contained herein. Claire Marcellin for initial studies of the phase inverting system as part of her MSc project. Dr Jian Liu for the critical nucleus work using the Span surfactant system. Dr Sharon Cooper for mathematical modelling of the revised nucleation theory.

Memorandum

The work reported in this thesis was carried out at the Department of Chemistry at the University of Durham between October 2003 and September 2006. The work has not been submitted for any other degree and is the original work of the author except where acknowledged by an appropriate reference.

Statement of Copyright

Financial Support

I gratefully acknowledge EPSRC funding for all work detailed in this thesis.

Abstract

The use of emulsions as an aid to the study of crystallisation has long been known. However, the exploitation of this technique has not yet been realised to its full potential. The various conditions that can be generated at, or near, an interfacial region provide a wide range of possibilities for the control, and probing of crystallisation mechanisms.

In this thesis, the effect of the interfacial curvature is considered for the case of ice crystallisation within water-in-oil emulsions. The use of a known ice nucleator, heptacosanol, acting as a co-surfactant enables the effect of a reduced epitaxial match to be monitored, with decreasing water pool diameter. The extreme case where the water pool does not contain enough material to form a crystalline nucleus such that $\Delta G \leq 0$ on complete crystallisation is found. This demonstrates for the first time that a direct experimental measurement of the critical nucleus size is possible.

The use of non-ionic surfactants allows emulsions to phase invert from water-in-oil to oil-in-water upon cooling, and on passing through the phase inversion, ultra low interfacial tensions are obtained. At the phase inversion, crystallisation by the surfactant layer is found to be greatly inhibited, even at high solute supersaturations for glycine and L-asparagine emulsions. Hence we achieve anomalous crystallization behaviour, with crystallisation achieved both on cooling and heating from the same system.

Another unique effect characterised is that of oil droplet inclusion into a single crystal. The highly polar octanoic acid oil phase adheres to the growing glycine crystal so strongly that crystal growth proceeds around the droplet without disruption to the overall resulting crystal to produce macroporous crystals. Where growth rates are uneven, highly fenestrated single crystalline structures result. Upon reducing the oil droplet diameter, dendritic morphologies, highly unusual for such low supersaturations of glycine, are formed. Moreover, the surfactant mixture also controls the polymorph produced, and reproducibly yields the desired β-glycine form.

Publications

Nicholson CE, Cooper SJ, Jamieson MJ:
"Unique crystal morphologies of glycine grown from octanoic acid-in-water emulsions"
Journal of the American Chemical Society **128** (24): 7718-7719

Nicholson CE, Cooper SJ, Marcellin C, Jamieson MJ
"The use of phase-inverting emulsions to show the phenomenon of interfacial crystallization on both heating and cooling"
Journal of the American Chemical Society **127** (34): 11894-11895

Jamieson MJ, Nicholson CE, Cooper SJ
"First study on the effects of interfacial curvature and additive interfacial density on heterogeneous nucleation. Ice crystallization in oil-in-water emulsions and nanoemulsions with added 1-heptacosanol"
Crystal Growth and Design **5** (2): 451-459

List of Symbols

E_t wt%	Weight % of ethylene oxide groups in brij surfactant
OH wt%	Weight % of hydroxide groups in brij surfactant
nH	Number of hydrophilic groups in brij surfactant
nL	Number of hydrophobic groups in brij surfactant
π	Reduction in surface tension also known as surface pressure
A	Area per molecule
k_B	Boltzmann constant
T	Temperature
γ	Surface tension
Γ	Surface excess concentration
c	Concentration
R	The gas constant
Δ	Change in a given quantity
ΔG	Gibbs free energy change
T_K	Krafft Temperature
p	Vapour pressure
υ_l	Liquid molecular volume
r	Radius
$\Delta\mu$	Superaturation, the difference in chemical potentials between 2 phases
ΔH	Enthalpy change
J	Rate of nucleation
W^*	Impingement rate of condensable nuclei
$n(i)^*$	Equilibrium concentration of critical nuclei
θ	Angle in degrees
°C	Degrees Celsius
R_g	Radius of gyration
R	Emulsion droplet radius
v	Molecular volume
f	Function of
τ	Induction Time

N	Number of particles per unit volume required for detection of a crystalline phase
V_m	Molecular volume

All subscripts associated with these symbols are defined in the body of the text associated with the relevant equation

List of Abbreviations

HLB	Hydrophile-Lipophile Balance
AOT	Dioctylsulfosuccinate (Sodium salt)
CMC	Critical Micelle Concentration
PEO	Polyethyleneoxide
EO	Ethylene Oxide
w/o	Water in Oil
o/w	Oil in Water
SDS	Sodiumdodecylsulfate
PIT	Phase Inversion Temperature
LNP	Liquid Nitrogen Pump
TMS93	Linkam Temperature Management System
PTFE	Polytetrafluoroethylene (Teflon)
WAXS	Wide Angle X-ray Scattering
SAXS	Small Angle X-ray Scattering
DSC	Differential Scanning Calorimetry
UVM	Ultrasound Velocity Measurement
UHQ	Ultra High Quality
H_2O	Water
NaCl	Sodium Chloride
$CaCO_3$	Calcium Carbonate
K-oleate	Potassium Oleate
HCl	Hydrochloric Acid
MIN	Minimal Interfacial Nucleation

Table Of Contents

Chapter 1

1.1 Background To Thesis

The design, function and formation of crystalline materials are of direct relevance to a wide range of research areas, and indeed everyday life. Industrial processes in the pharmaceutical industry, semiconductor production, amongst many others, often result in a crystalline material, of which the resulting properties are of utmost importance to its final application. Much of the fundamental science underpinning the formation of these crystalline materials remains an area of active research, particularly on the nano- and molecular scale. The work in this thesis aims to expand the current understanding of some of these processes by controlling the initial nucleation stage of crystallisation. In particular the effect of interfacial curvature, combined with interfacially active additives, achieves a new level of control over the crystals produced.

1.2 Aims & Objectives

The aims of this work are:

- To expand and add to the growing knowledge and models of the initial stages of crystallisation, particularly the nucleation step.
- To study the effects of interfacial curvature on the heterogeneous nucleation ability of interfacially adsorbed additives.
- To explore the amount of control over the resulting crystal achieved using additives to tailor the initial nucleus formed.

1.3 Layout Of Thesis & Route Map

Chapter 2 acts as both an introduction to surfactants and emulsions and as a brief outline to classical nucleation theory.

Chapter 3 details the equipment used for the experimental section of this thesis and contains a brief description of the operating conditions used.

Chapter 4 to 6 discuss the experiments and results carried out as part of the research for this thesis, and each contain a literature review of past material and discussion of the data obtained.

Chapter 4 contains all the initial studies of the range of surfactant systems chosen for the ice nucleation experiments and assesses the suitability of each for the ice nucleation studies.

Chapter 5 explains the modifications necessary to classical nucleation theory when considering a very small amount of crystallisable material and how this may lead to a direct measurement of the critical nucleus. This model is then tested by comparison to experimental evidence.

Chapter 6 moves on to consider the crystallisation of a solute in and around the dispersed phase of the emulsions. In this chapter glycine is used and its nucleation rate behaviour, morphology, and polymorph selection are all probed using interfacial-active additives to induce heterogeneous nucleation.

Chapter 7 provides a brief summary of the work and describes how this thesis fits in with the wider research area.

Appendix 1 gives a more detailed introduction to classical nucleation theory.

Appendix 2 contains movie files of crystallisation experiments from chapter 6; it is intended to provide a visual aid to the unusual crystallisation behaviour that has been observed.

Chapter 2

2.0 Introduction

The content of this chapter is intended as an introduction to the general background theory relevant to the work covered within this thesis. A more detailed introduction to previous work, and an in-depth theory corresponding to the work covered, is presented at the beginning of the subsequent chapters.

The use of emulsions to study the effects of interfacial curvature is a small step towards understanding the role of surface tension and epitaxial matching in the nucleation of crystals. An emulsion is comprised of oil, water and surfactant components to give either oil droplets dispersed in a water continuous phase (an oil-in-water emulsion) or water droplets dispersed in an oil continuous phase (a water-in-oil emulsion).

2.1 Surfactants

Surfactants are molecules which when present in low concentration will adsorb to the surfaces or interfaces of a system and alter the interfacial free energies of that system. The interfacial free energy is the work required to create unit area of an interface. Since the properties of matter at an interface can differ greatly from the bulk phase, surfactants can play an important role where there is a large interfacial area such as that in emulsions, foams and dispersions. True surfactants are distinguished by an ability to form oriented monolayers at the interface (here air/water or oil/water) and, most importantly, to form self-assembled structures (micelles, vesicles) in bulk phases.

This adsorption behaviour can be attributed to the solvent nature and to the chemical structure of surfactants that combines both a polar and a non-polar (amphiphilic) group into a single molecule. Due to their dual nature, amphiphiles

"sit" at interfaces so that their hydrophobic moiety is repelled from strong solvent interactions while the lipophilic part remains in solution.

Another characteristic of surfactant solutions is that when their aqueous concentration exceeds approximately 40%, they can form liquid crystalline phases (lyotropic mesophases). These systems consist of extended aggregates of surfactant molecules in large organised structures.

There are many possible head and tail group structures possible for surfactants. The head group can be charged or neutral, small and compact in size, or a polymeric chain. The tail group is usually a single or double, straight or branched hydrocarbon chain, but may also be a fluorocarbon, siloxane, or contain aromatic group(s). Since the hydrophilic part normally achieves its solubility either by ionic interactions or by hydrogen bonding, the simplest classification of surfactants is based on surfactant head group type, with further subgroups according to the nature of the lipophobic moiety. The four basic classes have therefore emerged as:

- The anionics and cationics, which dissociate in water into two oppositely charged species (the surfactant ion and its counter ion).
- The non-ionics, which include a highly polar (non-charged) moiety, such as polyoxyethylene (−OCH2CH2O−) or polyol groups.
- The zwitterionics (or amphoterics), which combine both a positive and a negative group.

2.1.2 Hydrophilic−Lipophilic Balance (HLB)

The hydrophilic−lipophilic balance (HLB) provides a numerical value that suggests whether an oil-in-water (o/w) or water-in-oil (w/o) emulsion will form. It relates molecular structure to interfacial packing and film curvature. As a guideline, for w/o emulsions the hydrophilic head groups must have strong interactions and for o/w emulsions the alkyl-alkyl interaction between the hydrophobic tail groups must be strong. The HLB value is generated by an

empirical equation (2.1) based on the relative proportions of hydrophobic and hydrophilic groups within the molecule. The HLB concept was introduced by Griffin[1] who characterized a number of surfactants, and derived an empirical equation for non-ionic alkyl polyoxyethylenes (CiEj) based on the surfactant chemical composition.[2]

$$HLB=(Ej\ wt\% + OH\ wt\%)/5 \qquad (2.1)$$

where Ej wt% and OH wt% are the weight percent of ethylene oxide and hydroxide groups respectively. Davies[3] proposed a more general empirical equation (2.2) that relates a constant to the different hydrophilic and hydrophobic groups:

$$HLB=[(nH \times H) - (nL \times L)]+7 \qquad (2.2)$$

where H and L are constants assigned to hydrophilic and hydrophobic groups respectively, and nH and nL are the number of these groups per surfactant molecule. For bicontinuous structures, i.e., those with zero curvature, it was shown that[4] HLB $\approx$ 10. Therefore by definition, w/o microemulsions form when HLB < 10, and o/w microemulsion when HLB > 10, see Table 2.1 for details. Tables 2.2 to 2.4 show common surfactant types and detail the surfactants used in this study.

Table 2.1 Showing HLB ranges and the typical applications for surfactants with that property.

HLB	Application
1 – 3.5	Antifoams
3.5 - 8	Water-in-oil emulsions
7 – 9	Wetting and spreading agents
8 - 16	Oil-in-water emulsions
13 - 16	Detergents
15 - 40	Solubilisers

Table 2.2 Showing common surfactant types where R= *an alkyl chain group*

Headgroup Class	Structure
Sulfonate	$R–SO_3^- M^+$
Sulfate	$R–OSO_3^- M^+$
Carboxylate	$R–COO^- M^+$
Phosphate	$R–OPO_3^- M^+$
Ammonium	$RxHyN^+X^-$ (x = 1-3, y = 4-x)
Quaternary ammonium	$R_4N^+X^-$
Betaines	$RN^+(CH_3)_2CH_2COO^-$
Sulfobetaines	$RN^+(CH_3^+)_2CH_2CH_2SO_3^-$
Polyoxyethylene (POE)	$R–OCH_2CH_2(OCH_2CH_2)nOH$
Polyols	Sucrose, sorbitan, glycerol, ethylene glycol, etc
Polypeptide	$R–NH–CHR–CO–NH–CHR'–CO–...–CO_2H$
Polyglycidyl	$R–(OCH_2CH[CH_2OH]CH_2)n–...–OCH_2CH[CH_2OH]CH_2OH$

Table 2.3 Illustrating examples of surfactant molecules

Group	General Structure	
Natural Fatty Acids	$CH_3(CH_2)_nCOOH$	n=12-18
Alkylphenols	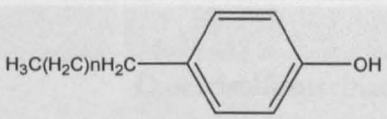	n=6-10 linear or branched
Polyoxypropylene	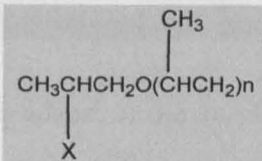	n=degree of oligomerisation X=initiator
Fluorocarbons	$CF_3(CF_2)_nCOOH$	n=4-8 linear or branched,or H terminated
Silicones	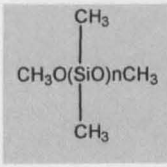	

Table 2.4 Surfactants commonly used in the experiments within this thesis

Surfactant Trivial Name	**HLB**	**Family**	**Derivative**
Brij30	9.7	Polyoxyethylene	$C_{12}E_4$
Brij35	16.9	Polyoxyethylene	$C_{12}E_{23}$
Brij52	5.3	Polyoxyethylene	$C_{16}E_2$
Brij72	4.9	Polyoxyethylene	$C_{18}E_2$
Span60	4.7	Sorbitan	Monostearate
Span65	2.1	Sorbitan	Tristearate
Span80	4.3	Sorbitan	Monooleate
Span85	1.8	Sorbitan	Trioleate
Tween20	16.7	Polyoxyethylene Sorbitan	Monolaurate
Tween60	14.9	Polyoxyethylene Sorbitan	Monostearate
Tween80	15	Polyoxyethylene Sorbitan	Monooleate
AOT		Dioctylsulfosuccinate, (sodium salt)	

When surfactants strongly adsorb at the interface a large reduction in surface tension is observed, even with small changes in concentration of the adsorbate. Practically, this enables the measurement of the surface activity of a surfactant to be determined directly from measurement of interfacial tension with respect to solute concentration.

2.1.3 Surface Or Interfacial Tension

The surface or interfacial tension is defined as the minimum amount of work required to create a unit area of interface due to the surface free energy of that interface.

2.1.4 Langmuir Monolayers[5]

A surfactant can drastically alter the interfacial tension due to its amphiphilic nature. Since the system energy is lowered when a surfactant molecule resides at the interface, surfactant accumulation at the interface is a spontaneous process resulting in the formation of a monolayer of surfactant at the water boundary and a reduction in the surface tension π, of the aqueous phase.

Langmuir films consist of surface-active material trapped between two phases, either liquid-liquid or liquid-gas. The hydrophilic part of the amphiphilic surfactant molecules is attracted to polar liquids, such as water, and the attraction is mainly coulombic. The interactions experienced by the hydrophobic tails are mainly of weaker Van der Waals type.

To form Langmuir monolayers, the surfactants are dissolved in a volatile organic solvent and gently introduced to the liquid interface at low concentration. The solvent evaporates leaving the surfactants partially oriented at the interface. The surfactant must possess the correct balance of a long hydrophobic tail group and a hydrophilic head group to ensure that it sits at the interface and forms just a single layer.

The use of a barrier to compress the monolayer causes the surfactant to form the 2D equivalent of a liquid, and then a solid if the film is sufficiently stable, see Figure 2.1. The 'solid' form of the monolayer produces an organised close-packed film known as a Langmuir film.

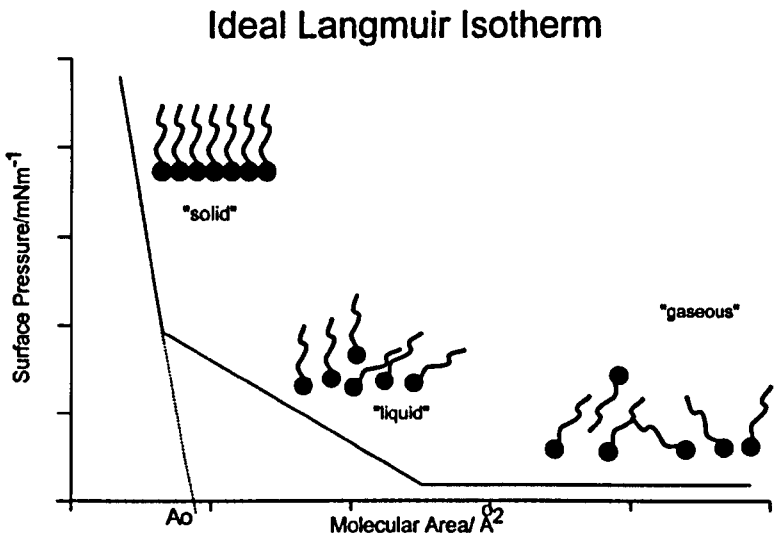

Figure 2.1 Langmuir monolayer surface pressure versus molecular area graph, shows the distinct phase transitions observed during an ideal trough experiment

Measurement of the surface pressure of these monolayers when in the gaseous state enables the molecular area to be approximated from the relationship

$$\pi A = kT \qquad (2.3)$$

where π is the surface pressure, A is the area per molecule, k is the Boltzmann constant and T is the temperature.

The surface pressure of a film can be measured using a Wilhelmy plate attached to a microbalance. The forces acting on the plate when it is in contact with the water are gravity, upthrust and surface tension. The first two may be cancelled out since the balance is zeroed when the plate is just immersed and kept at a constant level. Since the contact angle between water and the plate is zero, the surface tension is given by:

Surface Tension = Force/Perimeter (2.4)

where Perimeter is the perimeter of the plate in meters.

From this theory and subsequent application through experiment, both the state of the monolayer and the area per molecule can be measured.

2.1.5 Efficiency Of A Surfactant

The efficiency of a surfactant is the concentration of surfactant required to lower the surface tension by a given amount. Normally this value is set as the concentration of surfactant required to produce a reduction in surface tension γ of 20 mN m^{-1}.

The Frumkin adsorption equation, equation 2.5, relating the reduction in surface tension π to the surface excess concentration Γ verifies that the minimum concentration of surfactant required producing maximum adsorption at the interface lies close to this value. Since the maximum surface excess Γ_m generally lies in the range $1 - 4.4\times10^{-10}$ mol cm^{-2} solving the Frumkin equation shows that once the surface tension has been reduced by 20 mN m^{-1}, at 25°C, the surface is 84 – 99.9% saturated[6].

$$\gamma_0 - \gamma = \pi = -2.303RT\Gamma_m \log\left(1 - \frac{\Gamma}{\Gamma_m}\right) \qquad (2.5)$$

where γ_0 is the surface tension of pure liquid, γ is the surface tension of the liquid an surfactant, R is the gas constant (Boltzmann constant), T is the temperature of the solution Γ is the surface excess concentration and Γ_m is the maximum surface excess concentration of surfactant.

The negative logarithm of this surfactant concentration required to reduce the surface tension by 20 mN m^{-1}, pC_{20}, is useful as it can be related to the change in free energy $\Delta G°$ involved in the transfer of a surfactant molecule from the interior of the bulk liquid phase to the interface. A large value of pC_{20} indicates a

surfactant that is efficiently adsorbed at the interface and is efficient at reducing surface tension.

Other factors that contribute to surfactant efficiency are:

- A straight alkyl chain as the hydrophobic group, rather than a branched alkyl chain containing the same number of carbon atoms.
- A single hydrophilic group situated at the end of the hydrophobic group, rather than one (or more) at a central position.
- A non-ionic or zwitterionic hydrophilic group, rather than an ionic one.
- For ionic surfactants, a reduction in the effective charge by
  a) use of a more tightly bound (less hydrated) counterion and
  b) increase in ionic strength of the aqueous phase.

The use of a standard value of a decrease in surface tension of 20 mN m^{-1} for the definition of adsorption efficiency is not valid for systems where surfactants differ significantly in their maximum surface excess or when the surface pressure is less than 20 mN m^{-1}. Pitt et al.[7] circumvented this problem by defining $\Delta\gamma$ as half the surface pressure at the critical micelle concentration, or CMC.

2.1.6 Effectiveness Of A Surfactant

The effectiveness of a surfactant gives the maximum reduction in surface tension possible from a surfactant regardless of its concentration. This is equivalent to the surface excess concentration Γ_m at surface saturation. γ_{min}, and Γ_m, are controlled mainly by the CMC. Γ_m, through the Gibbs adsorption equation, gives a measure of the interfacial packing. The Gibbs adsorption equation is:

$$\Gamma = -\frac{c}{RT}\frac{d\gamma}{dc} \qquad (2.6)$$

where c is the concentration of the surfactant in the bulk solution, R is the gas constant and T is the temperature of the solution.

The effectiveness of a surfactant is related to its molecular structure; specifically to the relative size of the hydrophilic and hydrophobic portions of the adsorbing molecule. The area per molecule is determined either by the hydrophobic chain cross-sectional area, or the area required for closest packing of head groups, whichever is greater. Therefore, tightly or loosely packed films result in very different interfacial properties. Within a series of single straight chain surfactants, increasing the hydrocarbon chain length from C_8 to C_{20} will have little effect on adsorption effectiveness.[6]

2.2 Micellisation

In addition to forming oriented interfacial monolayers, surfactants can aggregate to form micelles, provided their concentration is sufficiently high. Micelles are typically clusters of between 50–200 surfactant molecules, whose size and shape are governed by geometric and energetic considerations, with the process being entropically driven.

Micelle formation occurs over a fairly sharply defined region called the critical micelle concentration (CMC). At and above the CMC, the maximum concentration of surfactant molecules at the interface has been reached and so additional surfactant molecules aggregate to form micelles, whereas the concentration of the unassociated monomers remains almost constant. This achieves a minimisation of the free energy of the system.

The driving force for micellisation in mainly entropic, as can be seen from the following considerations. Below the CMC, the hydrocarbon tail produces a cavity in the water structure. This cavity is lined by water molecules which differ in their organisation from that of the bulk water. The water exists in a more 'structured' environment. Furthermore, the hydrocarbon tail is less free to move in the solvated state because of the surrounding water.

On micelle formation, the bulk structure of water is restored and the entropy of the water increases. In the micelle core, which is essentially liquid hydrocarbon, there is greater freedom for movement and so the entropy associated with the hydrocarbon tails also increases.

Aggregation of surfactant molecules results partly from the tendency of the hydrophobic groups to minimise contacts with water by forming oily micro domains within the solvent. There, alkyl – alkyl interactions are maximised, while hydrophilic head groups remain surrounded by water. The head groups are little affected by micellisation since they are surrounded by water molecules at all stages of the process. However, interactions between headgroups (within the same micelle) will determine the size and shape of the micelle. These interactions will result in some of the hydrocarbon core being exposed to water because the surface cannot be covered by a close-packed arrangement of polar head groups.

2.2.1 The Cloud Point

For non-ionic surfactants, a common observation is that micellar solutions tend to become visibly turbid at a well-defined temperature. This is referred to as the cloud point, above which the surfactant solution phase separates. Above the cloud point, the system consists of an almost micelle-free dilute solution at a concentration equal to its CMC at that temperature, and a surfactant-rich micelle phase. This separation is caused by a sharp increase in the aggregation number and a decrease in micelle-micelle repulsions[8, 9] resulting in a difference in density of the micelle-rich and micelle-poor phases. Since much larger particles are formed, the solution becomes visibly turbid with large micelles efficiently scattering light.

The cloud point depends on the surfactants' chemical structure. For polyoxyethylene (PEO) non-ionics, the cloud point increases with increasing ethylene oxide (EO) content for a given hydrophobic group. At constant EO content the cloud point may be lowered by decreasing the hydrophobic groups'

size, broadening the PEO chain-length distribution, and branching in the hydrophobic group.[10]

2.2.2 The Krafft Point

Ionic surfactants are initially insoluble in water, but there is often a temperature at which the solubility suddenly increases very dramatically. This is known as the Krafft point or Krafft temperature, T_K, and is defined as the temperature at which the solubility of the monomeric surfactant is equivalent to its CMC at the same temperature. Below T_K, surfactant monomers only exist in equilibrium with the hydrated crystalline phase. No micelles are present, so the surfactant will not perform efficiently as its solubility is low. Above T_K, micelles are formed providing much greater surfactant solubility.

The Krafft point of ionic surfactants is found to vary with counterion[11], alkyl chain length and chain structure. Lowering T_K is usually achieved by introducing chain branching, multiple bonds in the alkyl chain or bulkier hydrophilic groups, thereby reducing intermolecular interactions that would promote crystallisation.

2.2.3 Emulsions

Microemulsions and emulsions can be formed by the swelling of micelles by an internal phase, for example the swelling of AOT micelles in an oil such as decane by addition of water will result in the formation of a w/o microemulsion. This uptake of a dispersed phase is the origin of detergent action. Extending this idea of swelling of micelles will result in a range of emulsion droplet sizes from microemulsion to emulsion by simply increasing the water content of the system see Table 2.5.

Table 2.5 Typical emulsion droplet sizes.

White Emulsion	Blue Emulsion (Nano-emulsion)	Micro Emulsion
White Creamy	Blue Semi-opaque	Transparent
Droplet Diameter > 400nm	Droplet Diameter ~100nm	Droplet Diameter <100nm

By putting energy into the system, by e.g. agitation, an emulsion can form but with time this will eventually revert to the lowest energy state of phase separation. Hence emulsions can only be classed as kinetically stable and not thermodynamically stable.

2.2.4 Microemulsions

Danielsson and Lindman[12] define a microemulsion as:
"A system of water, oil and an amphiphile which is a single optically isotropic and thermodynamically stable liquid solution".
In some respects, microemulsions can be considered as small-scale versions of emulsions, droplet type dispersions either of oil-in-water (o/w) or of water-in-oil (w/o) occur, with a size range in the order of 5−50 nm in drop radius, except that they are thermodynamically stable.

For microemulsions, once the conditions are right, spontaneous formation occurs. Microemulsion formation is dependent on surfactant type and structure. If the surfactant is ionic and contains a single hydrocarbon chain (e.g., sodium dodecylsulphate, SDS) microemulsions are often formed if a co-surfactant (e.g., a medium size aliphatic alcohol) and/or electrolyte (e.g., 0.2 M NaCl) are also present. With double chain ionics (e.g., AOT) and some non-ionic surfactants, a co-surfactant is not necessary. This results from one of the most fundamental properties of microemulsions, that is, an ultra-low ($\sim 10^{-3}$ mN m^{-1}) interfacial

tension between the oil and water phases, $\gamma_{o/w}$. The main role of the surfactant is to reduce $\gamma_{o/w}$ sufficiently, lowering the energy required to increase the interfacial area, so that spontaneous dispersion of water or oil droplets occurs due to the increase in entropy that arises on dispersion, and so the system is thermodynamically stable.

A well-known classification of microemulsions is that of Winsor[13] who identified four general types of phase equilibria:

- Type I: the surfactant is preferentially soluble in water and oil-in-water (o/w) microemulsions form (Winsor I). The surfactant-rich water phase coexists with the oil phase where surfactant is only present as monomers at small concentration.
- Type II: the surfactant is mainly in the oil phase and water-in-oil (w/o) microemulsions form. The surfactant-rich oil phase coexists with the surfactant-poor aqueous phase (Winsor II).
- Type III: a three-phase system where a surfactant-rich middle-phase coexists with both excess water and oil surfactant-poor phases (Winsor III or middle-phase microemulsion).
- Type IV: a single-phase (isotropic) micellular solution, that forms upon addition of a sufficient quantity of amphiphile (surfactant plus co-surfactant if necessary).

2.2.5 Nanoemulsions

Nanoemulsions are also known as mini-emulsions or blue emulsions. These are semi-opaque, blue-white coloured emulsions possessing an average droplet size of 0.1 μm - 0.4 μm in diameter. The surfactant concentration is much lower than that required to form microemulsions, typically 1-5% of the oil phase compared to 10-30% in microemulsions. Nanoemulsions also differ in that their surfactant mixture usually consists of an ionic surfactant and a long chain alcohol as a co-surfactant. (Typically $C_{12}H_{49}OH$ or greater)

The other contrasting property of nanoemulsions compared to microemulsions is that they are not thermodynamically stable, merely kinetically stable. The stability of a nanoemulsion can range from a few hours to several months, in either case this may be sufficient for the timescale of the measurements carried out upon them.

The suggested mechanism for the formation of nanoemulsions is the swelling of mixed micellular structures by solvent, followed by the breakdown of these structures into much smaller droplets, forming the nanoemulsion. It is proposed[6] that the driving force for nanoemulsion formation is the migration of surfactant to the oil-water interface and subsequent gain in entropy of mixing from this action.

2.2.6 Phase Inversion Temperature (PIT)

Non-ionic surfactants form w/o microemulsions (and emulsions) with high temperature sensitivity. In particular, there is a specific phase inversion temperature (PIT) where the film curvature changes from positive to negative. This critical point was defined by Shinoda et al.[14]:

- If T < PIT, an oil-in-water microemulsion forms (Winsor I[13]),
- If T > PIT, a water-in-oil microemulsion forms (Winsor II),
- At T = PIT, a middle-phase microemulsion exists (Winsor III) with a spontaneous curvature equal to zero, and a HLB number approximately equal to 10.

Increasing temperature increases the lipophilicity of the surfactant. Chains become dehydrated, and so micelles invert causing a w/o emulsion to be formed.

2.2.7 Ostwald Ripening & Coalescence

Microemulsions are thermodynamically stable, since the interfacial tension is low and is offset by the entropy of dispersion of the globules. Systems of larger droplet diameters are only kinetically stable, and develop into separate phases over time.

Ostwald ripening and coalescence are two distinct mechanisms of gradual degradation in emulsions. Ostwald ripening[15-19] is driven by the difference in Laplace pressure, Δp, of droplets of different radii, see equation 2.7, and the increased stability of smaller droplets, as shown by the Gibbs-Thomson equation. In particular the Laplace equation shows that,

$$\Delta p = \gamma\left(\frac{1}{r_1}+\frac{1}{r_2}\right) \qquad (2.7)$$

where γ is the interfacial tension and r_1 and r_2 are the radii of curvature of a deformed emulsion droplet.

Breaking of the droplets is feasible if the deforming force exceeds the Laplace pressure. It can be inferred from the Laplace relationship that a smaller droplet size requires a greater energy input (or more surfactant) to lower γ. Even in the absence of droplet rupture, larger droplets will tend to grow at the expense of smaller ones, due to the increased solubility of the material in the latter, as shown by the Gibbs-Thomson equation 2.8.

$$k_B T \ln\frac{p}{p_0} = \frac{2\gamma v_l}{r} \quad \text{or} \quad \Delta\mu = \frac{2\gamma v_i}{r} \qquad (2.8)$$

where p_0 is the vapour pressure of the liquid, p is that of the vapour, γ is the surface vapour-crystal interfacial tension, υ_l is the liquid molecular volume, and r is the radius of the droplet nucleus.

In the case of coalescence, the thin film between the droplets ruptures, causing them to fuse. Whether a coalescence or Ostwald ripening mechanism is predominantly operating is easily identified[20]; Ostwald ripening alone leads to a narrow size distribution and a growth rate that gradually vanishes. In the case of coalescence, the polydispersity increases.

2.2.8 Coagulation, Flocculation & Creaming

Coagulation is the term used to describe the formation of aggregates in an unstable emulsion or colloidal system. Some authors distinguish between coagulation and flocculation, with the latter referring to reversible aggregation and implying the formation of a loose or open network. If the coagulum density is lower than the surrounding medium, which is usually the case for oil-in water systems, the aggregate accumulates at the top. This is the effect known as creaming.

2.3 Nucleation Theory

Formation of a crystalline phase from a bulk solution requires the creation of an interface between two phases. The difference between the chemical potentials $\Delta\mu$ of these two phases gives the thermodynamic driving force towards a phase transition, in this case crystallisation, and is known as the supersaturation.

The supersaturation $\Delta\mu$ relies on a number of factors which depend upon the initial phase from which crystallisation occurs, as shown in Table 1.6.

Table 2.6 Calculation of Supersaturation

Process	$\Delta\mu$
Crystallisation from solution	$\Delta\mu = kT \ln \frac{C}{C_0} \quad \Delta\mu = \frac{\Delta_{sol} H \Delta T}{T_{sat}}$
Crystallisation from melt	$\Delta\mu = \frac{\Delta_{melt} H \Delta T}{T_m}$

Here: C and C_0 are the concentration of the solute, and its saturation concentration, respectively, $\Delta_{sol}H$ and $\Delta_{melt}H$ are the enthalpy of solution and melting, respectively and T_{sat} and T_m are the saturation and melting temperature, respectively. Supersaturation promotes the formation of small aggregates of molecules, i.e. crystal nuclei. However, the work done in creating this new surface makes these nuclei unstable with respect to the parent phase. For instance for condensation from the vapour phase, the vapour pressure of the newly formed nucleus is extremely high and so the nuclei will tend to evaporate back into the parent phase until a steady state is reached. Indeed, the Laplace and Gibbs Thompson equations, equations 1.7 and 1.8, show that the vapour pressure of a liquid nucleus is greater than that of the surrounding vapour phase.

2.3.1 Classical Heterogeneous Nucleation Theory

The crystallisation process is normally regarded as two processes:
Nucleation, the rate of formation of critical nuclei and
Crystal growth of the critical nuclei to micro/macroscopic dimensions.

Homogeneous nucleation refers to nucleation within a bulk parent phase whereas heterogeneous nucleation occurs upon a foreign substrate.

Nucleation occurring on a foreign substrate occurs at a greater rate than the homogeneous case, yet it may be represented in a similar way, i.e.

$$J = W^* n(i^*) \qquad (2.9)$$

where J is the rate of nucleation
W* is the impingement rate of condensable species on the nuclei
n(i*) is the equilibrium concentration of the critical nuclei
For heterogeneous nucleation:

$$n(i^*) = n_0 \exp\left[-\frac{\Delta G^*_{het}}{k_b T}\right] \qquad (2.10)$$

where n_0 is the concentration of the crystallising material adsorbed on the foreign substrate and ΔG_{het}^* is the Gibbs free energy of formation of the critical nucleus. ΔG_{het}^* depends on the shape of the critical nucleus on the substrate and also on the statistical distribution of the condensable species.

The energy barrier, ΔG_{het}, hindering the formation of a new crystalline phase is overcome simply by statistical fluctuations about the equilibrium.

The pivotal moment in the nucleation process is thus the attainment of the energy increase ΔG_{het} to form the critical nucleus, see Figure 2.2. Aggregates larger than the critical nucleus will tend to grow, whereas smaller ones will tend to evaporate/dissolve. Once the critical nucleus has formed, the bulk crystalline phase can occur by crystal growth.

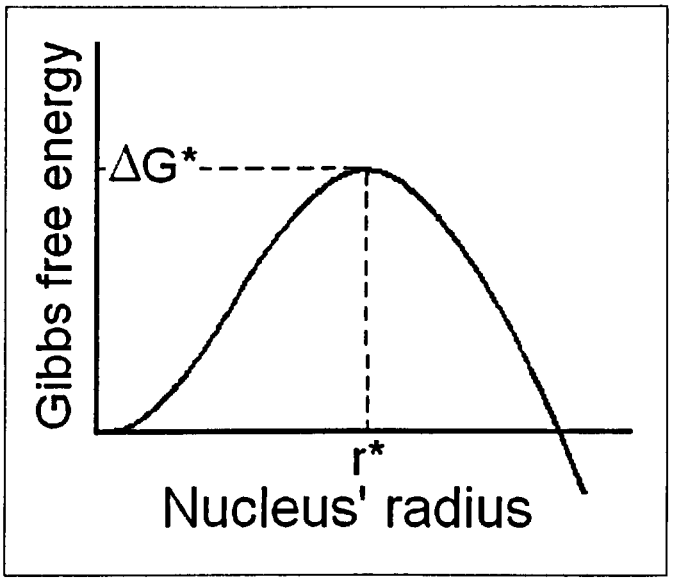

Figure 2.2 Profile of the change in Gibbs free energy with the size of a crystalline nucleus.

2.3.2 Improvements To, & Omissions In Classical Nucleation Theory

Classical nucleation theory can be improved by the incorporation of terms to account for the following, if appropriate[21-33].

- Statistical Mechanical Terms: These terms are collectively known as the replacement term and take into account the translational and rotational motion of the small aggregates.
- Zeldovich Factor: gives the steady-state concentration of critical nuclei, rather than the equilibrium concentration of critical nuclei.
- Thermal Non-Accommodation: Every time a cluster grows by the addition of an atom, its temperature will rise due to the liberated enthalpy of crystallisation. Hence the cluster will be more likely to evaporate.
- Quasi-Adsorption of Impingement Atoms: considers the scenario where an adatom re-evaporates before equilibrating with the surface.

- Time Dependent Nucleation (Time Lag): The time delay between a supersaturation occurring and the production of the steady state concentration of critical nuclei is termed nucleation time lag. Often this is much less than one second in duration, and so can be ignored.
- Correction for Small Critical Nuclei at High Supersaturation: For spherical particles the surface tension will tend to decrease with decreasing size. For anisotropic crystals (where the critical nucleus will not in general be spherical), edge and corner effects may also become important for very small nuclei.
- Strain or Dislocations: The critical nucleus may have some relatively large additional energy terms due to strain or dislocations, if the lattice dimensions of the substrate and critical nucleus differ greatly.

Classical nucleation theory is often adequate to describe nucleation in different systems. However, for the heterogeneous case, the substrate is assumed to be rigid and flat, which is clearly not the case for crystallisation induced by surfactants adsorbed at microemulsion or emulsion interfaces. Consequently, in this thesis I will investigate whether classical nucleation theory can be extended to model these systems.

2.3.3 Epitaxy

Epitaxy is the term used for the oriented growth of a crystalline material on a different material. The substrate may influence crystallisation to such an extent that a specific orientation or polymorph is induced.[34] Epitaxial theories examine the conditions required to achieve minimal interfacial energy from a single overgrowth orientation. Epitaxial growth differs from normal crystal growth in that the substrate and overgrown crystal have different chemical potentials.[35]

Epitaxial growth is favoured when there is a small lattice mismatch between the substrate and crystal, and when the interaction between the substrate and crystal is

strong. As a crystal is grown on the substrate any misfit between the crystal lattice is accommodated by misfit dislocations in the growing crystal to relieve any strain. Once the crystal reaches a certain size, past which the interaction of the substrate has diminished, the adatoms will revert to their usual lattice positions.

2.3.4 Growth Mechanisms

For a crystal surface that is atomically rough, continual growth is observed. Deposition of adatoms onto the crystal is diffusion controlled, and hence this growth rate depends linearly on the degree of supersaturation.

Growth of atomically flat surfaces requires the formation of a critical nucleus for each deposited layer. The rate of deposition is no longer linearly dependant upon the supersaturation. Instead the growth rate is given by a 2D equivalent of the nucleation rate. However once a critical supersaturation is reached nucleation of multiple 2D nuclei result in the surface becoming rough and continual growth begins.

Screw dislocations in the crystal face provide an alternate mechanism for atomic deposition allowing crystal growth at lower supersaturations.

2.3.5 Crystal Morphology

For crystals, the surface free energy is generally anisotropic. Consequently, the equilibrium shape of a crystal will not be spherical, but can be determined by the Gibbs-Wulff theorem[36].

Gibbs and Curie proposed that the equilibrium shape of a crystal, is given by the condition that the total surface Gibbs function of formation, should be a minimum for a constant volume of crystal[21, 37], i.e.

$$d\sum_n A_n\gamma_n = \sum_n \gamma_n dA_n = 0 \qquad (2.11)$$

where A_n is the area of face n and γ_n is the surface tension of face n.

Note that the surface tension is assumed to be constant across the face and independent of crystal shape.

Wulff showed that by assuming a fixed point, of distance Υ_n from face n, that the ratio γ_n/Υ_n is constant[36]. This allows determination of the equilibrium shape of the crystal from a Wulff plot (see Figure 2.3).

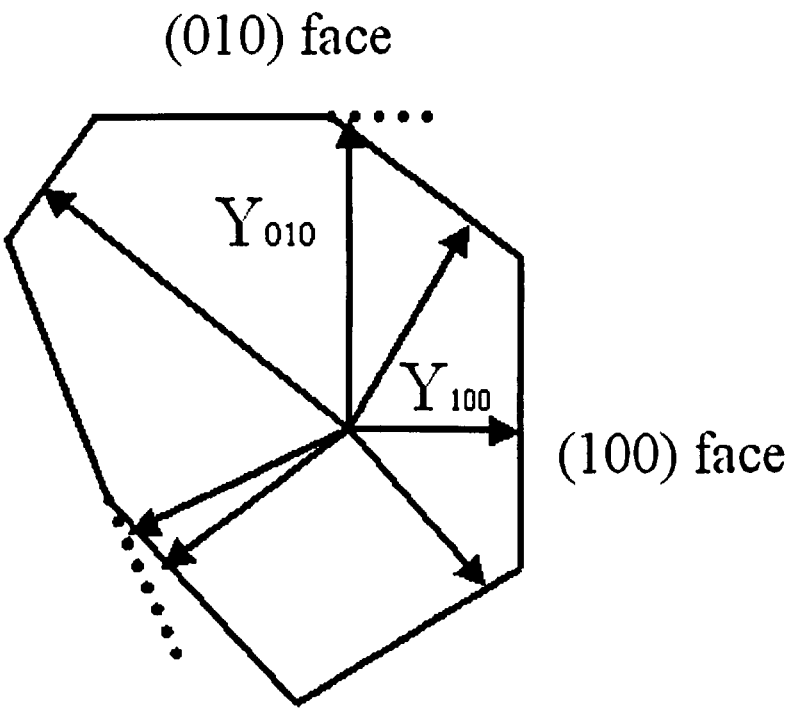

Figure 2.3. Illustration of a Wulff plot. According to the theory, the product $\Upsilon_{100}*\gamma_{100}$ is equivalent to $\Upsilon_{010}*\gamma_{010}$.

In a Wulff plot, vectors are drawn normal to all possible crystallographic faces from an arbitrary point, and the distances proportional to γ_n are marked on the

vectors. Planes normal to the vectors are constructed through the marks and the resulting polyhedron is the equilibrium form. As a consequence, faces with the lowest surface tension dominate the shape of the equilibrium crystal. This would be the (100) face for the hypothetical crystal illustrated in Figure 2.3.

The resulting morphology of a crystal will not typically be the equilibrium form, though. Instead the slowest growing faces will dominate the morphology. Many modelling programs have been created to try to predict the morphology of crystals simply from the interactions between molecules. The basic theory behind these programs is to minimise the potential of a pair/chain of molecules and consider the step energy of all available addition sites, from which it can be predicted where molecules will attach with the lowest energy expenditure. Hence the fastest growing faces are assigned. Since it is the slowest growing faces that determine the overall resulting shape of a crystal, a morphology can be predicted.

Control of crystalline morphology using additives is well known.[38-40] Incorporation of soluble additives in a solution whilst crystallising a substance can have profound effects upon the resulting morphology. Depending upon whether these additives adsorb to a fast or slow growing face, the resulting crystal shape is drastically altered. Should an additive attach to a fast growing face during the early stages of crystallisation and inhibit the growth of that face, it may now appear as one of the faces seen at the end of crystal growth, see Figure 2.4.

Additives may have an opposite effect, and promote the nucleation of a particular crystal face which will grow more quickly than it would normally, if the additives aggregate together, for instance at the air-water interface. Again this results in an altered morphology or indeed even a different polymorph appearing.

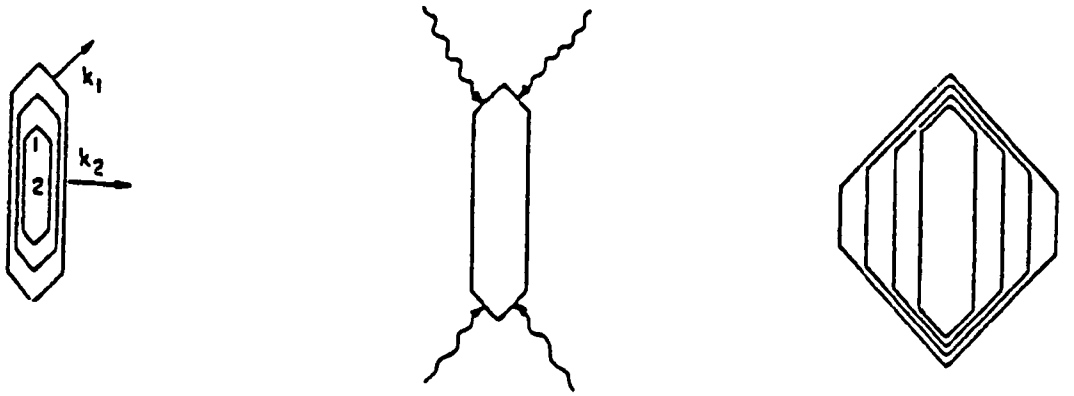

Figure 2.4. Showing that by inhibiting growth in the k1 direction the resulting crystal morphology is now dominated by this slowest growing facet.[40]

References

1 Griffin, W. C. J. *Cosmetics Chemists* 1949, ***1***, 311.

2 Griffin, W. C. J. *Cosmetics Chemists* 1954, ***5***.

3 Davies, J. T. In Proc. 2nd Int. Congr. Surface Act.: London, 1959; **Vol. 1**.

4 Israelachvili, J. N. Colloid Surf. A-Physicochem. Eng. Asp. 1994, **91**, 32.

5 NimaTechnologyLtd Operating Manual; 5th ed.

6 Rosen: Surfactants And Interfacial Phenomena USA, **1989**.

7 Pitt, A. R.; Morley, S. D.; Burbidge, N. J.; Quickenden, E. L. *Journal of Colloids and Surfaces: A* 1996, ***114***, 321.

8 Staples, E. J.; Tiddy, G. J. T. *J. Chem. Soc., Faraday Trans.* 1978, ***74***, 2530.

9 Tiddy, G. J. T. *Phys. Rep.* 1980, ***57***, 1.

10 Schott, H. *J. Pham. Sci.* 1969, ***58***, 1443.

11 Hato, M.; Tahara, M.; Suda, Y. *J. Coll. Interface Sci.* 1979, ***72***, 458.

12 Danielsson, I.; Lindman, B. *Journal of Colloids of Surfaces: A* 1981, ***3***, 391.

13 Winsor, P. A. *Trans. Faraday Soc.* 1948, ***44***, 376.

14 Shinoda, K.; Saito, H. Journal of Colloid and Interface Science 1969, **34**, 238.

15 Ostwald, W. *Lehrbruck der Allgemeinen Chemie:* Leipzig, Germany., 1896; Vol. 2 Part 1.

16 Ostwald, W. Z. *Phys. Chem.* 1897, 22, 289.

17 Ng, J. D.; Lorber, B.; Witz, J.; Theobald, D. A.; Kern, D.; Giege, R. *J. Cryst. Growth* 1996, ***168***, 50-62.

18 Boistelle, R.; Astier, J. P. *J. Cryst. Growth* 1988, ***90***, 14-30.

20 Schmitt, V.; Cattelet, C.; Leal-Calderon, F. *Langmuir* 2004, ***20***, 46-52.

21 Gibbs, J. On the Equilibrium of Heterogeneous Substances: New York, 1928; Vol. 1.

22 Frenkel, J. *Kinetic Theory of Liquids*; Oxford University Press: Oxford, 1946.

23 Rodebush, W. *Chem. Revs.* 1949, ***44***, 269-276.

24 Lothe, J.; Pound, G. *J. Chem. Phys.* 1962, ***36***, 2080-.

25 Lothe, J.; Pound, G. *In Nucleation*; Zettlemoyer, M., Ed.: New York, 1969; p 120.

26 Reiss, H. *Adv. Coll. & Interf. Sci.* 1977, ***7***, 1-66.

27 Russel, K.; Lothe, J.; Pound, G.; *Proceedings of the International Symposium on Condensation and Evaporation of Solids;* Rutner, G., Hirth, Gordon & Breach, Ed.: New York., 1964.

28 Zeldovich, J. *Acta Physicochim* 1943, ***18***, 1.

29 Chan, K. S.; Lee, J. K.; Shiflet, G. J.; Russell, K. C.; Aaronson, H. I. *Metallurgical Transactions A: Physical Metallurgy and Materials Science* 1978, ***9A***, 1016-1017.

30 Sigsbee, R.; Pound, G. *Adv. Coll. & Interf. Sci.* 1967, ***1***, 335.

31 Venables, J. A. *Thin Solid Films* 1973, ***18***, S11-14.

32 Shizgal, B.; Barrett, J. C. *J. Chem. Phys.* 1989, ***91***, 6505-6518.

33 Chukanov, V. N.; Korobitsin, B. A. *High Temperatures - High Pressures* 1997, ***29***, 319-325.

34 Weissbuch, I., M. Lahav, and L. Leiserowitz, *Crystal Growth & Design,* 2003. ***3***(2): p. 125-150.

35 Cooper, S.J., in Chemistry. 1993, University of Bristol: Bristol.

36 Wulff, G. *Z Kristallogr.* 1901, ***34***, 449.

37 Curie, P. Bull. *Soc. Franc. Mineral* 1885, ***8***, 49.

38 Berkovitchyellin, Z.; Addadi, L.; Idelson, M.; Lahav, M.; Leiserowitz, L. *Angewandte Chemie-International Edition in English* 1982, ***21***, 631-632.

39 Addadi, L.; Yellin, Z.; Weissbuch, I.; Lahav, M.; Leiserowitz, L. *Molecular Crystals and Liquid Crystals* 1983, ***96***, 1-17.

40 Weissbuch, I.; Addadi, L.; Berkovitchyellin, Z.; Gati, E.; Weinstein, S.; Lahav, M.; Leiserowitz, L. *Journal of the American Chemical Society* 1983, ***105***, 6615-6621.

41 Black, S. N.; Davey, R. J.; Halcrow, M. *Journal of Crystal Growth* 1986, ***79***, 765-774.

Chapter 3

3.1 Introduction

This chapter provides a brief outline of the procedures followed and experimental techniques used throughout the work of this thesis. It is intended to act as a 'how to' guide rather than describing in detail the theoretical background to each technique.

3.2 Background

There are a wide range of techniques available for investigating crystallisation and polymorphism, from optical techniques such as microscopy and observation, X-ray crystallography, solid state NMR, FTIR, for polymorph identification and resolution of crystal structures, to more indirect measurements of crystallisation from the latent heat of the phase transition, measured using DSC, to the use of ultrasound to observe the change in velocity when a slid phase is formed.

The uses of the techniques available were investigated and an appropriate method chosen for each application, for example:
w/o microemulsion with added nucleating agent heptacosanol

- Use optical microscopy to check stability of microemulsion at low temperatures and to ensure no crashing out of surfactant and co-surfactant.
- Use DSC to observe crystallisation temperature since droplet sizes are too small to be seen using optical microscopy.
- Use SAXS to determine droplet diameter, sine once again optical microscopy is of little use due to the extremely small droplet sizes.

3.3 Experimental Techniques

3.3.1 Optical Microscopy

Equipment used:

- Linkam F600 Coldstage, see Figure 3.2
- TMS93 Temperature Controller Module
- LNP94/2 Liquid Nitrogen Pump
- Olympus optical microscope, see Figure 3.1
- Olympus Camedia 2.1megapixel digital camera.
- Alternative camera Pixelink A602 2.0megapixel camera
- Linkam Linksys software, see Figure 3.3
- 10x objective, and 50x objective
- Cross polarizer and 590nm tint plate

The temperature programmer on the Linkam cold stage enabled the automatic control of a pre-programmed temperature profile leaving the observer to take photographs of important transitions of the emulsion. Purchase of appropriate Linksys software for PC and a fire-wire camera enabled this entire process to be automated for later parts of this work, see Figure 3.3. The most commonly used temperature profiles are shown below in Table 3.1.

Table 3.1 Examples of cooling profiles used for ice nucleation experiments in emulsions.

Cooling rate	**0.25**	**0.5**	**4**	**10**
Rate1	Hold 20°C for 2 min	Hold 20°C for 2 min	Hold 20°C for 2 min	Hold 20°C for 2 min
Rate2	5°C/min from 20°C to 0°C	5°C/min from 20°C to 0°C	4°C/min from 20°C to -40°C	10°C/min from 20°C to -40°C
Rate3	0.25°C/min from 0°C to -40°C	0.5°C/min from 0°C to -40°C	10°C/min from -40°C to 20°C	10°C/min from -40°C to 20°C
Rate4	5°C/min from -40°C to 20°C	5°C/min from -40°C to 20°C	Hold 20°C for 2 min	Hold 20°C for 2 min

Operation

- Fill dewar with liquid nitrogen and connect the line to the coldstage
- Connect the lines from the LNP94 to the coldstage.
- Switch on the LNP and TMS93
- Program the TMS 93 by pressing NEW then entering values for ramp number, rate, set temperature, and hold time, pressing enter after imputing each value.
- When program is complete press enter.
- Start the program by pressing start, selecting cycle if a repeat is required.
- The Linkam setup should then assume control of the coldstage and nitrogen pump so as to control the temperature as the program dictates.

Figure 3.1 Linkam cold stage & Olympus optical microscope.

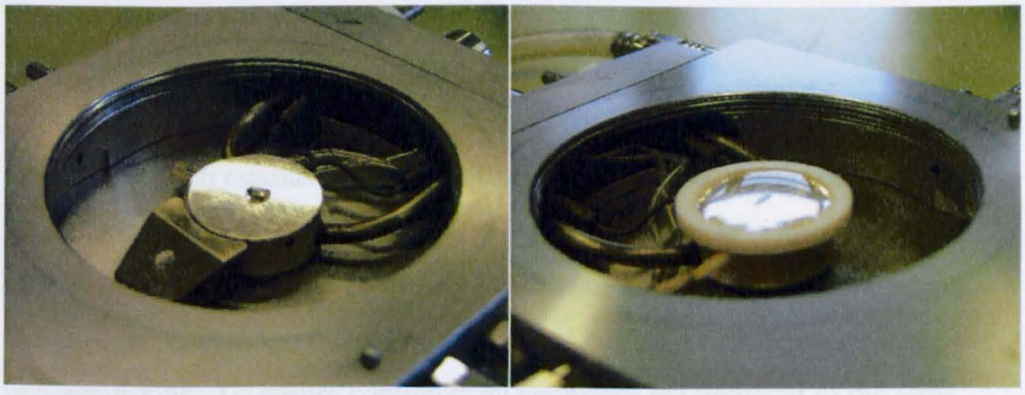

Figure 3.2 Close-up of sample stage Left: Water droplet placed on glass cover slip. Right: Fitted with PTFE ring to enable large water pool to be studied.

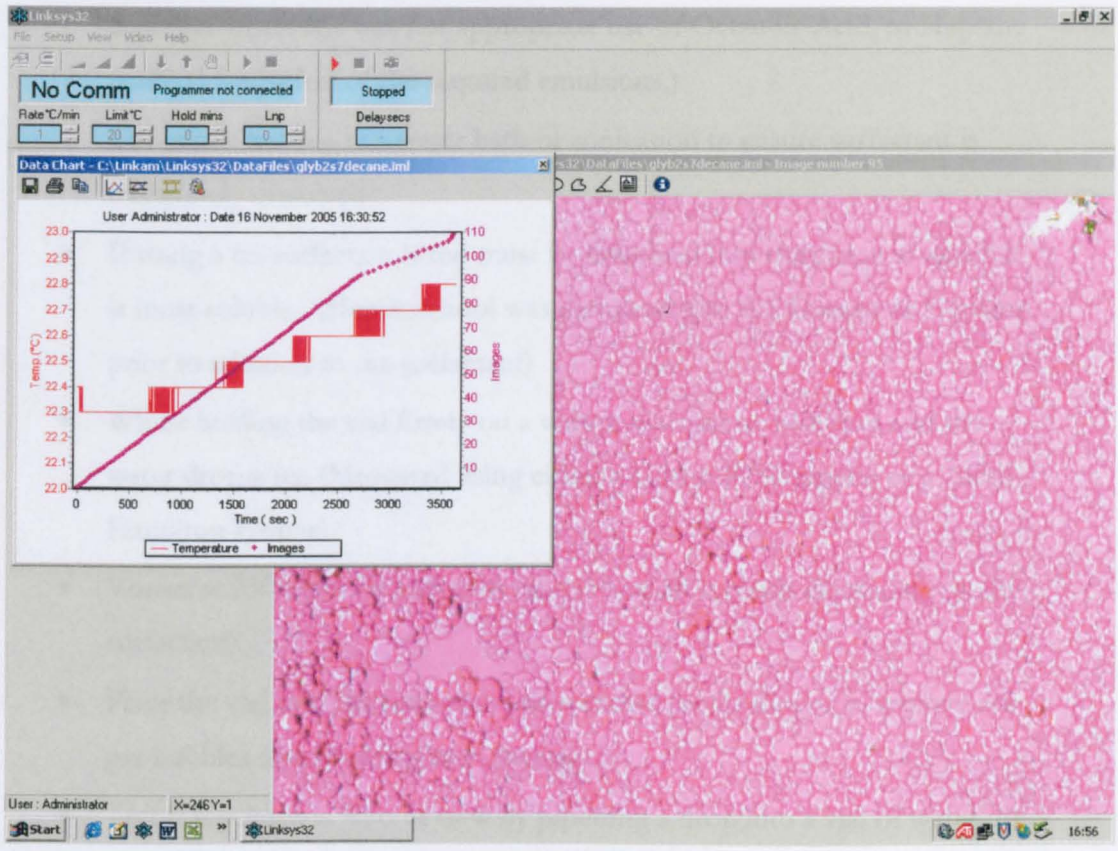

Figure 3.3 Linksys control software & analysis package, screenshot.

3.3.2 Emulsion mixing

Once it has been established whether the surfactant is more soluble in the oil phase or the aqueous phase a general procedure for mixing emulsions may be followed. Although order of mixing has little or no effect upon the resulting emulsion in most cases, the order of mixing is critical for the formation of nanoemulsions. To ensure continuity all emulsions are prepared to the same recipe.

- Decide which phase the surfactant is most soluble in. (In all cases mentioned here since w/o emulsions were being produced this was the oil phase)
- Weigh out the required amount of surfactant and oil into a vial. (To enable comparisons with previous work the oil of choice was Decane,

however when this was not appropriate use of Octanoic Acid, or Heptane enabled formation of the required emulsions.)

- Use gentle heating in a water bath or sonication to ensure surfactant is completely dissolved.
- If using a co-surfactant it too must be dissolved into the phase in which it is most soluble. (Heptacosanol was dissolved into the Decane or Heptane prior to addition to the surfactant)
- Whilst holding the vial firmly on a vortex machine at 1400rpm add the water drop wise. (Measured using either a Gilson P200 pipette or a 100µl Hamilton syringe)
- Vortex at 2500rpm for a chosen time (10 or 30 seconds depending on the surfactant)
- Place the vial into the sonicator and sonicate for 2 minutes to remove any gas bubbles dissolved whilst vortexing.
- Test if emulsion is w/o or o/w by pipetting a drop into a vial of water. If the droplet disperses it is an o/w emulsion, if it forms globules comparable to those seen in a lava lamp it is a w/o emulsion. If this test is insufficient, repeat, placing the droplet into a vial of the oil phase and observe its behaviour.
- Place a drop of the emulsion on a 22mm diameter BDH glass microscope slide and place the slide onto a Linkam coldstage.

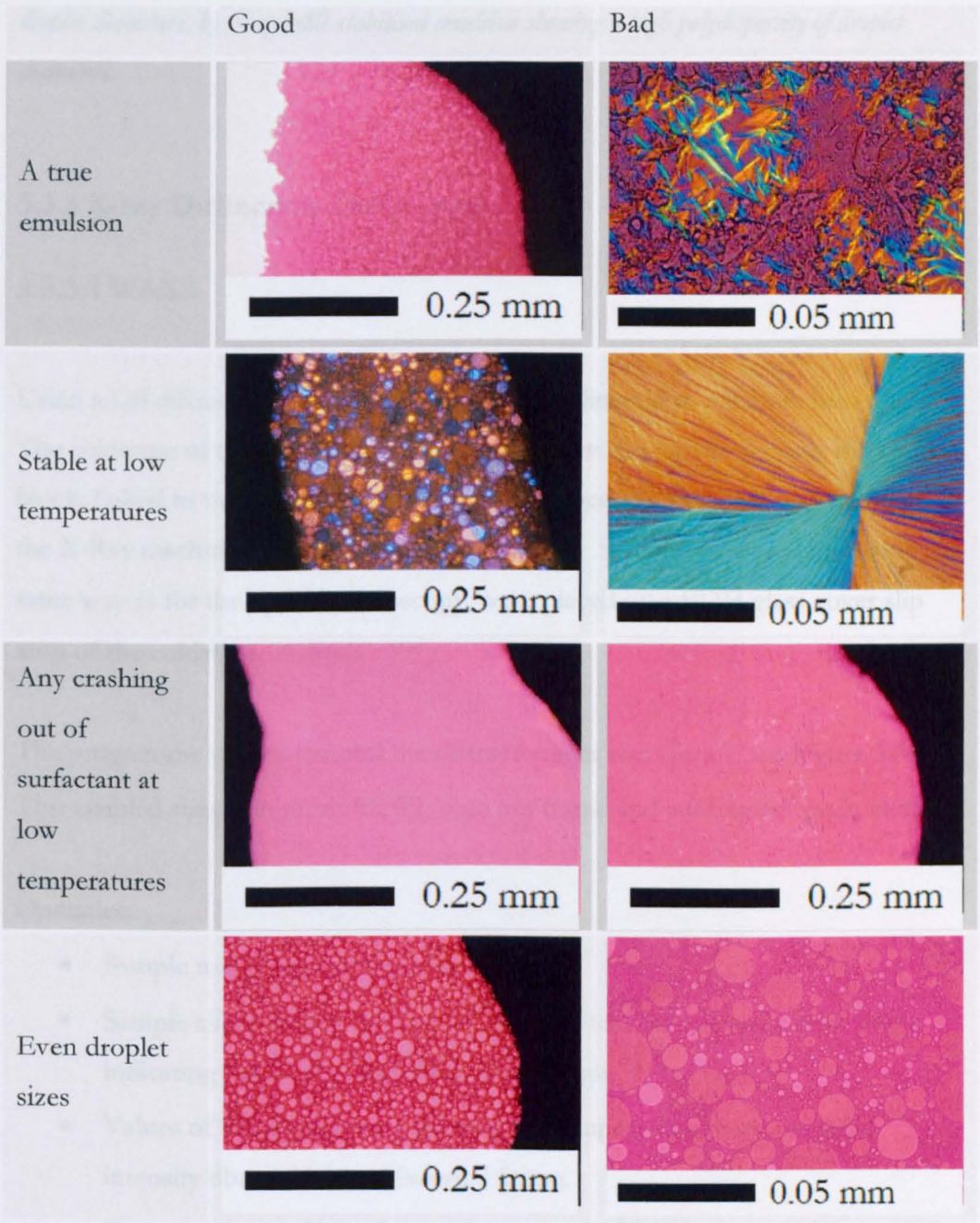

Figure 3.4. From top, left to right: a) A true white emulsion stabilised by the brij52 surfactant. b) A brij52 stabilised emulsion on cooling to 12 °C showing the birefringence texture characteristic of a lamellar liquid crystalline phase. c) A span65 stabilised water in decane emulsion, at ~ -25 °C, showing the crystalline ice confined within the droplets. d) Another lamellar liquid crystalline phase observed for water in hexane AOT stabilised emulsion on cooling. e) A microemulsion cooled to -30 °C showing no evidence of the heptacosanol cosurfactant crystallising into the oil phase. f) A similar microemulsion cooled to 12°C showing crystalline

heptacosanol in the oil phase. g) A span65 stabilised emulsion showing a low polydispersity of droplet diameters. h) A span80 stabilised emulsion showing a high polydispersity of droplet diameters.

3.3.3 X-ray Diffraction Techniques

3.3.3.1 WAXS

Using a D8 diffractometer, with a Mo source, collimated to a 0.3mm beam. The coldstage of the Linkam was removed from its casing leaving only the cooling block, linked to the control unit and liquid Nitrogen supply. This was clamped to the X-Ray machines' goniometer. See Figure 3.5. Samples prepared in exactly the same way as for the optical microscopy, were placed on a BDH glass cover slip atop of the coldstage.

The programme used to control the diffractometer was Gadds, see Figure 3.6. This enabled simple input of θ1, θ2, time per frame and subsequent peak analysis.

Operation

- Sample was placed on the Linkam
- Sample aligned using the manual goniometer controls and a laser beam indicating the focal point of the X-ray beam.
- Values of θ1, and θ2 were selected based upon maximum scattered intensity observed for a 60second frame.
- Temperature profile with a cooling rate of 4 °C/min from 20 °C to -40°C was chosen so that 15 second long frames corresponded to each °C that the sample was cooled through.
- The characteristic diffraction peaks of ice were observed when the emulsion droplets froze.

WAXS was also used in polymorph determination. Example scattering patterns obtained from the literature or calculated using Cerius2 given the molecular positions within the crystal (again obtained from the literature) showed the most intense peaks for a given polymorph. In these cases coupling to the Linkam was not required and so samples were placed on the goniometer either on the glass coverslip on which they had been grown or a silicon wafer. Peak positions were calculated using the Gadds software, calibrated using a polycrystalline corundum standard.

Figure 3.5 The Bruker D8 diffractometer, with Linkam cold stage & control unit in situ.

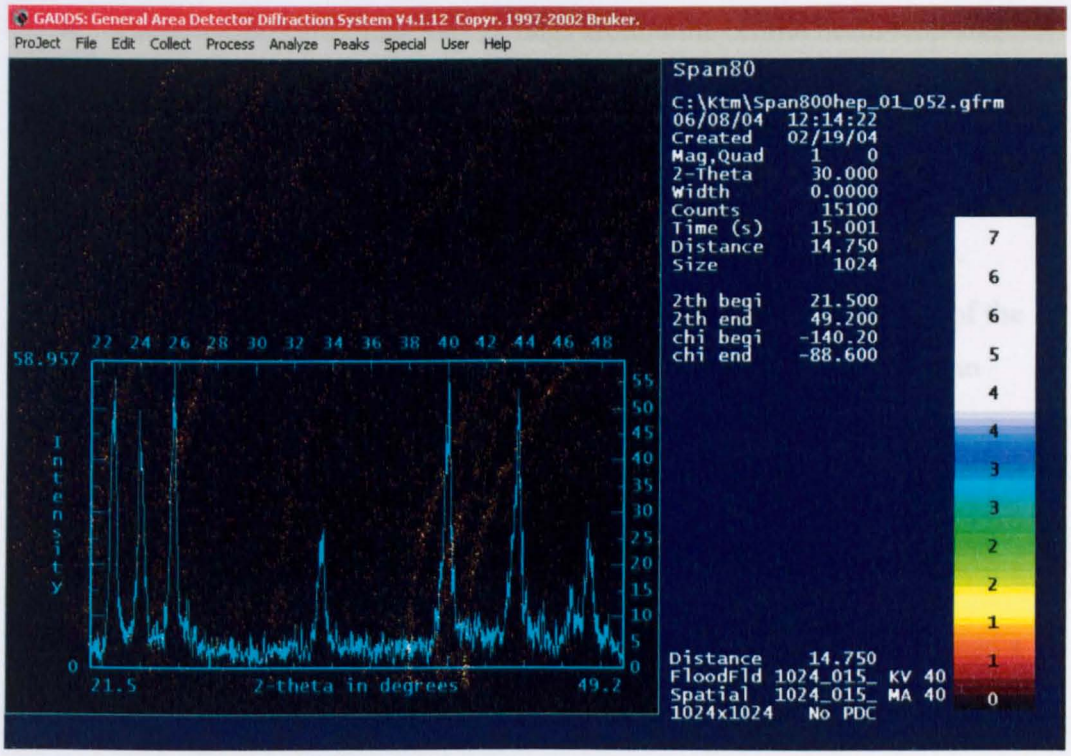

Figure 3.6 Typical diffraction pattern for the β polymorph of glycine, with peak integration analysis superimposed.

3.3.3.2 SAXS Nanostar

Small Angle X-ray Scattering (SAXS) is employed in the context of this thesis to obtain droplet sizes for microemulsion samples.

- The liquid sample is placed in a capillary and inserted into a holder inside the sample chamber. See Figure 3.8.
- The attenuator is dropped and the chamber evacuated.
- Using the Gadds program Radiography/Nanography is run, where the beam is fired at the sample and the sample stage is moved to determine the point of minimum transmission, hence the position of the capillary.
- Once the capillary position is accurately determined the sample stage is set to this position, the attenuator is raised and a diffraction pattern may be collected.

- The resulting pattern appears as rings around the central beam-stop and these rings correspond to a given angle of diffraction, hence a particle size. See Figure 3.9.
- This technique can be used for emulsions and vesicles only if there is a large difference in the scattering intensity of the oil and water phases.
- Analysis of the resulting pattern profile by integration over the area of the detector and subsequent application of the Guinier approximation can yield the radius of gyration for the smallest microemulsion droplets.
- By increasing the path length between sample and detector greater resolution at smaller scattering angles is possible. The longest path length of 106cm was used in all experiments here.
- The collection time was set at 2 hours as this proved sufficient to obtain a good signal to noise ratio.

Figure 3.7 The Bruker SAXS Nanostar instrument.

Figure 3.8 Left: the liquid capillary sample tube and Right: sample chamber.

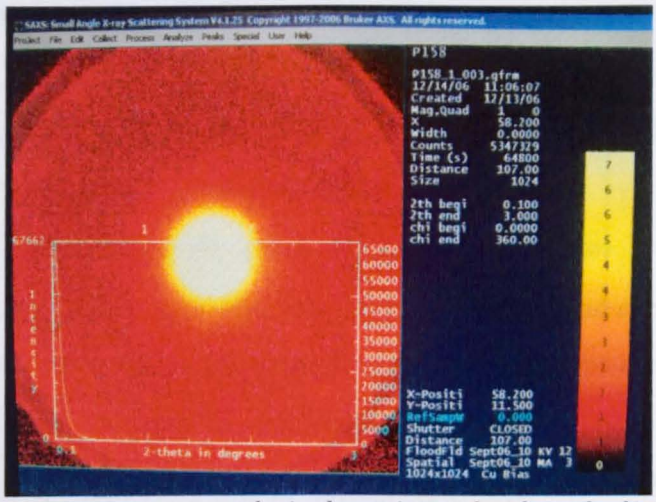

Figure 3.9 Typical diffraction patterns obtained superimposed with result of integration of that frame

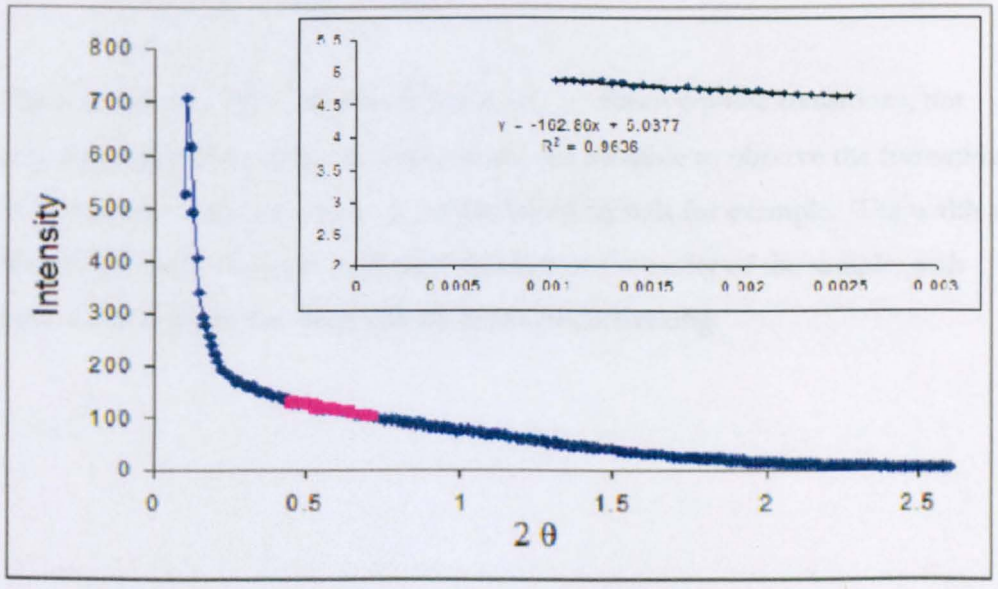

Figure 3.10 The Guinier (pink data points) region and inset data fitting using the Guinier approximation.

The Guinier region, that is very small-angle scattered X-rays can be used to determine the size of small spherical particles ~1-50 nm in diameter. To do this from the small region highlighted in Figure 3.10, where q*Rg ~1. Values of q^2 are plotted against ln Intensity. The gradient of this plot is related to the radius of gyration of the particles by a factor of $\sqrt{3}$[1,2].

3.3.4 Differential Scanning Calorimeter DSC

The instrument used was a Perkin Elmer Pyris1, see Figure 3.11, calibrated at 156°C with Indium and -87 °C with Cyclohexane.

- Sample was weighed into a 40µl Aluminium sample pan
- The change in voltage across the pan was measured and compared to a reference (empty pan) measuring the temperature of the sample within
- The machine recorded the heat input required to keep both pans at the same temperature when they were subjected to a cooling ramp
- ΔS and the specific heat capacity of the sample may be calculated from the value of ΔT ($T_{sample} - T_{reference}$)

The true value of DSC data lies in the ability to observe phase transitions, not only freezing and melting but it should also be possible to observe the formation of metastable states such as monotropic liquid crystals for example. The width of the dH/dT peak also gives a good indication of the purity of the sample, with pure substances giving sharp narrow peaks upon freezing.

Figure 3.11 The Perkin Elmer Pyris1 DSC

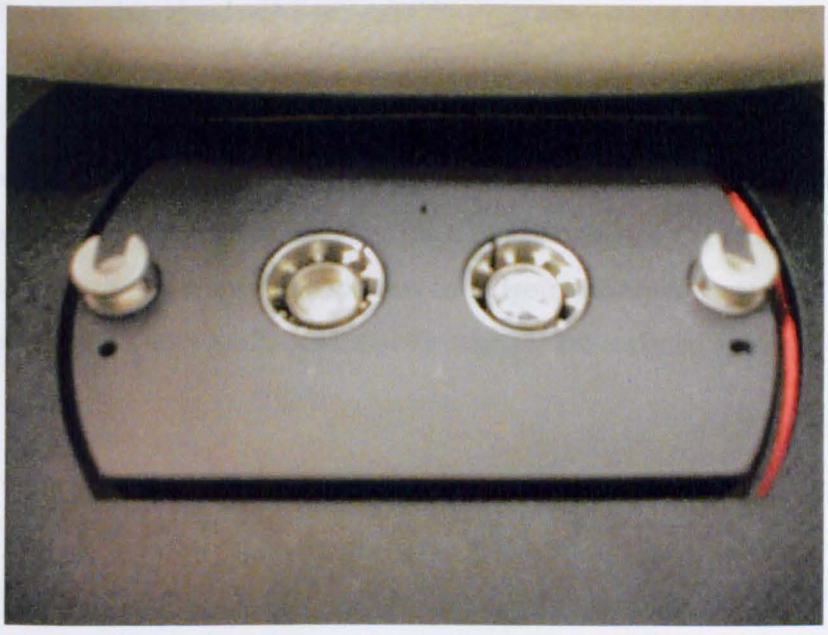

Figure 3.12 One of the reference 40 μl sample pans in the right hand furnace of the DSC

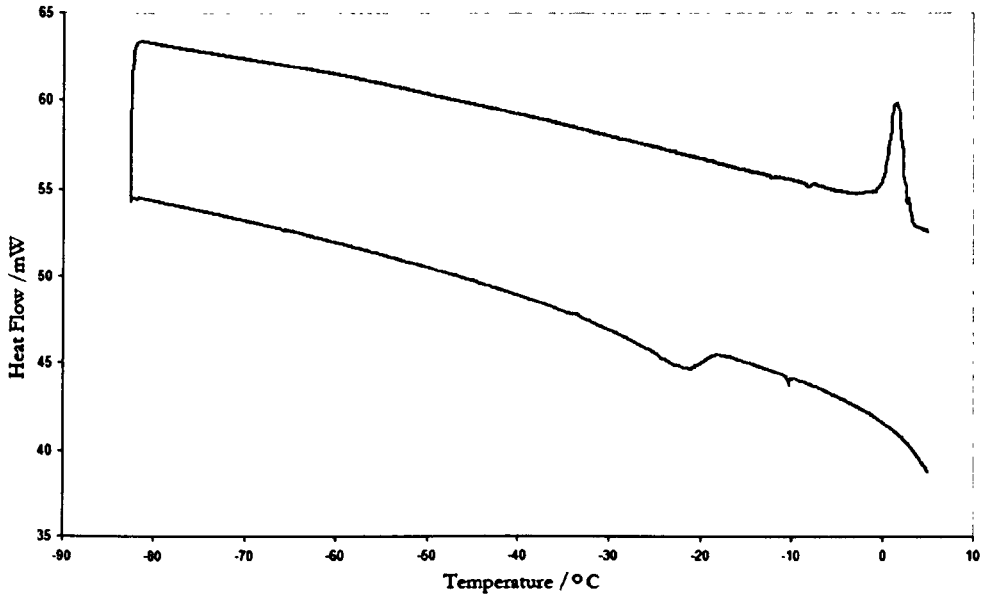

Figure 3.13 Typical DSC traces for ice crystallisation, sample under inspection is a w/o AOT stabilised microemulsion doped with heptacosanol.

Typical DSC traces as shown in Figure 3.12 can yield a lot of information about a sample when coupled with studies using polarising microscopy. Observed exotherms and endotherms in the DSC trace can be assigned to particular processes occurring within all the systems from lyotropic liquid crystal to microemulsions. Major peaks observed throughout are assigned as below.

Table 3.2 DSC peaks obtained during cooling of water in oil emulsions

Onset /° C	Peak /° C	Type of Peak	Attributed to
From -3 to -15	From -3 to -16	Sharp	Ice crystallisation induced by heptacosanol
From -18 to -28	From -20 to -39	Broad	Ice crystallisation, typically additive induced, dust or homogeneous at lowest temperatures
From -35 to -40	From -36 to -40	Large, Sharp	Decane crystallisation
From -96 to -100	From -96 to -100	Large, Sharp	Heptane crystallisation
From -40 to -80	From -40 to -80	Small	Water crystallisation, supercooled in extremely small droplet sizes

Table 3.3 DSC peaks obtained during heating of water in oil emulsions

Onset /° C	Peak /° C	Type of Peak	Attributed to
-96	-90	Large	Heptane melting
-39	-38	Large	Decane melting
-10	-10 to -8	Small, Broad	Bound / interfacial water melting
-1 to 2	0 to 2	Sharp	Water melting

3.3.5 Ultrasound Velocity Measurement UVM

The ultrasound velocity meter consists of a solid steel cylinder with an ultrasound source and sensor positioned at opposite sides of the cavity. See Figure 3.13. A temperature probe is positioned above the sensor to measure the temperature of the cells' contents. The base of the cylinder is made from a polymeric material to enable the use of a magnetic stirrer through the base. Constant stirring of the emulsion under inspection gives greater consistency of results and eliminates the

temperature gradient established when the vessel is cooled. Readings are recorded by a computer running the UVM1 software.

Operation:

- Place submersible magnetic stirrer beneath the UVM vessel in cooling bath (Haake Q60)
- De-gas the emulsion that is to be used by sonication.
- Place PTFE coated stirrer bar into vessel and pour in emulsion.
- Cooling of the emulsion is achieved by lowering the temperature of the bath.
- Measure and record the ultrasound velocity at 5 second intervals, (temperature readings are taken every 10 velocity measurements)
- Plot the ultrasound velocity as a function of temperature, observing a large discontinuity upon crystal formation.

Figure 3.13 UVM sample cell, the temperature probe can be seen protruding from cell wall.

The use of ultrasound to monitor crystallisation in emulsions is an established technique with much work carried out in the food science group at Leeds University[4-10]. The basic principle is that sound will travel faster through a solid than a liquid, so by monitoring the velocity of ultrasound passed through a sample an appreciable increase will be observed upon the formation of any crystalline

material. This principle seemed highly applicable to the study of ice crystal formation in w/o emulsions. Work carried out previously and published concerned the use of the technique for o/w emulsions, and upon further investigation the reasons for not studying w/o emulsions became apparent. For the w/o emulsions, the velocity measurements would jump randomly between a background level and that observed for a crystalline material, even when the sample was stable and held at room temperature. Initially it was suggested that this may be due to dissolved gas in the sample introduced upon agitating the mixture when emulsifying it. De-gassing the sample by vacuum or ultrasonic agitation did not remedy the problem, and so it was hypothesised that the erratic readings were due to the coalescence of the emulsion droplets.

After consultation with Prof. M Povey, he confirmed that his group had also encountered problems when trying to study w/o emulsions using ultrasound and the issue of coalescence was not isolated to a single surfactant system. He suggested the use of a siloxane based surfactant to remedy this problem. This remains an area for further investigation.

3.3.6 Langmuir Trough

In the course of these experiments a variety of troughs have been used. The experimental procedure for the Nima trough, shown in Figure 3.14, is outlined below[3]. These procedures used as good practice for any other trough used although the use of the microbalance was not possible with any of the smaller troughs. See Figure 3.15 for examples of other troughs used.

Operation:

- Thoroughly clean the trough using a lint free wipe soaked in chloroform, ensuring that no dust particles are contaminating the trough or the barriers.

- Fill the trough with ultra high quality (UHQ) water, so that the level of water stands proud of the trough sides, and the barriers are below the surface level.
- Using a vacuum gently sweep the surface clean holding the head of the suction tube parallel to the water surface to ensure surface contaminants are not forced into the bulk.
- If surface pressure measurements are to be taken, lower the Wilhelmy plate into the water, wait until fully soaked then gently raise it so that it is just held by the surface layer of water.
- Zero the balance and close the barriers, checking that the surface pressure does not alter by more than 0.03mN/m indicating that there are no contaminants on the surface.
- Open the barriers to the maximum then gently drop the monolayer solution onto the waters' surface, leaving for 3-5 minutes to allow the solvent to evaporate.
- Close the barriers to compress the monolayer to the 2D solid phase.
- Commence cooling the trough by pumping liquid coolant using the Haake Q60 re-circulating cooling bath.
- Observe if the ice is nucleated from the interface, Figure 2.15, and measure the temperature of the trough using a temperature probe, placed on the side of the section containing the water.

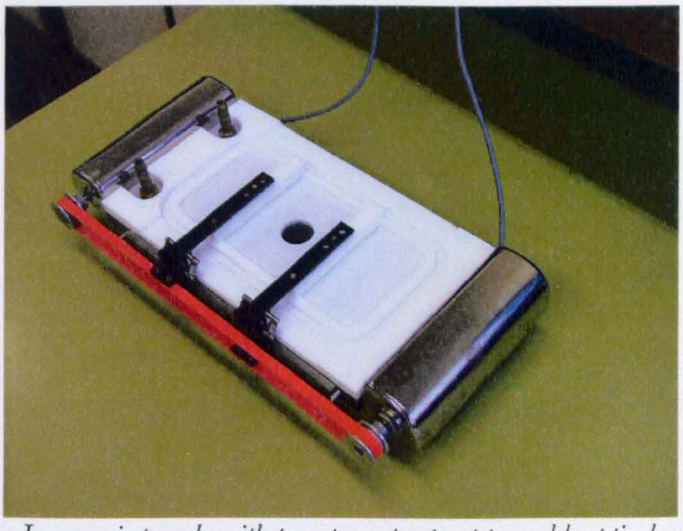

Figure 3.14 Nima Langmuir trough, with transparent cut-out to enable optical microscopy.

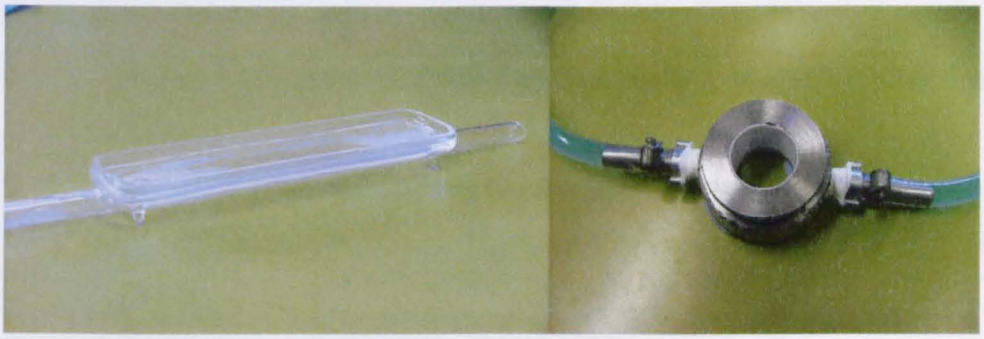

Figure 3.15 Left: Quartz glass trough, designed as shallow as possible to prevent thermal gradient over trough depth. Right: Aluminium PTFE-lined trough, cooled from sides and with glass base to enable microscopy

Figure 3.16 Water freezing from the surface, nucleated by heptacosanol, in quartz glass trough. 10× magnification, cross-polarisers and 539nm tint plate used to enhance image

References

1 Guinier, A.; Fournet, G. *Small Angle Scattering of X-rays*; Wiley; New York, 1955.

2 Glatter, O. *Small angle scattering and light scattering. In Neutron, X-ray and light scattering,* Lindner, P.; Zemb, Th.,Eds.;Elsevier Science: New York, 1991; pp33-60.

3 NimaTechnologyLtd, 'Operating Manual'.

4 McClements, D. J.; Povey, M. J. W. *Journal of Physics D-Applied Physics* 1989, ***22***, 38-47.

5 Dickinson, E.; Kruizenga, F. J.; Povey, M. J. W.; Vandermolen, M. *Colloids and Surfaces a-Physicochemical and Engineering Aspects* 1993, ***81***, 273-279.

6 Archer, G. P.; Kennedy, C. J.; Povey, M. J. W. *Cryo-Letters* 1996, ***17***, 391-396.

7 Dickinson, E.; Golding, M.; Povey, M. J. W. *Journal of Colloid and Interface Science* 1997, ***185***, 515-529.

8 Povey, M. J. W. *Contemporary Physics* 1998, ***39,*** 467-478.

9 Wang, Y. T.; Povey, M. J. W. *Colloids and Surfaces B-Biointerfaces* 1999, ***12***, 417-427.

10 Challis, R. E.; Povey, M. J. W.; Mather, M. L.; Holmes, A. K. *Reports on Progress in Physics* 2005, ***68***, 1541-1637.

11 Chow, R.; Blindt, R.; Chivers, R.; Povey, M. *Ultrasonics* 2005, 43, 227-230.

Chapter 4

4.1 Introduction

This chapter is intended to demonstrate the starting point of the work in this thesis. The simplest case to consider for emulsion crystallisation is simply crystallisation of the dispersed phase; water. The nucleation of ice has been an area of active research for over 60 years and remains extremely relevant today considering the amount of frozen goods society has come to rely upon. The nucleation of ice in emulsions provides and environment in which homogenous nucleation can be observed, and with the use of an interfacially active ice nucleator such as heptacosanol, the heterogeneous nucleation can be studied using the same system and conditions.

4.2 Literature Review

4.2.1 Ice Freezing In Supercooled Water

Crystallisation of ice from the metastable liquid state below the generally accepted freezing point of 0 °C has been the subject of much interest over the past century. Contrary to popular belief, if the nucleation of ice was purely homogeneous, supercooled water would not crystallise until -40 °C[2,3]. However due to the many impurities and heterogeneous nuclei present such low crystallisation temperatures are only observed under very controlled conditions. Early experiments to determine the rate of homogeneous nucleation of ice required extreme care to be taken when purifying the water for use. In particular, the methodology involved using triple distillation in dedicated glassware until resistivity measuring greater than 10 MΩ cm^{-1} was obtained.

Langham and Mason[1] established a simple relationship (equation 4.1) between the rate of nucleation and the degree of supercooling for homogeneous nucleation

(since the volume dependant theory proposed by Bigg[74] held only for heterogeneous nucleation).

$$\log_{10} I = 32.84 + \log_{10} T - \frac{U}{2.303} kT - \frac{1.1*10^{17}\sigma_{sl}^3}{L_f^2 T \ln^2 \frac{T_0}{T}} \quad (4.1)$$

Where I is the rate of production of nuclei per cm^3 per second, U is the activation energy for the self diffusion of a molecule in the liquid, k is the Boltzmann constant, σ_{sl} is the specific surface free energy of the liquid crystal interface L_f is the latent heat of fusion, T is the absolute temperature and T_0 is 273 K the thermodynamic freezing point.
The rate depends upon the free energy of the liquid-crystal interface, the activation energy of diffusion in the liquid and inversely upon the latent heat of fusion and degree of supercooling.

The specific volume of water has been measured to -40 °C by Schufle[2] with the highest density of water occurring at 4 °C. As the water is supercooled its density decreases, indicating a more open ice-like packing of the H_2O molecules[3]. Combined with the specific heat measurements of supercooled water showing greater intermolecular bonding as temperature decreases, Frenkel suggested the possibility of water clusters. Romussen and MacKenzie[3] calculated that the smallest cluster with an ice-like structure took the form of a 6 membered ring, but the extent of ice-likeness is small until the water is highly supercooled.

Diffuse interface analysis modelling was unable to predict a homogeneous mechanism for ice nucleation, showing rather, a bulk heterogeneous mechanism instead. This was due to the model being unable to account for the structural changes that occur in liquid water when it is supercooled[4].

When studying the nucleation of ice in confined geometry, or on a substrate the substrate can introduce defects in the ice crystal, or even growth of the cubic form of ice, instead of the usual hexagonal polymorph[5]. When ice was grown in

aluminosilicate pores 40 Å in diameter, only the cubic form was observed by neutron diffraction. Increasing the pore size to 200 Å created mainly the cubic form, but some hexagonal, and increasing again to 500 Å pores in a sol-gel formed only hexagonal ice[6].

The effect of surface roughness was also significant when considering a scale of less than 500 Å . At this level, several H_2O molecules can be anchored to the surface in a geometry incompatible with crystalline ice, thereby introducing defects into the crystal structure. A smooth surface will enable the H_2O molecules to move and rearrange into the most favourable geometry on freezing.[5] It is therefore desirable to carry out nucleation studies with the water placed on (or more importantly) in a hydrophobic medium, thereby eliminating any surface interactions.

4.2.2 Ice Nucleation In Emulsions

The freezing of water in emulsions enables a greater degree of supercooling. Statistically any dust or heterogeneous nucleating particles are dispersed into only a few droplets, enabling the rest to experience homogeneous nucleation, provided that the surfactant used does not promote ice crystallisation itself.
Slow rates of crystallisation are observed due to the slow diffusion rates and non coalescence of droplets, preventing the transfer of ice nuclei from one water pool to another.

Hence detailed studies of the rates of ice nucleation and crystallisation are possible when considering freezing of emulsions due to the ability of obtaining purely homogeneous nucleation. Previous methods[7] using a cloud chamber to mimic atmospheric nucleation are subject to dust particles and other heterogeneous nuclei contaminating the water droplets[8].

The rate of crystallisation is found to be related to the droplet size in the emulsions. As expected a range of droplet sizes are present within an emulsion,

hence a range of freezing temperatures are observed[9]. If the nucleation is induced at the interface, nucleation is affected not by the volume of the droplet but by the extent of the surface[8].

Pre-cooling of w/o emulsions increases the rate of homogeneous nucleation, with pre-cooling to -30 °C resulting in the water droplets crystallising at the fastest rate[10]. This is due to a memory effect where the water retains some of its ordered pre-critical nuclei short range order, and as such there already results some degree of water clustering within the emulsion.

The rate of nucleation in emulsion droplets was found to be greater than that predicted by Mason[1], but may be accounted for by the temperature dependant interfacial free energy between water and ice. It was argued that an alternate nucleation mechanism based upon forming the critical nucleus by aggregation of ordered sub clusters, rather than stepwise addition of single H_2O molecules, could also account for the high rate of nucleation in ordered liquids[8].

4.2.3 Ice Nucleation Using Long Chain Alcohols

The ice nucleating ability of long chain alcohols has been well documented[11-21]. The effect is only observed for alcohols with a carbon chain length greater than 16 for the air-water interface, or greater than 22 for the oil-water interface[11]. Straight chain alcohols form a monolayer at the interface with the OH groups pointing into the water. The orientation of the OH groups is such that they provide an epitaxial match for the ab lattice of hexagonal ice. X-ray studies have shown[12, 21] that the alcohol monolayer 'freezes' into a 2D crystalline domain at temperatures below 9 °C. Epitaxial matching for the crystalline structure of ice is a compromise between the long range order induced by the hydrophobic chains and the tilt angle at which they stack at the interface. It was found that the hydrocarbon chains are all in the trans-conformation.

An intriguing consequence of the stacking that was observed was the 'odd-even' effect. Alcohols with an odd number of carbon atoms in their chain were far more effective ice nucleators than the adjacent even numbered chain alcohols. It was proposed that this effect resulted from different molecular packing, giving a different orientation of the OH groups for the odd numbered chains compared to the even ones[18]. To investigate the epitaxial match further, a fluorocarbon surfactant was used as a matrix to host segregated domains of the alcohol and the decrease in nucleating efficiency was measured. The results showed that the nucleating efficiency was proportional to the number of nucleating domains, and furthermore that the area of lattice match was comparable to the size of the critical nucleus for ice, approximately 25-30Å[16, 22]. The domain size match was later confirmed using FTIR methods and clearly showed the aggregates, along with the increased ice nucleating efficiency, however some conflicting results from grazing angle X-ray diffraction showed that the alcohols did not separate into domains, rather that they completely mixed with the co-surfactant.

4.2.4 W/O Emulsions Using Non-Ionic Surfactants

Non-ionic surfactants such as the Brij series can be used to produce microemulsions, nanoemulsions and emulsions of either o/w or w/o type. Formation of w/o type emulsions is usually achieved by heating the mixture above the phase inversion temperature,[23] resulting in water droplet sizes between 0.5-0.8μm, or smaller if the mixture is agitated whilst being heated. Lowering of the phase inversion temperature is achieved by using a Brij surfactant with 4 ethylene-oxide groups and a long carbon chain, while using a shorter chain length hydrocarbon as the oil phase.[24] The order of mixing for the Brij30 surfactant resulting in nanoemulsion formation is critical to the size of dispersed phase droplets[25], yet order of mixing has no effect if increased surfactant concentrations are used as in this case a thermodynamically–stable microemulsion forms.

Previous studies on the supercooling of water in w/o emulsions employed the Span65 surfactant, sorbitan tristearate[3] and suggested that these emulsions were

stable at low temperatures. Since the results were obtained by densiometry and dilatometry, the observation of any of the liquid crystalline phases or phase separation that was observed in my studies would not have been observed. The result of this study clearly showed the homogeneous nucleation of ice occurring at ~39 °C.

4.2.5 Effect Of Alcohols On Emulsion Stability

Alcohols can be of sufficient amphiphilic character to act as co-solvents in emulsions, sitting between the oil rich and water rich phases in the interfacial layer. This results in a lowering of the interfacial tension between the water and oil[26]. The chain length of the alcohol will determine its behaviour at the interface. Some short chain alcohols have abnormal pressure-concentration behaviour as a function of temperature, possibly a consequence of the ordering of water by the OH headgroups[27]. For the oil/Brij/alcohol/water system the amount of water solubilised decreases with increasing alcohol chain length, and the % area of the phase diagram for the w/o emulsion decreases.

A favourable effect of the addition of alcohols to an emulsion is the destabilisation of the liquid crystalline phase.[28] In the liquid crystalline system it has been observed that the alcohols at the interface will twist from the trans orientation at the head group end, to adopt the most favourable packing orientation[29]. Addition of a short chain alcohol such as ethanol, or isopropanol to the Brij52/coconut oil/water system resulted in stabilisation of the w/o microemulsion phase[30].

4.2.6 Templating Crystal Nucleation

Pseudo 2D 'crystalline' monolayers assembled on the surface of water can provide a planar arrangement complementary with the 3D crystal it is nucleating. There

are many applications for this technique of templating crystal growth, including control of polymorphs, resolution of enantiomers, and biomimicry[15].

Nucleation of amino acids such as glycine[31] that crystallise in an enantiotropic space group may be controlled in that the face of the crystal nucleated must complement that of the monolayer nucleating it. That is, if a layer of D-Leucine forms the monolayer, the glycine will be nucleated from the (010) face. If L-Leucine is used glycine is nucleated from the (0 0) face. α-amino acids acting as surfactants have also been shown to nucleate NaCl crystals, with the face nucleated depending upon the headgroup charge of the monolayer[32]. Induced nucleation of $CaCO_3$ has also been demonstrated, with each of the three polymorphs of calcium carbonate, i.e. calcite, aragonite and vaterite, induced by different reaction conditions[33-35].

Generation of microcrystalline materials in emulsions has been documented for several examples[49-73]. Simply mixing two emulsions, one containing an inorganic salt, the other containing a strong reducing agent is a straightforward method to achieving metallic nanoparticles[36-38]. Improved crystallinity was obtained by using an anionic surfactant with the corresponding counter-ion being that of the metal to be crystallised[22, 39].

4.3 Context

The work detailed in this chapter was aimed at firstly determining the ice nucleating ability of a long chain alcohol, heptacosanol, when in a well-characterised monolayer state at the planar air-water and oil-water interface. Then identifying the best surfactant-based system to use in extending these studies to ice crystallisation in emulsions and microemulsions.

4.3.1 Ice Crystallisation Under Well-Defined Monolayers

In work carried out by Lahav et al[13], a 10μl droplet of water was simply placed onto a glass slide then a drop of a long chain alcohol in chloroform was dropped upon the surface of the water droplet and the system then cooled to find the ice freezing temperature. Early tests of this method, using heptacosanol ($C_{27}H_{55}OH$), soon showed that this was an extremely uncontrolled manner of obtaining a monolayer coating of the heptacosanol, with most of the chloroform solution running off the droplet. It was therefore one of my aims to repeat this experiment under a well-characterised monolayer held in a Langmuir trough. Using a Wilhelmy plate microbalance, and PTFE barriers, the surface pressure and surface area could be measured; hence the surface area per molecule could be determined accurately.

4.3.2 Ice Crystallisation In A W/O Emulsion, Microemulsion & Nanoemulsion.

The study of the ice nucleating ability of heptacosanol at a curved interface is also one of the main aims of this work. In attempting to quantify the effect of surface curvature on formation of the critical nucleus, w/o emulsions/microemulsions were an obvious choice for study. The nucleating agent, heptacosanol, resides as a cosurfactant at the oil/water interface and the water droplet radius can be altered by changing the composition of the emulsion/ microemulsion mixture. For emulsions, measurement of the droplet radius can be carried out by optical microscopy and hence the surface curvature calculated.

Formation of a microemulsion requires a large amount of surfactant and due to the small droplet size; the droplets have a large surface area to volume ratio. Since conditions close to the interface differ from that of the bulk solution, there may be a more pronounced effect of the nucleating ability of the heptacosanol. Since microemulsions have droplet sizes smaller than 50 nm, they cannot be observed optically. Hence differential scanning calorimetric analysis is the method of choice for measurements of freezing temperatures in microemulsions.

Nanoemulsions form the intermediate size between the emulsion and the microemulsion. They are only kinetically stable, but require much lower surfactant concentrations than microemulsions for their formation. These systems, along with microemulsions, form the area of greatest scientific interest, not only with respect to the effect of surface curvature upon ice nucleation, but as micro reactors for the crystallisation of many other substances.

4.3.3 Comparison Of Crystallisation Temperatures & Curvature

The crucial aim of this chapter is to compare the ice Crystallisation temperatures of all of these systems and in doing so, determine if the epitaxial lattice match observed at the planar interface will be enhanced or reduced by increasing interfacial curvature. If a curvature-dependent effect is found, it shows that the additive is effectively integrated into the surfactant interfacial layer. If no effect is found, the additive may reside in segregated domains, and it is the presence of these domains not the droplet curvature that will have a large effect on the freezing temperature. The surfactant mixtures chosen not only provides a means of stabilising an emulsion but may also produce an environment at the interface chemically similar to that which the heptacosanol would form itself, and in doing so increases the solubility and the interfacial activity of the nucleating additive.

4.4 Experimental Details & Methodology

4.5 Results & Discussion

4.5.1 Ice Crystallisation Under Monolayers At The Air-Water Interface

The attractively simplistic approach of dropping 10μl of water onto the hydrophobic glass cover slip placed on the Linkam coldstage, and then spreading a consistent amount of alcohol onto the water surface proved problematic. On gently dripping 1-10μl of the alcohol of interest dissolved in chloroform onto the

water droplet, the chloroform solution slipped off the water and onto the glass slide, due to the surface curvature of the water droplet. Consequently, this resulted in an un-characterisable monolayer state. Even in the face of these difficulties it could clearly be seen using optical microscopy that the alcohols heptacosanol, eicosanol and nonadecanol were efficiently nucleating ice, and that the effect was surface specific. The elevated freezing points were not as high as expected compared to those of Lahav et al.[13] in particular the highest temperature observed for ice crystallisation was -4 °C, where the published work cites -1.9 °C for heptacosanol. However, the odd-even effect and the effects of chain length were clearly demonstrated see Table 4.1 and Figure 4.1.

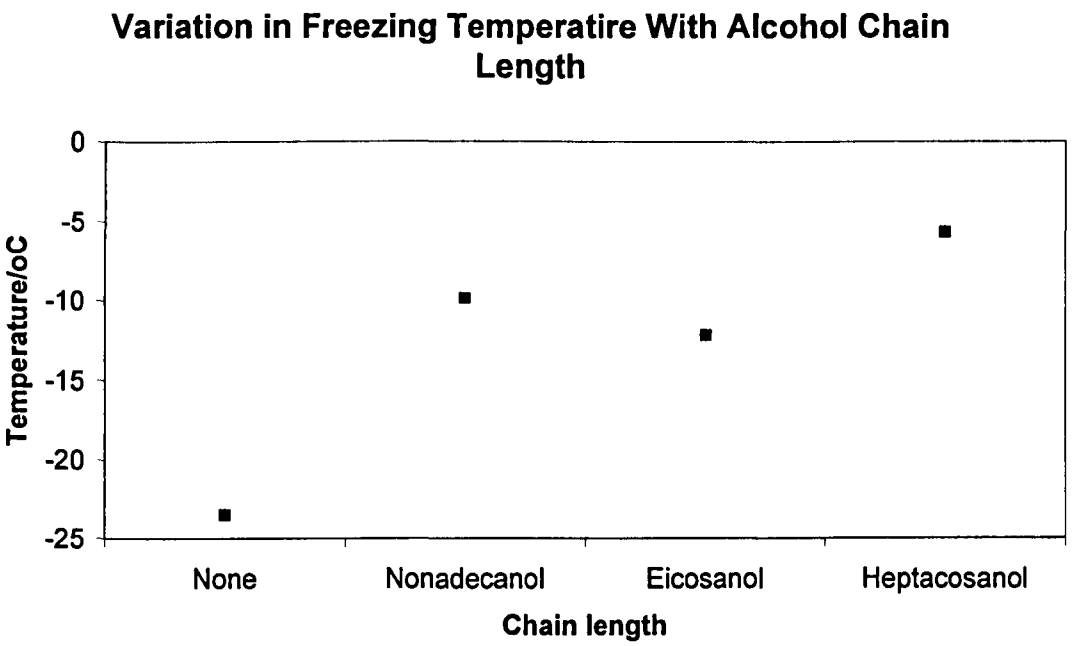

Figure 4.1 Showing the variation in ice freezing temperature with added surface monolayer

Table 4.1 Experimental results from freezing of water using the method of Lahav et al[13]

Alcohol	Concentration /moldm^{-3}	Amount	Freezing Temperature /°C
None			-23.5
Nonadecanol	1.8E-2	5ul	-9
Nonadecanol	1.8E-2	5ul	-11
Nonadecanol	1.8E-2	5ul	-9.5
Eicosanol	1.7E-2	5ul	-12.7
Eicosanol	1.7E-2	5ul	-11.5
Heptacosanol	1.0E-3	5ul	-6.5
Heptacosanol	1.0E-3	5ul	-7.5
Heptacosanol	1.0E-3	5ul	-7.5
Heptacosanol	1.0E-3	2.5ul	-5.5
Heptacosanol	1.0E-3	1ul	-2.9
Heptacosanol	5.0E-3	5ul	-5
Heptacosanol	5.0E-3	2ul	-4.8
Heptacosanol	1.0E-3	2ul	-4.8

In order to better control and understand the state of the monolayer that was so effectively nucleating the ice, it seemed logical to study the nucleating properties of an alcohol monolayer in the 2D solid state. This would enable a measurement of the area per molecule and also observation of the ice nucleating properties of the alcohols over a large planar interface.

Again this simple goal was troublesome, the problems beginning to surface when checking the freezing temperature of ultra high quality (UHQ) water in the Nima PTFE Langmuir trough. The trough was cooled by passing a liquid coolant through an aluminium block to which the PTFE trough was fused. Should the trough be cooled too much then the PTFE (which has a very large thermal expansion coefficient) may have broken away form the aluminium base plate. Also since the cooling was applied from the bottom of the trough, the temperature gradient formed over the depth of the water in the trough was almost 10 °C. This temperature gradient, and the scratches in the PTFE itself, resulted in

the water freezing from the bottom to the top, regardless of the nucleating ability of any monolayer spread onto its surface. It is believed that the presence of scratches on the PTFE trough bottom was the major contributing factor to the heterogeneous nucleation of ice at these sites.

Eventually two solutions to the problem were devised:
Placing of a PTFE ring around the glass slide on the Linkam cold-stage, so that a puddle of water with a more planar surface could be studied under the microscope, see Figure 4.2.
Fabrication of a small trough entirely out of quartz glass (measuring 13x2x0.5cm) as it was known that glass did not act as a nucleating agent for the water and its transparency enabled it to be placed under the transmission microscope, see Figure 4.2.

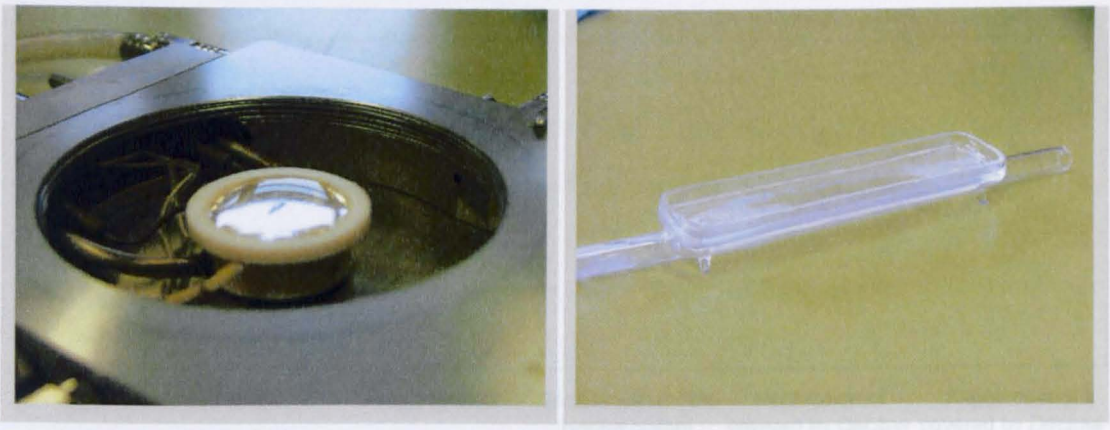

Figure 4.2 Left Water pool on Linkam coldstage, held by PTFE ring, Right Quartz glass trough used for planar nucleation studies.

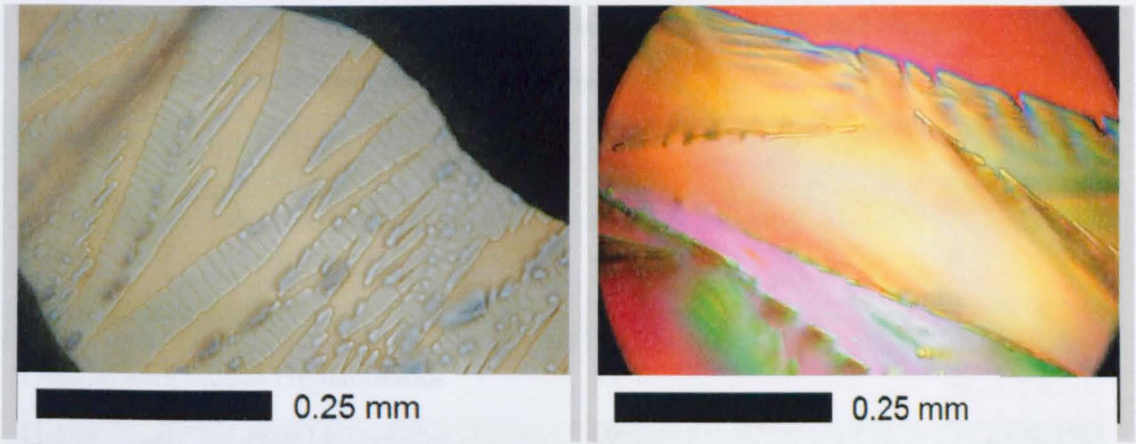

Figure 4.3 Left Ice freezing under heptacosanol monolayer on water droplet, Right Ice freezing under heptacosanol and decane layer in quartz glass trough.

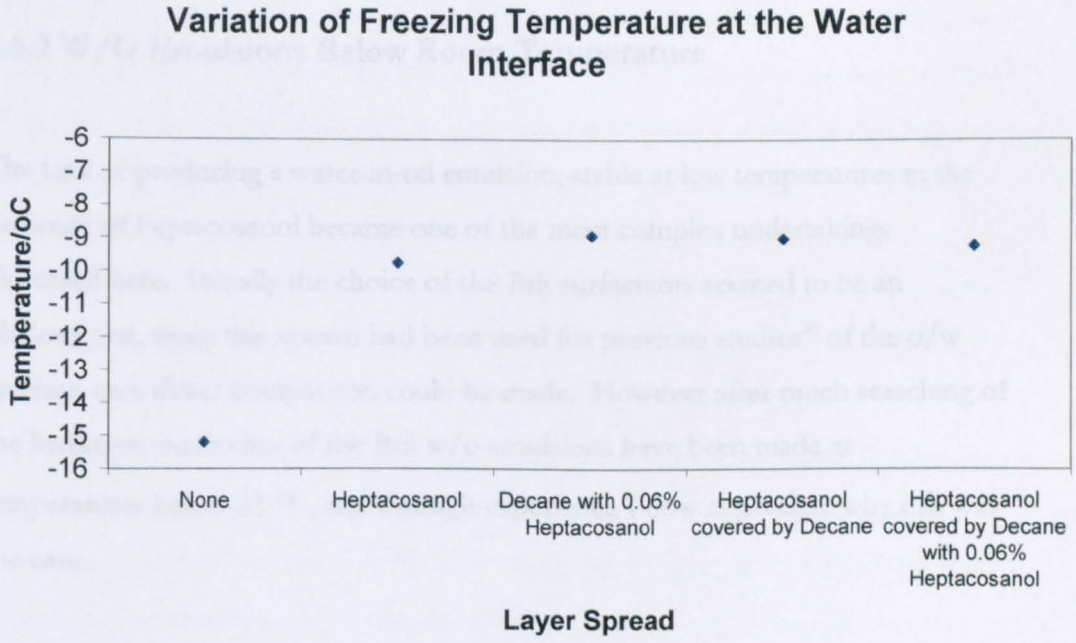

Figure 4.4 Shows the observed change in freezing temperature of water with addition of nucleating agent, heptacosanol.

The data shown in Figure 4.4 and in Table 4.2 shows little or no effect due to the addition of an oil phase, indicating that the heptacosanol will behave as a surfactant molecule and as such will be present in the interfacial region in sufficient concentration to nucleate the ice crystals at elevated temperatures compared to the homogeneous case.

Table 4.2 shows the variation of the mean freezing point from three repeats, with the type of interfacial region that is presented in the graph in Figure 4.4.

Layer Spread	Mean Freezing Temperature/°C	Standard Deviation
None	-15	4
Heptacosanol	-9.8	0.1
Decane with 0.06% Heptacosanol	-9	2
Heptacosanol covered by Decane	-9	2
Heptacosanol covered by Decane (0.06% Heptacosanol)	-9.2	0.4

4.5.2 W/O Emulsions Below Room Temperature

The task of producing a water-in-oil emulsion, stable at low temperatures in the presence of heptacosanol became one of the most complex undertakings discussed here. Initially the choice of the Brij surfactants seemed to be an obvious one, since this system had been used for previous studies[30] of the o/w systems, so a direct comparison could be made. However after much searching of the literature, no studies of the Brij w/o emulsions have been made at temperatures below 25 °C, and through experience I now appreciate why this was the case.

The phase inversion from the w/o emulsions to the o/w is due to a decrease in the Brij surfactants lipophilicity with decreasing temperature. Use of a short chain alcohol co-surfactant was reported to increase the stability of the w/o emulsions[29]. However the use of a longer chain alcohol decreased the % area of the phase diagram in which the w/o emulsion was found. The low temperatures required for supercooling the water combined with the destabilising of the w/o emulsion by the heptacosanol prevented any of the systems using the Brij surfactants to remain stable enough for nucleation studies.

More surprising was the formation of the liquid crystalline phases upon cooling the emulsions, particularly at relatively low surfactant concentrations of 3-15% wt.

4.5.3 Lamellar Liquid Crystalline Phases

Formation of the lamellar liquid crystalline phases observed for the Brij surfactant emulsions at temperatures below 25 °C was not entirely unexpected, as the surfactants lipophilicity decreased and the system phase inverted from a w/o to an o/w emulsion. However it is surprising that the liquid crystals formed and remained stable over such a low surfactant concentration range. The emulsions studied typically contained between 3-15% wt surfactant, whereas the formation of lamellar liquid crystals usually requires a much higher surfactant concentration of 30% or more. Moreover, the use of DSC to try to observe the phase transition to this liquid crystalline phase failed, yet optical microscopy clearly showed the correct extinction effects characteristic of a liquid crystalline phase, when using the cross polarisers, see Figure 4.5. Further DSC experiments showed the possibility of a liquid crystalline transition occurring at ~24 °C, much higher than that observed in optical microscopy (~10-17 °C). Since this transition is so close to room temperature one would have expected it to have been reported previously, a possible reason for this discrepancy between techniques may be attributed to the different containers that the emulsion is held in for the different experiments, or simply that the DSC was not sensitive enough to record the small energy change associated with this transition.

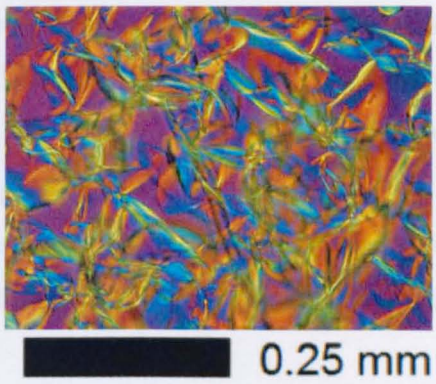

Figure 5.5 Lamellar lyotropic liquid crystalline phase observed at 17 °C. Viewed through crossed polarisers and red tint plate.

Preliminary ice freezing experiments were conducted on these lamellar lyotropic liquid crystal phases to determine whether this would be an interesting area of research to conduct alongside the proposed emulsion and microemulsion studies. Unfortunately, though, the ice nucleating ability of the alcohol in the lamellar lyotropic liquid phase appeared greatly reduced, see Figure 4.6, with samples containing 0.1% wt in the oil fraction increasing the freezing point of the water by just 2 °C. This disappointing result indicated that perhaps the alcohol was not residing at the interface in the lamellar liquid crystalline systems, or perhaps a greater concentration was required before an appreciable effect is observed. It may also be postulated that the alcohol is unable to form the segregated crystalline domains large enough for the formation of the critical nucleus where the lattice match between alcohol and ice is sufficient to induce crystallisation.

Further freezing experiments and studies using small angle X-ray scattering (SAXS) with a cooling stage attached to the sample chamber may yield some answers as to the state of the water between the lamellae, and the lamellar spacing of these liquid crystalline samples. However, this remains an area for future research, since it was not possible to carry out sub-ambient experiments on the SAXS Nanostar as the cooling accessory was not available at this time.

The freezing points shown in Figure 4.6 for the KTLC series were obtained by DSC analysis. There was no evidence of the phase change to the liquid crystalline state evident, perhaps indicating that the process is too gradual to observe clearly. It seems from the results shown that in the presence of heptacosanol a smaller % wt of water achieves the greatest nucleating effects, while in the absence of nucleating agent the reverse seems true, with the greater volume of water giving the highest nucleation temperature. Further studies are required though, to verify this.

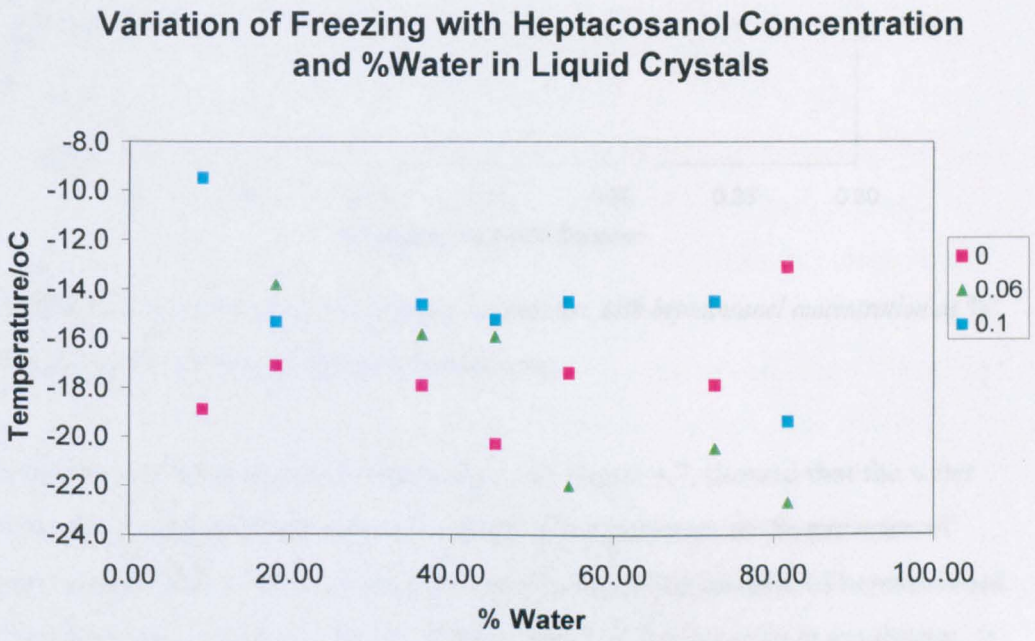

Figure 4.6 preliminary experiments showing the variation in the freezing point of water in lamellar liquid crystalline systems with varying water content and heptacosanol concentration. O (pink squares) means no added heptacosanol, 0.06 (triangles) is 0.06% wt heptacosanol in the oil phase and 0.1(blue squares) is 0.1% wt heptacosanol in the oil phase, respectively.

4.5.4 Stable W/O Emulsions

Formation of a stable w/o emulsion required the use of a different family of non-ionic surfactants. The sorbitan esters (Span 65 and 80) were of sufficiently low HLB value to generate w/o emulsions. Initially Span 65 was used but the emulsions produced had a wide range of water droplet sizes and so Span 80 was

adopted instead, producing emulsions with droplet sizes ranging from 20 μm to 80 μm.

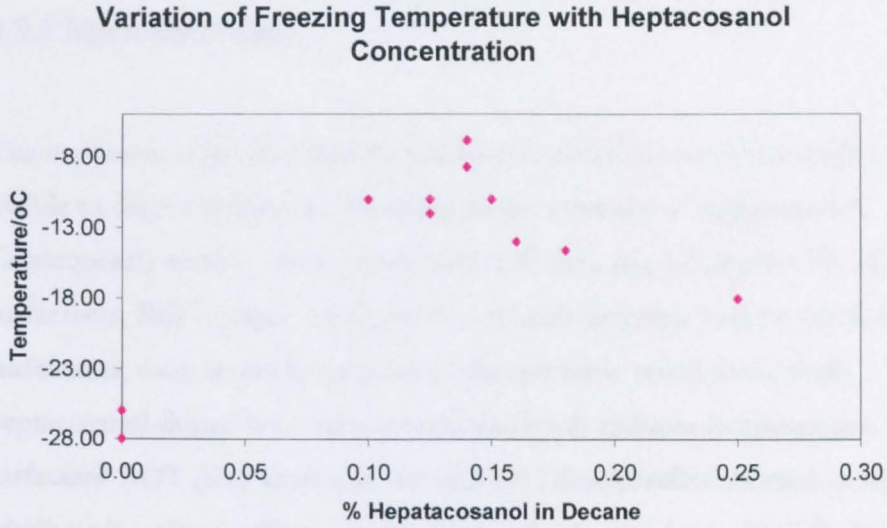

Figure 4.7 shows the variation in ice freezing temperature with heptacosanol concentration as % wt of the oil phase for the Span80 stabilised emulsions.

Results obtained from optical microscopy, see Figure 4.7, showed that the water in the emulsion droplets froze over a range of temperatures in the presence of heptacosanol. This may be a consequence of a broad distribution of heptacosanol in the droplets, combined with the polydispersity of droplet sizes in emulsions. It may also be that the partitioning of the heptacosanol in the interfacial monolayer is such that it is unable to form aggregated domains large enough to nucleate ice effectively in some instances.

Although the Span surfactants were capable of producing normal white emulsions, the formation of blue nanoemulsions, or transparent microemulsions remained impossible at low temperatures, and in the presence of heptacosanol.

Eventually the use of the anionic surfactant AOT was employed to achieve the formation of a stable w/o microemulsion. Despite initial concerns over the effect of the Na^+ counterion and the charged head group of the surfactant, these seemed to have no effect upon the nucleation temperature, indicating that any effects of

the presence of charged species were small compared to the large effects of the heptacosanol nucleating the ice crystallisation.

4.5.5 Microemulsions

The non-ionic surfactant Span85 that was used for the emulsion studies was unable to form stable microemulsions in the presence of heptacosanol. Consequently various other surfactants, including Brij 52 doped with alcohol co-surfactants, Brij 72, Span 65, Span60, and other Brij type polyoxyethylene surfactants, were tested to determine whether these could form stable heptacosanol-doped w/o microemulsions at sub ambient temperatures. The ionic surfactant AOT (also known as Aerosol-OT, dioctyl sulfosuccinate or bis (2-ethylhexyl) sodium sulfosuccinate) was finally chosen due to its well characterised behaviour when forming w/o microemulsions. Indeed the droplet radius size/nm can be calculated from the simple ratio of water to surfactant[41-48] by 0.15 $[H_2O]$/ [AOT], assuming that the thickness of the AOT plus bound water layer is 1.5 nm.

Initial experiments were conducted to determine the amount of heptacosanol required to produce efficient ice nucleation, see Figure 4.8. Although the AOT microemulsions show that ice nucleation occurs at higher temperatures in the presence of heptacosanol optical microscopy shows that the solubility of the alcohol is reduced when the emulsion is cooled, in some cases resulting in the precipitation of crystals of heptacosanol from the emulsion, see figure3.9. Hence great care was taken to ensure that the heptacosanol concentration subsequently used would not result in heptacosanol crystallisation prior to the ice freezing. A very small heptacosanol concentration of 0.10% wt in the oil phase satisfied this criterion but still provided good ice nucleation promotion.

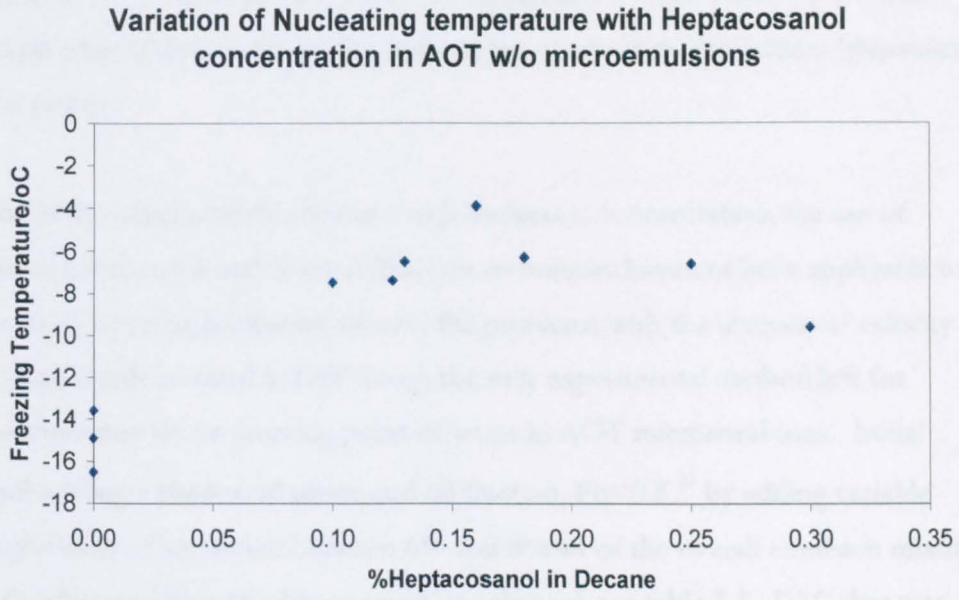

Figure 4.8 shows a preliminary study of the variation of freezing temperature with heptacosanol concentration as % wt of the oil phase for an AOT and decane microemulsion system.

Note that the oil phase chosen for these studies was decane to ensure continuity from the emulsion studies. However as can be seen in Figure 4.8 the freezing temperature of these emulsions with no added heptacosanol is much higher than expected from previous data in the literature which quoted values of ~ -39 ^{0}C.[2] This is considered in more detail later.

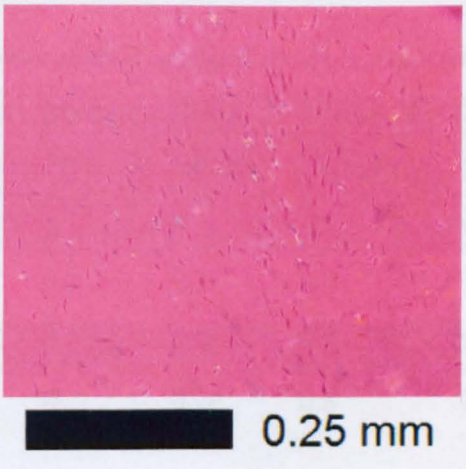

Figure 4.9 AOT Microemulsion with 0.18% heptacosanol in decane cooled to 8 oC viewed through crossed polarisers and red tint plate showing crystallisation of the additive heptacosanol upon cooling.

Due to the small particle sizes and high surfactant concentration, the use of optical microscopy and X-ray diffraction techniques have not been applicable to the study of microemulsions. Hence, the problems with the ultrasound velocity measurements resulted in DSC being the only experimental method left for determination of the freezing point of water in AOT microemulsions. Initial studies using a decane oil phase and oil fraction, Fo=0.8 [φ] by adding variable proportions of surfactant between 6% and 8% wt of the overall emulsion mixture both white and blue emulsions could be achieved, see table 3.3. DSC data was collected from these emulsions in triplicate and the ice freezing temperature measured. Note, there were slight variations in the bulk ice melting temperature of ±1 °C, from the expected value of 0 °C, measured on the DSC heating run. Hence the ice freezing temperatures in °C were given by the difference, ΔT, in the ice freezing and melting temperature, to negate the variation in the DSC measured ice melting temperature.

Typical compositions and results are shown below in Table 4.3 and Figure 4.10:

Table 4.3 Typical composition of AOT stabilised emulsions and resulting droplet radii

	Mass H20 / g	**Mass AOT / g**	**Mass Decane / g**	**Predicted Radius / Å**
Microemulsion	0.2	0.1	0.8	74
Blue emulsion	0.12	0.05	0.8	89
White emulsion	0.2	0.06	0.8	124*

[φ] $F_O = \frac{O}{O+W}$ where O is the mass of oil and W is the mass of water

*NB that by definition that this predicted droplet radius is far too small for a white emulsion, this was later observed to form a microemulsion on cooling.

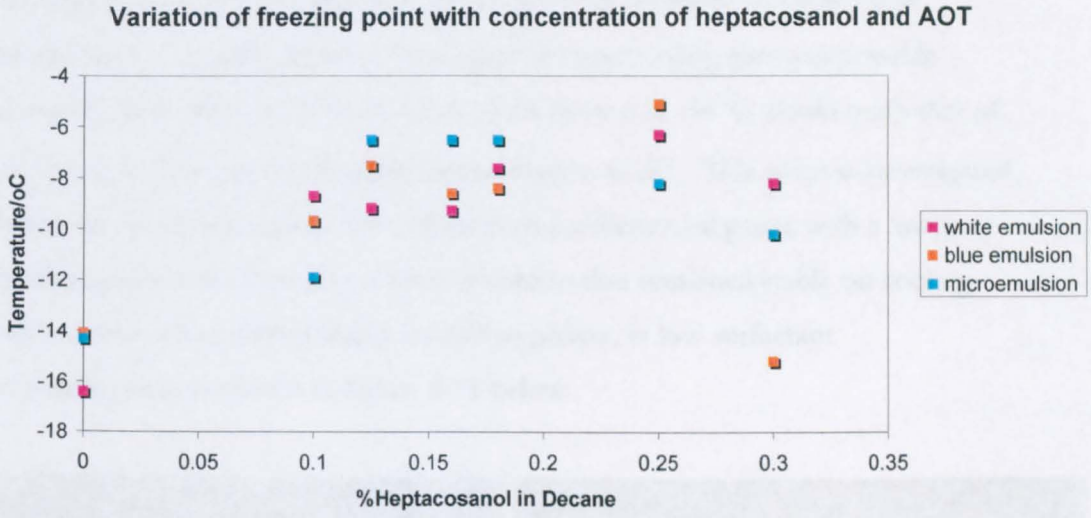

Figure 4.10 shows the variation in the freezing temperature with emulsion composition. Results for the white emulsion are shown by pink squares, for the blue emulsions by orange squares and for the microemulsions by blue squares.

Once again the freezing temperature of the water for the emulsions containing no heptacosanol is much higher than expected. These peaks in the DSC spectra were relatively small and it is assumed that the true crystallisation peak of the water freezing homogeneously at ~-40 °C was masked by the freezing of the oil at this temperature. Subsequent studies on this system have also shown that a certain amount of phase separation occurs for the larger w/o microemulsion droplets resulting in a small pool of water lying on the DSC pan, which will then freeze at around -18 °C.

Upon repeating the sample preparation however it was found that the blue emulsions were not stable for long periods of time, but upon standing for a few hours resulted in stable microemulsions. Optical microscopy of these 'blue-emulsions' also showed that upon cooling a small amount of phase separation could occur, or the emulsion would turn white as the droplets coalesce. Since slow cooling rates of 2 °C min^{-1} were employed for these systems to accurately

observe the supercooling, few, if any of the blue emulsions retained their room temperature character.

Another crucial problem with this system that was observed was that upon decreasing the droplet diameter the degree of supercooling that was possible increased, and often the freezing peak of the decane at -38 °C would mask that of the water, and so prevent accurate determination of ΔT. This point is investigated further in the next chapter. The selection of a different oil phase with a lower freezing point would not give a white emulsion that remained stable on cooling and resulted once more in liquid crystalline phases, at low surfactant concentrations, as shown in Figure 4.11 below.

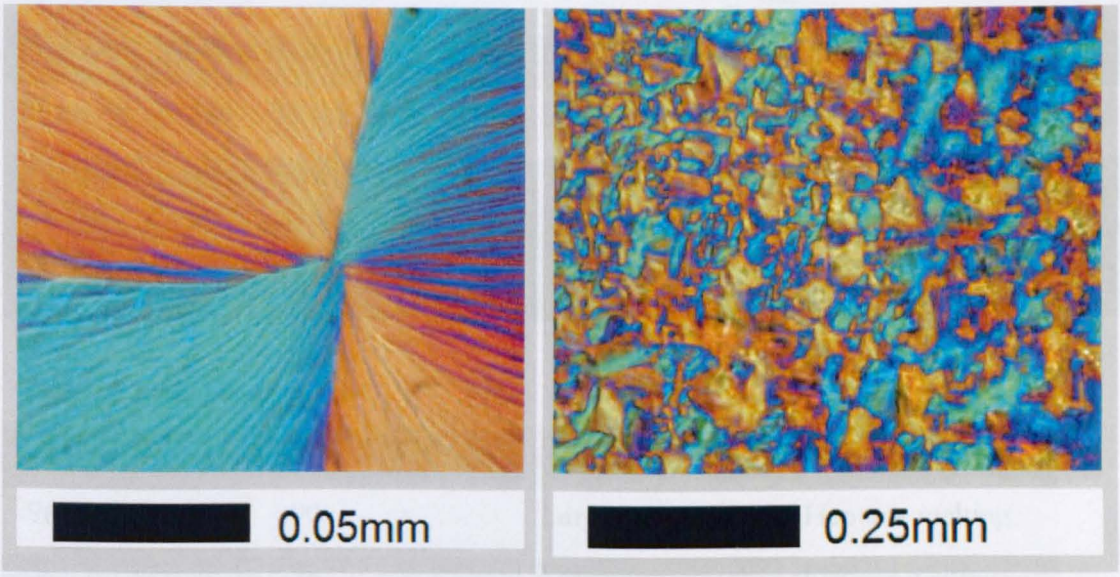

Figure 4.11 Left: heptane and AOT emulsion cooled and then forming a lamellar liquid crystalline phase. Right: octane and AOT emulsion also giving liquid crystalline behaviour on cooling.

Typical DSC traces as shown in chapter 3 Figure 3.13, can yield a lot of information about a sample when coupled with studies using polarising microscopy. Observed exotherms and endotherms in the DSC trace can be assigned to particular processes occurring within all the systems from lyotropic liquid crystal to microemulsions. Major peaks observed throughout are assigned as below in Tables 4.4 and 4.5.

Table 4.4 DSC Cooling cycle

Onset / °C	Peak / °C	Type of Peak	Attributed to
12	10	Small, Sharp	Heptacosanol crashing out of >0.12% wt solution (Precise temperature depends upon Heptacosanol concentration).
From -3 to -15	From -3 to -16	Sharp	Ice crystallisation induced by heptacosanol in AOT/decane systems.
From -18 to -28	From -20 to -39	Broad	Non-specific ice nucleation, due to either the aluminium pan or dust.
From -35 to -40	From -36 to -40	Large, Sharp	Decane crystallisation
From -96 to -100	From -96 to -100	Large, Sharp	Heptane crystallisation
From -40 to -80	From -40 to -80	Small	Water crystallisation, supercooled in extremely small droplet sizes

Table 4.5 DSC Heating Cycle

Onset / °C	Peak / °C	Type of Peak	Attributed to
-96	-90	Large	Heptane melting
-39	-38	Large	Decane melting
-10	-10 to -8	Small Broad	Interfacial water melting
-1 to 2	0 to 2	Sharp	Water melting

4.5.6 Cooling Rate Effects

A problem with all methods outlined in this report, is the simple fact that using a constant cooling rate the observation of the water freezing will not occur at the temperature of formation of the critical nucleus, hence introducing a systematic error into the results. Although it is impossible to eliminate this effect entirely, slower cooling rates should provide more accurate results.

4.5.7 Effect Of Heptacosanol On The Nucleation Of Ice

It can clearly be seen in all the results that the presence of heptacosanol greatly enhances the nucleation of ice in supercooled water; ice is nucleated at a much higher temperature than in pure water emulsions. It can also be seen that there is only a slight reduced nucleating efficiency at the oil-water interface compared to the air-water interface. The precise interactions or composition at the interface remains unknown for the curved systems, though.

4.5.8 Potassium Oleate Emulsions

The use of a single surfactant system to span the full range of w/o and o/w emulsions so that a comparison of concave and convex curvature could be made on the same interfacial conditions was found to be possible using a potassium oleate and hexanol surfactant mixture. From this system by varying the ratio of water to oil from 1:9 to 9:1, blue o/w, through white o/w, to all w/o emulsions were achievable and stable at low temperatures in the presence of heptacosanol.

The potassium oleate surfactant was only available as a paste from Aldrich, comprising 60%water, so initial studies were carried out on just the surfactant mix with the oil phase to compare the emulsion freezing points. Table 4.6 shows the initial results.

Table 4.6 where Mix 0%, 0.05% and 0.10% represent heptacosanol concentration as % wt of the oil fraction of a surfactant/oil mixture of 61.5% wt decane, 15.4% wt hexanol and 23.1% wt potassium oleate paste.

Sample	ΔT /°C	ΔT /°C	ΔT /°C	Mean ΔT /°C	Standard Deviation
MIX0%	-37.6	-38.0	-37.0	-37.5	0.50
MIX0.05%	-38.5	-30.8	-37.0	-35.4	4.08
MIX0.10%	-27.3	-27.8	-26.3	-27.1	0.76

These data could be interpreted as the freezing points of the water pools in the smallest w/o microemulsion possible with this system, due to the water already present with the surfactant mix. Drying of the surfactant mix was not attempted as the safety instructions suggested that heating or drying of the paste would result in decomposition of the surfactant, and as such it must be kept refrigerated until used. Hence the overall water content of these mixes is ~14% wt. These data show approximately a 10 °C increase in freezing temperature with just 0.1% wt heptacosanol in the oil phase.

Using the compositions shown below a range of emulsions was prepared and studied by DSC. Typically the cooling rate used was 5 °C minute^{-1} from 30 to -45 °C. See Table 4.7.

Table 4.7 Composition of potassium oleate emulsions studied by DSC

Emulsion Type	K-oleate /% wt	Hexanol /% wt	Decane /% wt	Water /% wt	Heptacosanol as % wt of Decane Fraction
Blue o/w	8.31	13.85	55.38	10.00	0
White o/w	6.46	10.77	43.08	30.00	0
White w/o	4.62	7.69	30.77	50.00	0
Blue w/o	2.77	4.62	18.46	70.00	0
Micro w/o	0.92	1.54	6.15	90.00	0
Blue o/w	8.31	13.85	55.38	10.00	0.05
White o/w	6.46	10.77	43.08	30.00	0.05
White w/o	4.62	7.69	30.77	50.00	0.05
Blue w/o	2.77	4.62	18.46	70.00	0.05
Micro w/o	0.92	1.54	6.15	90.00	0.05
Blue o/w	8.31	13.85	55.38	10.00	0.10
White o/w	6.46	10.77	43.08	30.00	0.10
White w/o	4.62	7.69	30.77	50.00	0.10
Blue w/o	2.77	4.62	18.46	70.00	0.10
Micro w/o	0.92	1.54	6.15	90.00	0.10

As could be seen from this initial study, it appeared that again, for the microemulsion droplets, a large degree of supercooling was possible without added heptacosanol, and that the low concentration of heptacosanol was still highly effective at promoting ice nucleation, see Table 4.8.

Table 4.8. Initial study showing the ice freezing temperatures / °C for various compositions of potassium oleate emulsions, for a single set of measurements

Heptacosanol % wt of oil phase	0	0.05%	0.10%
blue o/w	-19.63	-10.02	-15.35
white w/o	-19.39	-14.73	-12.68
blue w/o	-31.04	-21.8	-22.55
micro w/o	-29.13	-23.9	-19.13

Results indicated that for the blue o/w emulsion, the higher surfactant concentrations of heptacosanol required previously[40] to achieve increased nucleation temperatures, was not necessary in this case, possibly due to the different interactions between surfactant, co-surfactant and additive resulting in an increased interfacial occupancy by the additive.

Along with the large increase in nucleation temperature for the o/w nanoemulsions the w/o emulsions also show an increase in nucleation temperature with added heptacosanol. This trend seems to indicate that as the surface curvature increases for the convex case, the lattice match also increases, and in so doing increases the nucleation temperature. However increasing the additive concentration to 0.10% of the oil phase results in an increase in freezing temperature once again.

Further investigation into this system due to the stochastic nature of nucleation, did not provide good statistical results, see Table 4.9, indicating that the enhanced nucleating ability of heptacosanol for this system was not showing as dramatic an effect as initial results had indicated and so the system chosen for further investigation was that using the AOT surfactant.

Table 4.9. Shows the mean ice freezing temperatures / °C for various compositions of potassium oleate emulsions, mean results of 3 repeats shown, all with standard deviations of less than 1%

Heptacosanol % wt of oil phase	0%	0.05%	0.10%
blue o/w	-17.5	-17.9	-16.9
white o/w	-17.5	-20.0	-17.8
white w/o	-19.6	-19.8	-15.9
blue w/o	-27.0	-23.2	-25.5
micro w/o	-28.9	-30.1	-25.7

4.6 Summary Discussion

For the o/w case, despite the K-oleate systems' reduced nucleating ability for the blue emulsion, the trend is comparable to previous work, a slight reduction of nucleating ability is observed for the blue emulsion compared to the white emulsion. However, in the later studies a contradictory result is obtained implying that the blue o/w emulsions are actually better at nucleating ice than their white counterparts. Since the distribution of data is so wide in this case that further studies are required.

For the w/o white emulsion all systems seem to show a nucleating temperature of ~-11°C. The only increase on this was for the AOT system with increased heptacosanol concentration of 0.16% in the oil phase, showing a nucleating temperature of -6.5°C This is due to the optimal interfacial concentration of the nucleating species being achieved, but this may be due to ice freezing on heptacosanol that crystallises out on cooling.

The blue w/o emulsions have a slightly more complex behaviour, particularly due to their ability to phase separate or coalesce upon cooling for the AOT systems. If it is assumed that the emulsion retains its' room temperature character the results shown indicate that for the AOT systems the nucleating temperature

increases, implying an enhanced lattice match. This is highly unlikely as the expected epitaxial match between hexagonal ice and heptacosanol should decrease with increasing interfacial curvature, as found in studies of Crystallisation in oil-in-water emulsions and nanoemulsions.[40] So the more believable K-oleate system may be more indicative of the true behaviour, showing a large reduction in nucleating ability for the blue w/o emulsions compared to their larger white counterparts.

Micro-emulsion behaviour takes another turn back to higher nucleating temperatures. For the K-oleate system this is not as marked an increase as hoped, but further increase of the heptacosanol concentration was not possible due to its reduced solubility on cooling. For the AOT microemulsion the loading of heptacosanol could be increased up to 0.25% wt of the oil phase resulting in nucleation temperatures as high as -3.9°C, almost comparable to the planar case. However the possibility of heptacosanol crystallising out on cooling could not be ruled out for this system, and so in future studies it was decided to keep to a low 0.06 % wt of heptacosanol to ensure this did not arise.

In conclusion the K-oleate system provided a possible route to study the effects of interfacial curvature upon epitaxial lattice matching of the heptacosanol to the ice for the full range of curvatures. However other competing interfacial effects could be affecting the data and its interpretation. In particular, we have the competing factor of the hexanol co-surfactant. It is known that short chain alcohols are used as antifreeze agents due to their ability to disrupt the nucleation of ice and as a consequence of this depress the freezing point observed. If hexanol does this then we have competing crystallisation promotion and inhibiting effects.

A key observation in all these studies is that of the stochastic nature of nucleation. Even from a given batch of samples identical in composition a range of nucleation temperatures may be observed, varying by as much as 5°C, and as such

if the enhancement of nucleation temperature is less than that, it may not be observed and drowned out in statistical noise.

4.7 Conclusion & Forward Look

The ability to use emulsions as a method of studying homogenous and heterogeneous nucleation seem apparent from these results. The reduced effect of an epitaxial match when a highly curved nucleation additive site is used clearly demonstrates that a good lattice match between substrate and crystal nucleus are essential.

The most highly curved systems of the microemulsions have shown the greatest effect of this reduced lattice match. Consequently, it was decided just to concentrate on the AOT microemulsion system for more detailed studies of the effect of interfacial curvature on the ability of heptacosanol to promote ice freezing.

References

1 E. J. Langham and B. J. Mason, *Proceedings of the Royal Society A*, 1958, ***247***, 493.

2 J. A. Schufle and M. Venugopalan, *Journal of Geophysical Research*, 1967, ***72***, 3271.

3 D. H. Rosmussen and M. A.P., *Journal of Chemical Physics*, 1973, ***59***, 5003.

4 L. Gránásy, Journal of Physical Chemistry, 99, 14182.

5 S. Trakhtenberg, R. Naaman, and S. R. Cohen, *Journal of Physical Chemistry B*, ***101***, 5172.

6 J. M. Baker and J. C. Dore, *Journal of Physical Chemistry B*, 1997, ***101***, 6226.

7 W. G. Courtney, Journal of Chemical Physics, **36**, 2018.

8 G. R. Wood and A. G. Walton, *Journal of Applied Physics*, 1970, ***41***, 3027.

9 E. Tombari, C. Ferrari, G. Salvetti, and G. P. Johari, *Journal of Chemical Physics*, 1999, ***111***, 3115.

10 D. Clausse, L. Babin, F. Broto, M. Agverd, and M. Clausse, *Journal of Physical Chemistry*, 1983, ***87***.

11 R. Popovitzbiro, M. Lahav, and L. Leiserowitz, *Journal of the American Chemical Society*, 1991, ***113***, 8943.

12 R. Popovitzbiro, M. Gavish, M. Lahav, and L. Leiserowitz, *Makromolekulare Chemie-Macromolecular Symposia*, 1991, ***46***, 125.

13 R. Popovitzbiro, J. L. Wang, J. Majewski, E. Shavit, L. Leiserowitz, and M. Lahav, *Journal of the American Chemical Society*, 1994, ***116***, 1179.

14 J. L. Wang, F. Leveiller, D. Jacquemain, K. Kjaer, J. Alsnielsen, M. Lahav, and L. Leiserowitz, *Journal of the American Chemical Society*, 1994, ***116***, 1192.

15 I. Weissbuch, M. Lahav, and L. Leiserowitz, *Crystal Growth & Design*, 2003, ***3***, 125.

16 J. Majewski, R. PopovitzBiro, R. Edgar, M. ArbelHaddad, K. Kjaer, W. Bouwman, J. AlsNielsen, M. Lahav, and L. Leiserowitz, *Journal of Physical Chemistry B*, 1997, ***101***, 8874.

17 J. Majewski, R. Popovitzbiro, K. Kjaer, J. Alsnielsen, M. Lahav, and L. Leiserowitz, *Journal of Physical Chemistry*, 1994, ***98***, 4087.

18 J. Majewski, R. Popovitzbiro, W. G. Bouwman, K. Kjaer, J. Alsnielsen, M. Lahav, and L. Leiserowitz, *Chemistry-a European Journal*, 1995, ***1***, 304.

19 M. Gavish, R. Popovitzbiro, M. Lahav, and L. Leiserowitz, *Science*, 1990, ***250***, 973.

20 R. Edgar, J. Y. Huang, R. Popovitz-Biro, K. Kjaer, W. G. Bouwman, P. B. Howes, J. Als-Nielsen, Y. R. Shen, M. Lahav, and L. Leiserowitz, *Journal of Physical Chemistry B*, 2000, ***104***, 6843.

21 M. Arbel-Haddad, M. Lahav, and L. Leiserowitz, *Journal of Physical Chemistry B*, 1998, ***102***, 1543.

22 A. Courty, I. Lisiecki, and M. P. Pileni, *Journal of Chemical Physics*, 2002, ***116***, 8074.

23 J. Esquena, G. R. Sankar, and C. Solans, *Langmuir*, 2003, ***19***, 2983.

24 V. N. Paunov, S. I. Sandler, and E. W. Kaler, *Langmuir*, 2000, ***16***, 8917.

25 A. Forgiarini, J. Esquena, C. Gonzalez, and C. Solans, *Langmuir*, 2001, ***17***, 2076.

26 M. Kahlweit, R. Strey, and G. Busse, *Journal of Physical Chemistry*, 1991, ***95***, 5344.

27 G. Caminati, D. Senatra, and G. Gabrielli, *Langmuir*, 1991, ***7***, 1969.

28 A. Yaghmur, A. Aserin, and N. Garti, Colloids and Surfaces a-Physicochemical and Engineering Aspects, 2002, **209**, 71.

29 Y. Sasanuma, F. Nishimura, H. Wakabayashi, and A. Suzuki, *Langmuir*, 2004, ***20***, 665.

30 A. Acharya, S. P. Moulik, S. K. Sanyal, B. K. Mishra, and P. M. Puri, *Journal of Colloid and Interface Science*, 2002, ***245***, 163.

31 I. Weissbuch, L. Addadi, Z. Berkovitchyellin, E. Gati, M. Lahav, and L. Leiserowitz, *Nature*, 1984, ***310***, 161.

32 E. M. Landau, R. Popovitzbiro, M. Levanon, L. Leiserowitz, M. Lahav, and J. Sagiv, *Molecular Crystals and Liquid Crystals*, 1986, ***134***, 323.

33 B. R. Heywood and S. Mann, *Advanced Materials*, 1994, ***6***, 9.

34 S. Mann and G. A. Ozin, *Nature*, 1996, ***382***, 313.

35 D. Walsh and S. Mann, *Nature*, 1995, ***377***, 320.

36 M. Boutonnet, J. Kizling, and P. Stenius, *Colloids and Surfaces*, 1982, ***5***, 209.

37 H. Weller, Angewandte Chemie-International Edition in English, 1993, **32**, 41.

38 M. Boutonnet, J. Kizling, R. Touroude, G. Maire, and P. Stenius, *Catalysis Letters*, 1991, ***9***, 347.

39 M. P. Pileni, *Nature Materials*, 2003, ***2***, 145.

40 M. J Jamieson, C. E.Nicholson, S.J. Cooper, S. *Cryst. Growth Des.* 2005, ***5***, 451-459.

41 S.Nave, J. Eastoe, R.K. Heenan, D Steytler, I. Grillo, *Langmuir* 2000, ***16***, 8741-8748.

42 S. Nave, J. Eastoe, J. Penfold, *Langmuir* 2000, ***16***, 8733-8740.

43 A. Beeby, I. M. Clarkson,J. Eastoe, S. Faulkner, B. Warne, *Langmuir* 1997, ***13***, 5816-5819.

44 J. Eastoe, S. Stebbing, J. Dalton, R.K. Heenan, *Colloid Surf. A-Physicochem. Eng. Asp.* 1996, ***119***, 123-131.

45 J. Eastoe, A. R. Cox, Colloid Surf. A-Physicochem. Eng. Asp. 1995, **101**, 63-76.

46 R. Hasegawa, T. Sugimura, Y. Suzaki, Y. Shindo, A. Kitahara, *J. Phys. Chem.* 1994, ***98***, 2120-2124.

47 J. Eastoe, G. Fragneto, B. H. Robinson, T. F. Towey, R. K. Heenan, F. J. Leng, *J. Chem. Soc.-Faraday Trans.* 1992, ***88***, 461-471.

48 J. Eastoe, B. Warne, *Curr. Opin. Colloid Interface Sci.* 1996, ***1***, 800-805.

49 G. D. Rees, R. Evans-Gowing, S. J. Hammond, and B. H. Robinson, *Langmuir*, 1999, ***15***, 1993.

50 A. Agostiano, M. Catalano, M. L. Curri, M. Della Monica, L. Manna, and L. Vasanelli, *Micron*, 2000, ***31***, 253.

51 M. Lade, H. Mays, J. Schmidt, R. Willumeit, and R. Schomacker, *Colloids and Surfaces a-Physicochemical and Engineering Aspects*, 2000, ***163***, 3.

52 P. Calandra, A. Longo, and V. T. Liveri, *Colloid and Polymer Science*, 2001, ***279***, 1112.

53 J. Zhang, L. D. Sun, C. Qian, C. S. Liao, and C. H. Yan, *Chinese Science Bulletin*, 2001, ***46***, 1873.

54 M. Summers, J. Eastoe, and S. Davis, *Langmuir*, 2002, ***18***, 5023.

55 S. Xu, H. C. Zhou, J. Xu, and Y. D. Li, *Langmuir*, 2002, ***18***, 10503.

56 G. Hota, S. Jain, and K. C. Khilar, Colloids and Surfaces a-Physicochemical and Engineering Aspects, 2004, **232**, 119.

57 J. Xu and Y. D. Li, Journal of Colloid and Interface Science, 2003, **259**, 275.

58 J. P. Cason, M. E. Miller, J. B. Thompson, and C. B. Roberts, *Journal of Physical Chemistry B*, 2001, ***105***, 2297.

59 Y. F. Chen and Z. Rosenzweig, *Nano Letters*, 2002, ***2***, 1299.

60 S. Y. Chang, L. Liu, and S. A. Asher, *Journal of the American Chemical Society*, 1994, ***116***, 6739.

61 M. L. Curri, A. Agostiano, L. Manna, M. Della Monica, M. Catalano, L. Chiavarone, V. Spagnolo, and M. Lugara, *Journal of Physical Chemistry B*, 2000, ***104***, 8391.

62 E. C. Hao, H. P. Sun, Z. Zhou, J. Q. Liu, B. Yang, and J. C. Shen, *Chemistry of Materials*, 1999, ***11***, 3096.

63 J. Eastoe and B. Warne, Current Opinion in Colloid & Interface Science, 1996, **1**, 800.

64 H. F. Gao, Y. Q. Zhao, S. K. Fu, B. Li, and M. Q. Li, *Colloid and Polymer Science*, 2002, ***280***, 653.

65 R. A. M. Hikmet, D. V. Talapin, and H. Weller, *Journal of Applied Physics*, 2003, ***93***, 3509.

66 G. N. Karanikolos, P. Alexandridis, G. Itskos, A. Petrou, and T. J. Mountziaris, *Langmuir*, 2004, ***20***, 550.

67 B. Liu, H. P. Li, C. H. Chew, W. X. Que, Y. L. Lam, C. H. Kam, L. M. Gan, and G. Q. Xu, *Materials Letters*, 2001, ***51***, 461.

68 B. Liu, G. Q. Xu, L. M. Gan, C. H. Chew, W. S. Li, and Z. X. Shen, *Journal of Applied Physics*, 2001, ***89***, 1059.

69 H. Ohde, M. Ohde, F. Bailey, H. Kim, and C. M. Wai, *Nano Letters*, 2002, ***2***, 721.

70 J. Perez-Conde and A. K. Bhattacharjee, *Physical Review B*, 2003, ***67***, art. no.

71 B. A. Simmons, S. C. Li, V. T. John, G. L. McPherson, A. Bose, W. L. Zhou, and J. B. He, *Nano Letters*, 2002, ***2***, 263.

72 L. D. Sun, X. F. Fu, C. Qian, C. S. Liao, and C. H. Yan, *Chemical Journal of Chinese Universities-Chinese*, 2001, ***22***, 879.

73 B. Wang, F. Gao, B. He, D. B. Zhang, H. M. Cheng, J. M. Ma, and L. M. Qi, *Acta Physico-Chimica Sinica*, 2003, ***19***, 21.

74 E. K. Bigg, *Proc. Phys. Soc B*, ***66***, 688.

Chapter 5

5.1 Introduction

In this chapter the use of emulsion droplets as a method of limiting the amount of crystallisable material present is explored. The initial concept for this chapter may me summarised in one question. What happens when the size of the droplets containing the water are smaller than required to form a critical nucleus?

5.2 Literature Review

Previous investigations into ice nucleation within emulsion droplets have not considered the limiting case of droplet volume approaching the critical nucleus size[7-11]. Instead studies have concentrated on the formation of ice nuclei within lamellar liquid crystalline phases[12] and within the pores of mesoporous materials such as MCM-41[13] Typically a decrease in the freezing temperature of water within a confined volume is observed for the smallest pore radii. This has led to the proposition that $\Delta T \propto 1/R$ where R is the pore radii, $\Delta T = T_0 - T_c$ and T_0 and T_c are the equilibrium melting temperature and actual crystallisation temperature, respectively.

The melting point depression found for small droplets of radii, R is often modelled[14,15] using the Gibbs-Thomson equation,

$$\Delta T = T_0 - T_m = (2\gamma v T_0)/R\Delta_{fus}H \qquad (5.1)$$

where T_m is the melting temperature, γ is the melt-crystal interfacial tension, v is the liquid molecular volume and $\Delta_{fus}H$ is the enthalpy of fusion. Theoretical treatments have shown[16-18], though, that this in fact provides an upper limit for the melting temperature, for which the transition pathway has no energy barrier. The thermal energy in the sample then means that we would expect the real melting temperature to be lower. Another major problem with this equation is

that the bulk values of $\Delta_{fus}H$ and γ are used. The small droplet volumes and nuclei sizes under consideration are such that this cannot be held as true.

Along with this predicted upper limit for melting, the thermodynamic criterion of $\Delta G \leq 0$ must be observed, since the process of crystallisation cannot cause the system to achieve an overall gain in ΔG. [19,20] This introduces a lower limit to the melting temperature, such that melting must fall between the value predicted by the Gibbs-Thomson equation and

$$\Delta T = (3\gamma v T_0)/R\Delta_{fus}H \qquad (5.2)$$

In both cases, the assumption is made that a surface layer of liquid is present, should this not be the case then melting/freezing must occur via a nucleation mechanism.

From the theoretical work of Cooper[21] et al crystallisation and melting can be predicted from classical nucleation theory, above a limiting size R_{min}, and as such the need for these upper and lower boundaries on the process of melting is rendered obsolete. This model is based upon the use of confined volumes of crystallisable material and the contact angle that these form with the confining vessel. This theoretical model is detailed in section 5.4 below. Below R_{min} classical nucleation theory cannot be used because melting temperatures would be predicted to be below crystallisation temperatures, which is not possible. See Figure 5.1. This occurs because at the predicted phase transition temperatures for $R < R_{min}$, there is limited material within the droplet, and this results in an overall increase in the Gibbs free energy of the system, which is not thermodynamically allowed. Hence, below R_{min} the melting and crystallisation temperatures are both given by:

$$\Delta T = \frac{3\gamma v T_0 \cos\theta}{R\Delta_{trans}H}. \qquad (5.3)$$

As equation 4.3 applies to both melting and crystallisation, there should be no hysteresis between melting and freezing provided the phase transitions leave the droplet structure unchanged. Equation 5.3 becomes equation 5.2 when $\theta = 0°$ and a surface liquid layer for melting (or a surface crystalline layer for crystallisation) is present. Since the Gibbs-Thompson equation is not used below R_{min} to calculate r^*, bulk values are not applied to the prediction. Consequently from experimental data a direct measurement of the critical nucleus is possible for the first time and is confirmed by comparison with this theory.

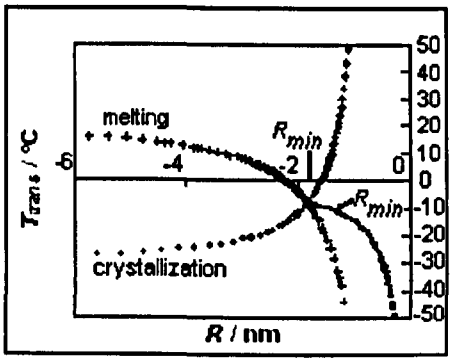

Figure 5.1 Variation in the predicted heterogeneous ice Crystallisation and melting temperatures within spherical substrates with $\theta c = 110°$ as a function of droplet radius, R. For R < Rmin, both the melting and Crystallisation temperatures are given by the 'Rmin' branch.

5.3 Context

As shown in chapter 2 classical nucleation theory shows that nucleation can proceed provided that a free energy increase ΔG^* occurs.

This maxima in ΔG^*, gives the critical nucleus, and represents the pivotal point of nucleation. Nucleus sizes below this critical size will tend to dissolve, larger than this and they will tend to grow into crystals. Hence knowing the size of the critical nucleus is important, but to date this has not been directly measured.

Use of microemulsions to provide a means of studying supercooled water is not a novel idea by any means; however there have been relatively few quantitative investigations [1-6] into ice freezing temperatures within microemulsion droplets of varying size.

5.4 Theoretical Model

This model is based upon the concept of a critical nucleus, which is that in any nucleation process there is an energy barrier to the creation of a new phase from a parent phase. This energy barrier ΔG^* will differ depending upon whether nucleation is homogeneous or heterogeneous, the latter having a lower energy barrier to the formation of a new phase.

Considering for example the homogeneous case. Classical nucleation theory[22] states that the value of ΔG^*_{hom} is given by

$$\Delta G^*_{hom} = \frac{16}{3\Delta\mu^2}\pi\gamma^3 v^2 \qquad (5.4)$$

where $\Delta\mu$ is the supersaturation, given by:

$$\Delta\mu = \Delta_{fus} H \Delta T / T_0 . \qquad (5.5)$$

For this theory to be valid at the small confined volumes under consideration here, then the Helmholtz free energy should be used instead of ΔG^*. But we assume that the phases are incompressible and that there is no change of volume upon crystallisation and so use ΔG^* throughout to highlight the connection with the classical theory. The more general heterogeneous form of this energy barrier

is ΔG^* which can be expressed as a product of a function of the contact angle between the critical nucleus and the planar nucleating substrate θ_p and ΔG^*_{hom}.

$$\Delta G^* = \Delta G^*_{\text{hom}} f(\theta_p) \qquad (5.6)$$

For a curved substrate the function of θ_p is based upon the angle between the planar surface that lies tangential to the curved surface of the nucleating substrate, i.e. the additive doped droplet interface in this instance, see Figure 5.2.

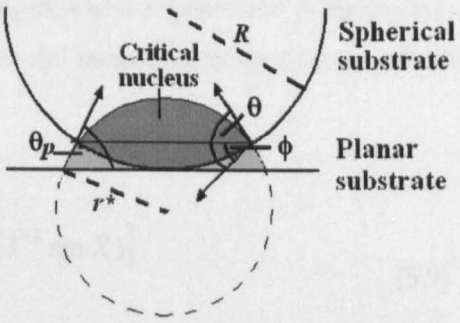

Figure 5.2 Parameters from which $f(\theta_p)$ is calculated for nucleation within a spherical droplet.

$f(\theta_p)$ is given by

$$f(\theta_p) = 0.25(2 - 3\cos\theta_p + \cos^3\theta_p) \qquad (5.7)$$

where $x=R/r^*$, where r^* is the critical nucleus radius and $y=\pm(x^2-2x\cos\theta+1)^{0.5}$ and $\cos\theta_p = x-y$. Then the values of R and y are given as negative values, when the nucleation is occurring within the droplet and the curvature is concave, whilst these values are positive for the convex curvature systems relating to Crystallisation upon a droplet.

To relate this to a given temperature of a transition, T_{trans}, the rate of nucleation needs to be set to a low rate, for ease of illustration lowest observable rate of $1cm^2$

s^{-1}. The nucleation rate, J, is given by $J = A\ exp\ (-\Delta G^*/k_B T_{trans})$ where A is a pre exponential factor assumed to be constant and k_B is the Boltzmann constant.

Rearrangement to give $\Delta G^* = k_B T_{trans}\ lnA$ and substitution into equation 5.6 gives: (where ΔG^*_{hom} has also been substituted by equation 5.4)

$$\Delta T^3 - \Delta T^2 T_0 + \frac{16\pi\gamma^3 v^2 T_0^{\,2} f(\theta_p)}{3k\Delta_{fus} H^2 \ln A} = 0 \qquad (5.8)$$

This has three roots, one of which gives a critical nucleus of only one molecule and as such gives an unphysical crystallisation temperature close to 0 K. The other two solutions give the transition temperatures for melting and crystallisation,

$$T_{trans} = \frac{T_0}{3}\left\{2 + \cos X - (3^{0.5} \sin X)\right\} \qquad (5.9)$$

and

$$T_{trans} = \frac{T_0}{3}\left\{2 + \cos X + (3^{0.5} \sin X)\right\} \qquad (5.10)$$

where

$$X = \frac{1}{3}\arccos\left[1 - \frac{72\pi\gamma^3 v^2 f(\theta_p)}{k\Delta_{fus} H^2 T_0 \ln A}\right]. \qquad (5.11)$$

From these formulae alone, predictions can be made for any system, whether nucleation is homogeneous or heterogeneous, or nucleation is within confined volumes, or the typical case of melting by the thickening of pre-existing surface layers.

The variations in the predicted ice crystallisation and melting temperatures with substrate radius determined using equation 5.9 and 5.10 are shown in Figure 5.1 for the case where $\theta = 100°$. It can be seen from Figure 5.3 that as $R \sim r^*$ crystallisation and melting occur at smaller ΔT values, due to the volume of the critical nucleus being reduced, see Figure 5.6.

The crystallisation and melting curves cross at a value of $R = R_{min}$. For $R < R_{min}$ we have the unphysical situation where the melting curve is below that of the crystallisation curve. This occurs because the complete phase transformation of the droplet results in an increase in the free energy of the system at these predicted temperatures. This cannot occur. Hence below R_{min} classical nucleation theory cannot be used and so the limiting condition of $\Delta G = 0$ must be imposed to determine the phase transformation temperature.

The effect of imposing the limiting condition that $\Delta G = 0$ on the total phase transformation of the droplet is easily obtained by setting $R = R_{min}$ and retaining the convention that this radius takes a negative value for nucleation on a concave surface. Then,

$$\frac{4\pi R_{min}^3 \Delta\mu}{3v} + 4\pi R_{min}^2 (\gamma_2 - \gamma_1) = 0 \qquad (5.12)$$

i.e.

$$R_{\min} = \frac{3v(\gamma_1 - \gamma_2)}{\Delta\mu} = \frac{3v\gamma}{\Delta\mu}\cos\theta = \frac{3r^*}{2}\cos\theta \qquad (5.13)$$

Equation 5.13 shows that R_{min} only takes the required negative values for phase transformations within spherical substrates when $\theta > 90°$ and r^* is positive, or when $\theta < 90°$ and r^* is negative. Hence the R_{min} condition occurs at $T_{trans} < T_0$ for $\theta > 90°$ and at $T_{trans} > T_0$ for $\theta < 90°$, as is expected.

From equation 5.13, substitution of the supersaturation gives

$$T_{trans} = T_0\left(1 - \frac{3\gamma v \cos\theta}{R\Delta_{trans}H}\right) \qquad (5.14)$$

and this phase transition temperature applies both to melting and crystallisation and so there should be no hysteresis between the two.

Once this condition is met the θ_p and ϕ values are invariant for a given contact angle. This is important as it means that the volume of the critical nucleus relative to the droplet volume is constant. In particular

$$\frac{\text{Critical nucleus volume}}{\text{droplet volume}} = \frac{f(\theta+\phi)}{x^3} - f(\phi) \qquad (5.15)$$

and since $\cos(\theta+\phi) = \frac{x\cos\theta - 1}{y}$ and $\cos\phi = \frac{x-\cos\theta}{y}$ with and $x = 1.5\cos\theta$

$y = -0.5(4 - 3\cos^2\theta)^{0.5}$ for $R \le R_{min}$, then we have:

$$\frac{\text{Critical nucleus volume}}{\text{droplet volume}} = \frac{4}{27|\cos^3\theta|}\left\{1 - \frac{27\cos^3\theta}{8} + \frac{2 - (3/4)\cos^2\theta + (9/8)\cos^4\theta}{\pm(4 - 3\cos^2\theta)^{0.5}}\right\} \qquad (5.16)$$

This shows that the dependence of the critical nucleus volume/droplet volume is dependant solely on θ and the dependence is relatively weak, see Figure 5.3.

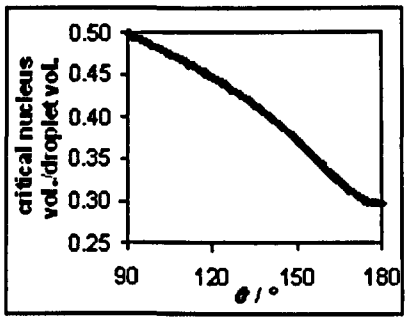

Figure 5.3 Variation of a) R_{min} with θ and b) critical nucleus volume/ droplet volume with θ for $R \leq R_{min}$

This means that we can determine the number of molecules in the critical nucleus with good precision, provided we know R, even if the exact contact angle is not known.

The number of molecules in the critical nucleus is

$$= \frac{16\pi R^3}{81v|\cos^3\theta|}\left\{1 - \frac{27\cos^3\theta}{8} + \frac{2-(3/4)\cos^2\theta+(9/8)\cos^4\theta}{\pm(4-3\cos^2\theta)^{0.5}}\right\} \quad (5.17)$$

This means that we have a direct measurement of critical nucleus size that does not rely on the Gibbs-Thomson equation. So bulk values of the interfacial tension and enthalpy of fusion are not required to describe the minute critical nucleus.

5.5 Experimental Details & Methodology

Crystallisation experiments in microemulsions were conducted with and without the addition of 0.06 wt% of the cosurfactant, heptacosanol ($C_{27}H_{54}OH$), which is a known [23,24] ice nucleator.

The water-in-oil microemulsion system investigated here uses di(2-ethylhexyl) sodium sulfosuccinate (AOT) as the stabilising surfactant. This is a commonly used ionic surfactant due to the simple relationship between water droplet radius

and water concentration in the overall microemulsion mixture relative to that of the AOT, i.e. droplet radius / nm = 1.5 + 0.15 $[H_2O]/[AOT]$ [25-29]. Heptane, heptacosanol and AOT, were mixed and sonicated in a water bath at 60 °C to ensure that all the heptacosanol had dissolved. Water was added to the cooled solution and the microemulsion was obtained by vortexing for 30 seconds at 25000 rpm. The composition of the microemulsions used is listed in tables 5.1-5.3. The percolation temperature of AOT microemulsions is quite low (~ 27 °C)[25,26] and so care was taken to ensure that these microemulsions were always stored well below this temperature to avoid the enhanced droplet clustering and increase in droplet size polydispersity associated with this transition temperature.

5.6 Results & Discussion

5.6.1 Droplet Size Analysis

Confirmation of the droplet sizes was achieved by SAXS analysis on the samples at 2°C to determine if the small amount of added heptacosanol or the change in temperature perturbed the droplet sizes from that predicted by the model of Eastoe.[27] Two hour small angle X-ray scattering (SAXS) experiments were carried out using a Bruker Nanostar, with the sample-to-detector distance of 1.07 m. The mean droplet radius of each sample was obtained by Guinier analysis[33,34] on the SAXS data, see chapter3 for a description of this technique. Data was also collected from a selection of the samples at 25, -5, -15, -20 and -30°C. This showed that down to -30°C there was very little fluctuation in the droplet diameter. In agreement with many previous studies on AOT microemulsions,[25-29] the water pool size is given by 0.15 $[H_2O]/[AOT]$, assuming that the thickness of the AOT plus bound water layer is 1.5 nm. Figure 5.4 shows the comparison of the SAXS data collected and the fit of the line 0.15 $[H_2O]/[AOT]$.

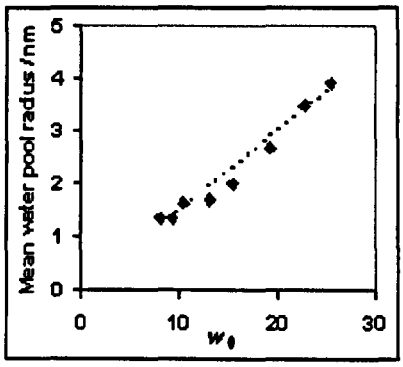

Figure 5.4. Variation of the mean water pool radii with $w_0 = [H_2O]/[AOT]$ for the AOT microemulsions. The dashed line shows the fit to $0.15w_0$ nm.

5.6.2 Determination Of Ice Crystallisation Temperatures & Comparison With Predicted Data.

DSC data were acquired at a heating and cooling rate of 5 °C min^{-1} and to an accuracy of ± 1 °C across a temperature range of 10 to –80 °C. The exothermic peak and endothermic peak in the cooling and heating runs are attributed to the ice Crystallisation and melting, respectively. Typical DSC cooling traces for microemulsions are shown in Figure 5.5.

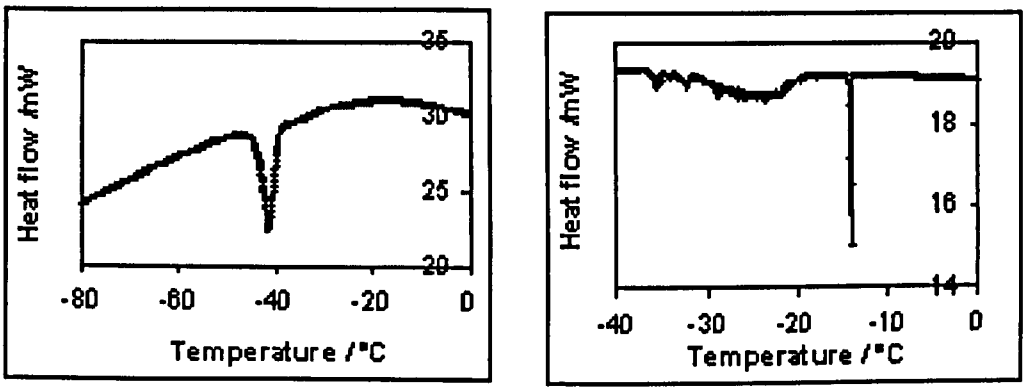

Figure 5.5 Typical DSC traces of the cooling cycle a) without additive and so homogeneous nucleation occurs and b) with 0.06%wt heptacosanol in the heptane oil phase, so heterogeneous nucleation occurs.

The interfacial concentration of heptacosanol in these microemulsions is 0.18%, corresponding to on average <1 molecule of additive per droplet. Higher concentrations of heptacosanol were not used due to its low solubility in heptane, and upon cooling higher concentrations would crystallise within the oil phase. Besides, higher concentrations up to 0.35%wt in the heptane phase were tested and did not provide any further enhancement of the nucleation temperature. Nevertheless, a significant increase in ice Crystallisation temperatures was observed with this small amount of 0.06 wt% added heptacosanol, which indicates that some droplets contain (far) more than one heptacosanol molecule. This is backed up by the fact that we generally see two peaks in the DSC spectra; the first one being small and sharp, the second one typically much larger and

broader, see Figure 5.5 above. The higher T_c peak is assigned to the optimum crystallisation temperature, and the lower temperature, broader peak represents the mean nucleating ability of heptacosanol.

The mean freezing temperatures and water pool radii are shown in Tables 5.1 to 5.3 below, along with the microemulsion composition. In determining the composition of the microemulsions, it was noted that the AOT itself is hygroscopic and so when stored it is kept in a tightly sealed container. An AOT sample was submitted for Thermal Gravimetric Analysis (TGA) to determine the amount of residual water that would be present in all microemulsions prior to the addition of the aqueous phase. The sample was heated at 10 °C min^{-1} to 130 °C and held at that temperature for 2 hours, after which there was no further loss of material. Overall a total of 2.6% by weight was lost. This systematic error was accounted for throughout all the experiments using this surfactant and equates to 5 μl of water for every 0.10 g of surfactant. Note that for a more definitive proof that the TGA mass loss was due to loss of water, the system can be coupled to a mass spectrometer. However there was no suspicion that any other contaminants were present.

Table 5.1 AOT microemulsion composition, water pool radii, and ice Crystallisation data.

Water weight fraction	Heptane weight fraction	AOT weight fraction	w_0 = $[H_20]$/ [AOT]	Water pool radius / nm	T_c / °C	Contact angle/°	No. of molecules in critical nucleus
0.035	0.858	0.107	8.05	1.2	-48.1	180.0	67
0.038	0.856	0.107	8.67	1.3	-47.6	180.0	84
0.040	0.853	0.107	9.29	1.4	-44.2	180.0	103
0.045	0.849	0.106	10.52	1.6	-43.5	180.0	150
0.050	0.844	0.106	11.76	1.8	-41.7	180.0	209
0.055	0.840	0.105	12.99	2.0	-41.2	180.0	281
0.065	0.831	0.104	15.46	2.3	-41.7	180.0	363
0.075	0.823	0.103	17.93	2.7	-41.6	180.0	365
0.079	0.818	0.102	19.17	2.9	-42.0	180.0	354
0.084	0.814	0.102	20.40	3.1	-41.0	180.0	381
0.093	0.806	0.101	22.87	3.4	-41.4	180.0	370

Table 5.2 AOT plus heptacosanol microemulsion composition, water pool radii, and ice Crystallisation data using highest T_c peak data.

Water weight fraction	Heptane + $C_{27}H_{55}OH$ weight fraction	AOT weight fraction	w_0 = $[H_20]$/ [AOT]	Water pool radius / nm	T_c /°C	Contact angle/ °	No. of molecules in critical nucleus
0.048	0.846	0.106	11.14	1.7	-14.4	103.2	330
0.050	0.844	0.106	11.76	1.8	-9.1	100.5	358
0.055	0.840	0.105	12.99	2.0	-9.1	97.4	406
0.060	0.835	0.104	14.23	2.1	-8.2	92.1	456
0.070	0.827	0.103	16.70	2.5	-8.3	85.8	545
0.075	0.823	0.103	17.93	2.7	-6.0	80.0	609
0.079	0.818	0.102	19.17	2.9	-6.9	78.5	627
0.084	0.814	0.102	20.40	3.1	-7.3	77.4	676
0.093	0.806	0.101	22.87	3.4	-6.9	73.2	751

Table 5.3 AOT plus heptacosanol microemulsion composition, water pool radii, and ice Crystallisation data using largest T_c peak data.

Water weight fraction	Heptane + $C_{27}H_{55}OH$ weight fraction	AOT weight fraction	w_0 = $[H_20]$/ [AOT]	Water pool radius / nm	T_c /°C	Contact angle/°	No. of molecules in critical nucleus
0.035	0.858	0.107	8.05	1.2	-30.5	143.4	88
0.036	0.857	0.107	8.30	1.2	-32.3	141.6	98
0.038	0.855	0.107	8.79	1.3	-32.0	138.2	119
0.039	0.854	0.107	9.04	1.4	-27.9	136.6	131
0.041	0.852	0.107	9.53	1.4	-29.0	133.3	157
0.044	0.850	0.106	10.27	1.5	-26.5	128.7	202
0.048	0.846	0.106	11.14	1.7	-22.6	123.6	263
0.050	0.844	0.106	11.76	1.8	-25.4	120.3	344
0.055	0.840	0.105	12.99	2.0	-24.8	118.6	372
0.060	0.835	0.104	14.23	2.1	-19.5	107.2	414
0.065	0.831	0.104	15.46	2.3	-23.0	109.5	425
0.070	0.827	0.103	16.70	2.5	-20.8	103.7	461
0.075	0.823	0.103	17.93	2.7	-20.0	100.5	490
0.079	0.818	0.102	19.17	2.9	-21.3	100.6	495
0.084	0.814	0.102	20.40	3.1	-21.3	98.9	510
0.093	0.806	0.101	22.87	3.4	-22.7	98.9	527

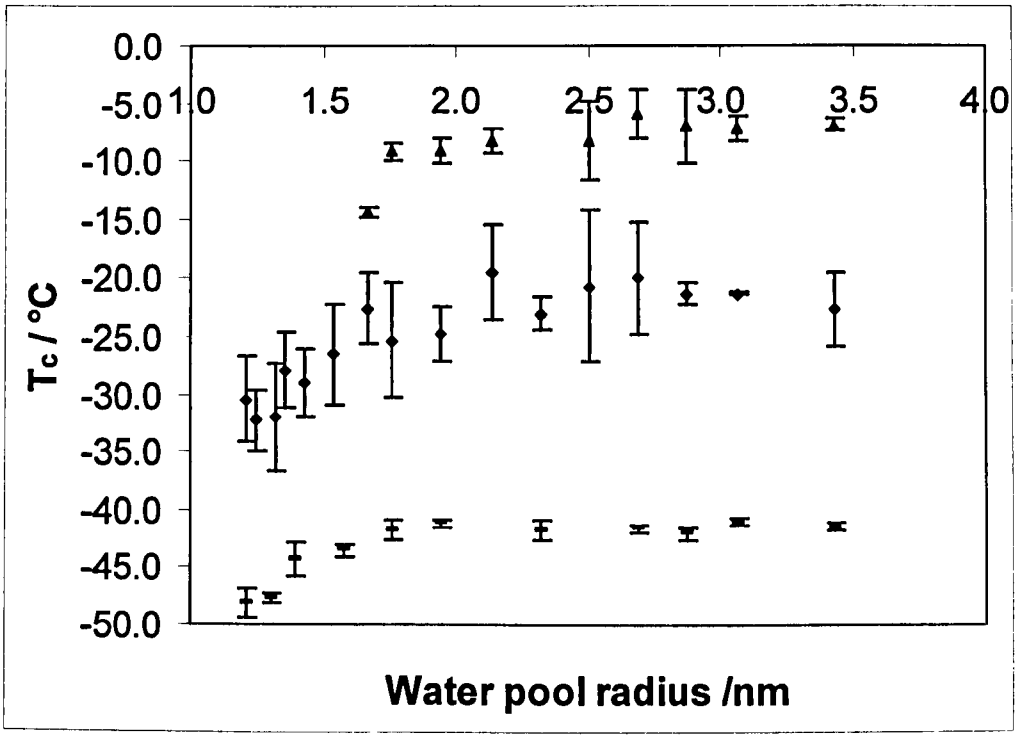

Figure 5.6 Variation of observed Crystallisation temperatures with water pool size for microemulsions with a) AOT (triangles), b)AOT plus heptacosanol, highest T_c peak (diamonds) and c)AOT plus heptacosanol, largest T_c peak (squares).

The drop off in crystallisation temperatures observed below ~2 nm seen in Figure 5.6 is attributed to the condition of $\Delta G = 0$ having to be met, i.e. the limiting thermodynamic criterion that the system cannot gain free energy overall if crystallisation is to occur.

For emulsions without added heptacosanol, the AOT is not seen to nucleate the ice at temperatures above -40°C, showing that homogeneous nucleation is occurring and so the contact angle is 180°. The work of Boned et al[3], Nucci and Vanderkooi[4] using DSC to study ice crystallisation in AOT microemulsions is consistent with these observations, as they too observed homogeneous ice crystallisation. Since the contact angle is known in this system, any discrepancy between predicted values and experimentally observed ones is due to either uncertainty in the experimental values or the variation in r^* from that predicted using the Gibbs-Thomson equation and bulk values of $\gamma/\Delta_{fus}H$. Fitting the

experimental data results in a maximum decrease of 5% from the bulk values and as such, these can be considered as appropriate for this system. This also confirms that the R_{min} value of 2.2 nm ($= 3\gamma v T_0 / \{\Delta_{fus} H \Delta T\}$) predicted for this system is accurate.

For the AOT and heptacosanol systems T_c is greater than -40 °C above R_{min}, and we find that to fit the data, θ must be allowed to increase with curvature. The error achieved in the fit by doing this is less than 0.1 °C in T_c, and 0.1 nm in R. These errors are actually lower than the experimental errors. The contact angle values used to fit the theoretical data are shown in Tables 5.1 to 5.3.

An increase in θ with curvature for the heterogeneous nucleation mechanism is not unexpected. If the concentration of heptacosanol is kept constant, and surface curvature increased, then the lattice match between heptacosanol and ice is decreased, resulting in a reduced nucleating ability. This is comparable to the data of Jamieson et al [24], which when this model is applied also shows an increase in θ with surface curvature.

For the heptacosanol-doped AOT microemulsions, heterogeneous crystallisation occurs within the water pools nucleated by the interfacial layer. This interfacial layer comprises: heptacosanol, AOT molecules, and bound/interfacial water layer (deemed unfreezable within the temperature range considered here). Hence from Young's equation, $\cos\theta = \frac{\gamma_{sv} - \gamma_{sx}}{\gamma_{vx}}$, θ depends on the difference between the interfacial tension between this layer and water, and the interfacial tension between this layer and ice. Since it is the interfacial tension between this layer and water that needs to be considered and not the ultra low oil-water interfacial tension value, this has the result of allowing θ to be less than 90°. Values of θ > 90° would only be required if we were replacing surfactant molecules at the oil-water interface with the ice critical nuclei, and this is clearly not happening.

For the homogeneous case, the uncertainty in the value of θ is removed completely as θ is fixed at 180° i.e. nucleation is removed from the interface. The

sole error in this data is then the experimental value of T_c and the water pool radius. Below R_{min}, the values of r^*, that is the radius of the critical nucleus, deviate significantly from that predicted using the bulk value of $\gamma/\Delta_{fus}H$, particularly for $R<1.3$ nm, see Table 5.1. Note that this means that the value of T_c does not fall as dramatically as expected below R_{min}, since the drop off that might be expected for a constant contact angle is offset somewhat by the decrease in $\gamma/\Delta_{fus}H$.

It was found that for the homogeneous case that the critical nucleus size was ~ 103 molecules for $R=1.4$ nm.

For the heterogeneous crystallisation in the heptacosanol-doped microemulsions, the variation of contact angle with water pool size can be fitted to a quadratic of equation 4.18 above R_{min}, see Figure 5.7. Below R_{min} it was assumed that the contact angle also varied in accordance with this equation.

$$y = 1.20\times10^{19}x^2 - 7.61\times10^{10}x + 219 \qquad (5.18)$$

N.B. that the actual contact angles below R_{min} are given by the last contact angle value above R_{min} + an added amount corresponding to the gradient (i.e. the differential) of this equation.

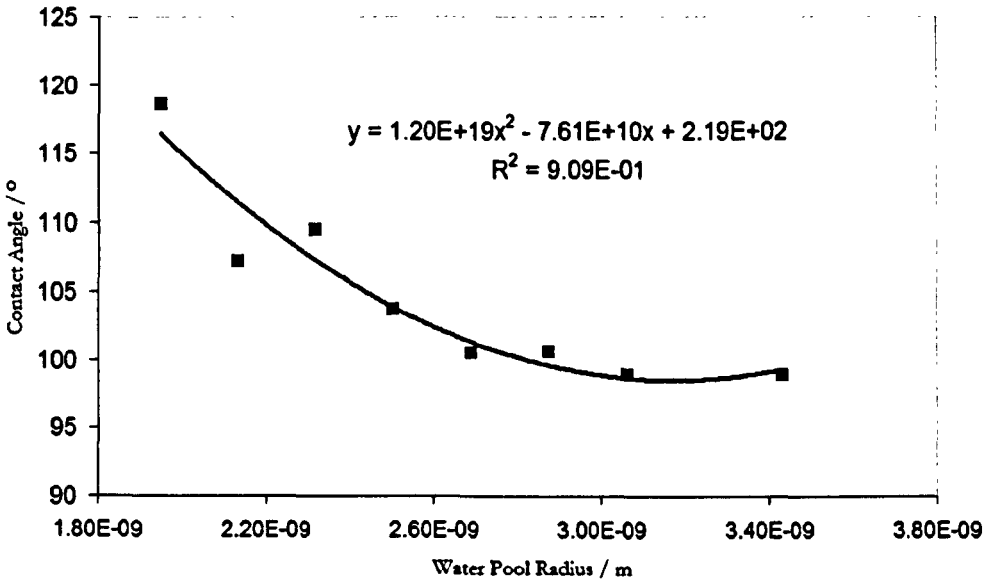

Figure 5.7 Fitting of contact angle data above Rmin to determine the likely contact angles below Rmin.

For the heterogeneous case, this means that below above R_{min} the critical nucleus sizes range from 202 molecules to 358 molecules for water pool radii between 1.5 to 1.8 nm. These values are expected to be accurate since there is a relatively low dependence of the critical nucleus size on the contact angle calculated using equation 4.18. For instance, with a 5% and 10% error in the contact angles, the number of ice molecules in the critical nucleus for water pool radii of 1.9 to 1.5 nm would change by 3-4% and 6-7%, respectively, and for an unrealistically large 20% error, the change would be 10-13%.

5.6.3 Comparison With Critical Nucleus Sizes Of Other Systems

Comparison of this system with that of ice freezing in heptacosanol-doped microemulsions stabilized with a 1:1 ratio by wt of Span80/Tween80,[36] shows very good agreement with the predicted and experimentally determined critical nucleus sizes for the heterogeneous case, see Tables 5.4 and 5.5.

Table 5.4. Span 80/Tween 80 plus heptacosanol microemulsion composition, water pool radii, and ice Crystallisation data.

Water weight fraction	Heptane + heptacosanol weight fraction	1:1 Span 80/Tween 80 weight fraction	Water pool radius / nm	T_c / °C	Contact angle /°	No. of molecules in critical nucleus
0.060	0.740	0.200	1.1	-32.3	180.0	55
0.065	0.735	0.200	1.5	-29.0	128.8	179
0.070	0.730	0.200	1.8	-27.0	124.2	348
0.075	0.725	0.200	2.1	-24.6	115.9	392
0.080	0.720	0.200	2.3	-21.4	107.0	434
0.090	0.710	0.200	2.8	-17.4	94.5	520
0.100	0.700	0.200	3.4	-15.8	87.5	592
0.110	0.690	0.200	3.6	-13.1	81.5	669
0.123	0.677	0.200	3.9	-14.1	81.5	676
0.130	0.670	0.200	3.7	-11.4	78.2	717
0.140	0.660	0.200	3.6	-11.6	79.5	687
0.150	0.650	0.200	3.4	-11.9	81.0	655
0.173	0.627	0.200	4.7	-10.0	70.5	862
0.200	0.600	0.200	5.1	-8.3	66.0	971

Table 5.5 Comparison of data for $R < R_{min}$, *showing the good agreement of the critical nucleus sizes.*

System	†No. of molecules in critical nucleus	Contact angle /°	Factor by which $(\gamma_1 - \gamma_2)/\Delta_{fus}H$ deviates from values at R_{min}	T_c / °C	Water pool radius / nm
AOT + heptacosanol	88	143.4	0.52	-30.5	1.2
	98	141.6	0.58	-32.3	1.2
	119	138.2	0.64	-32.0	1.3
Largest T_c peak	131	136.6	0.59	-27.9	1.4
	157	133.3	0.68	-29.0	1.4
	202	128.7	0.74	-26.5	1.5
	263	123.6	0.77	-22.6	1.7
	344	120.3	1.00	-25.4	1.8
Span 80 / Tween 80 + heptacosanol	70	148.7	0.48	-32.3	1.1
	200	133.5	0.74	-29.0	1.6
	348	124.2	1.00	-27.0	1.8

†Calculated using the water pool radius value and the contact angle between the critical nucleus and droplet interface.

For example, in the AOT plus heptacosanol series, the critical nucleus size ranges from 202 molecules to 344 molecules, as the water pool size increases from 1.5 nm to 1.8 nm, whilst for the Span 80 / Tween 80 and heptacosanol system, the critical nucleus contains 200 and 348 molecules for water pool radii of 1.6 nm and 1.8 nm, respectively. As expected, these values are larger than those in the AOT microemulsions without heptacosanol, because homogeneous nucleation occurs in the undoped system, and so the Crystallisation temperatures are lower.

5.6.4 Consideration Of The Cation Na^+ In The Water Pools.

A concern when using an ionic surfactant compared to the non-ionic ones is the effect of the counter-ion on the water crystallisation. Should the Na^+ be present in the water pools, the melting point and freezing point would be depressed by the colligative effect of this impurity. There was no evidence of this colligative effect in any of the DSC spectra. Because ice crystallisation also resulted ultimately in phase separation in the AOT micro emulsions, on heating the samples back to room temperature, the ice always meted at 0 °C, and there was never any evidence of water melting ~10 °C below its' normal melting temperature which would be indicative of 'interfacial' water that experiences strong interactions with the surfactant and effectively forms a chemically different environment to the 'bulk water'.

5.6.5 Water Shedding

A curious property of AOT microemulsions recently found is that of water shedding at ~ -35°C.[25, 26] whereby the water pool is released from the microemulsion droplet. After water shedding, the water pool is immersed in the organic solvent. However, since the Crystallisation is not initiated at the water pool interface for the AOT microemulsions without heptacosanol, this will not affect the ice Crystallisation temperatures. The AOT plus heptacosanol microemulsions typically freeze prior to, or at the expected temperature range for water shedding, and so water shedding should not have occurred to a significant degree prior to crystallisation occurring.

5.6.6 Phase Separation

It was found that the AOT microemulsions with 0.20 weight fraction of water or greater partially phase separated on cooling. This phase separation in larger microemulsion droplets has also been observed in other AOT microemulsion

systems previously investigated in chapter 4. A direct consequence of this is ice nucleation occurring at the higher temperature of ~-20 °C in this phase separated region. This explains the high nucleation temperatures observed for the expected homogeneous nucleation in the AOT/decane microemulsions in chapter 4. So in fact we now believe that homogeneous nucleation does occur in this AOT/decane microemulsion system, like it does in our water-in-heptane AOT undoped microemulsions, but that the expected peak at -40 °C is masked by the decane crystallizing at ~-35 to -40 °C, and the observed higher ice freezing peak at ~-20 °C is due to some phase separation occurring.

5.7 Conclusion & Forward Look

The variation of the ice crystallisation temperature with the water pool size, R, has been successfully modelled by using equation 5.9 and equation 5.14 for $R > R_{min}$, and $R \leq R_{min}$, respectively. The size of the critical nucleus can be found simply just by measuring the droplet size and crystallisation temperature of the confined phase in sufficiently small microemulsion droplets with $R \leq R_{min}$. It has also been shown that nanoscale systems lower the value of $\gamma / \Delta_{fus} H$ from that found for the bulk phase. In particular, the fitting of experimental data both for the AOT and Span80/Tween80 systems suggest that this ratio has a value similar to its bulk value for water pool radii of 2 nm and above, but below this size the value begins to decrease markedly, with the value decreasing to ~0.7 of its bulk value for radii ~1.5 nm. Recently the size of critical nuclei has been inferred from scattering data[35]. In comparison, the method detailed in this chapter provides an attractively simple and direct measurement of critical nucleus size.

References

1 Senatra, D.; Zhou, Z.; Pieraccini, L. *Progr. Colloid Polym. Sci.* 1987, ***73***, 66-75.

2 Munson, C. A.; Baker, G. A.; Baker, S. N.; Bright, F. V. *Langmuir* 2004, ***20***, 1551-1557.

3 Boned, C.; Peyrelasse, J; Moha-Ouchane, M. *J. Phys. Chem.* 1986, ***90***, 634-637.

4 Nucci, N. V.; Vanderkooi, J. M.. *J. Phys. Chem. B* 2005, ***109***, 18301-18309.

5 Senatra, D.; Pratesi, R.; Pieraccini, L. *J. Thermal Anal. Cal.* 1998, ***51***,79-90.

6 Senatra, D.; Gambi, M. C.; Carlà, M.; Chittofrati, A. *J. Therm. Anal. Cal.* 1999, ***56***,1335-1346.

7 Schulz, P. C. *J. Therm. Anal. Cal.* 1998, ***51***, 135-149.

8 Garti, N.; Aserin, A.; Ezrahi, S., Tiunova, I.; Berkovic, G. *J. Colloid Interf. Sci.* 1996, ***178***, 60-68.

9 Garti, N.; Aserin, A.; Tiunova, I.; Fanun, M. *Colloids and Surfaces A: Physiochem. Eng. Aspects* 2000, ***170***, 1-18.

10 Ezrahi, S., Nir, I.; Aserin, A.; Kozlovick, N.; Feldman, Y.; I.; Garti, N. *J. Dispers. Sci. Tech.* 2002, ***23***, 351-378.

11 Morishige, K.; Kawano, K. *J. Chem. Phys.* 1999, ***110***, 4867-4872.

12 Casillas, N.; Puig, J. E.; Olayo, R.; Hart, T. J.; Franses, E. I *Langmuir* 1989, ***5***, 384-389.

13 Schmidt, R.; Hansen, E. W.; Stöcker, M.; Akporiaye, D.; Ellestad, O. H. *J. Am. Chem. Soc.* 1995, ***117***, 4049-4056.

14 Christenson, H. K.. *J. Phys.: Condens. Matter* 2001, ***13***, R95-R133

15 Alba-Simionesco, C.; Coasne, B.; Dosseh, G.; Dudziak, G.; Gubbins, K. E.; Radhakrishnan, R.; Sliwinska-Bartkowiak, M. *J. Phys.: Condens. Matter* 2006, ***18***, R15-R68.

16 Vanfleet, R. R.; Mochel, *J. M. Surf. Sci.* 1995, ***341***, 40-50.

17 Denoyel, R.; Pellenq, R. J. M. *Langmuir* 2002, ***18***, 2710-2716

18 Petrov, O.; Furó, I. *Phys. Rev. E* 2006, 011608

19 Couchman, P. R.; Jesser, W. A. *Nature* 1977, ***269***, 481-483

20 Enustun, B. V.; Gunnink, B. W.; Demirel, T. *J. Colloid Interface Sci.* 1990, ***134***, 264-274

21 Cooper, S. J.; Nicholson, C. E.; Liu, J. *submitted to Phys. Rev. E.*

22 Sigsbee, R. A.; Pound, G. M. Adv. *Colloid Interface Sci.* 1967, ***1***, 335-390.

23 Popovitz-Biro, R.; Wang, J. L.; Majewski, J.; Shavit, E.; Leiserowitz, L.; Lahav, M *J. Am. Chem. Soc.* 1994, ***116***, 1179-1191.

24 Jamieson, M. J.; Nicholson, C. E.; Cooper, S. *Cryst. Growth Des.* 2005, ***5***, 451-459.

25 Zulauf, M.; Ericke, H. *J. Phys. Chem.* 1979, ***83***, 480-486

26 Ricka, J.; Borkovec, M.; Hofmeier, U.. *J. Chem. Phys.* 1991, ***94***, 8503-8509

27 Maitra, A. *J. Phys. Chem.* 1984, ***88***, 5122-5125

28 Moulik, S. P.; De, G. C.; Bhowmik, B. B.; Panda, A. K. *J. Phys. Chem. B* 1999, ***103***, 7122-7129

29 Nazario, L. M. M.; Hatton, T. A.; Crespo, J. P. S. G. *Langmuir* 1996, ***12***, 6326-6335

30 Van Horn, W. D.; Simorellis, A. K.; Flynn, P. F. *J. Amer. Chem. Soc.* 2005, ***127***, 13553-13560.

31 Simorellis, A. K.; Van Horn, W. D.; Flynn, P. F. *J. Amer. Chem. Soc.* 2006, ***128***, 5082-5090.

32 S.Nave, J. Eastoe, R.K. Heenan, D Steytler, I. Grillo, *Langmuir* 2000, ***16***, 8741-8748.

33 Guinier, A.; Fournet, G. *Small Angle Scattering of X-rays*; Wiley; New York, 1955.

34 Glatter, O. *Small angle scattering and light scattering. In Neutron, X-ray and light scattering*, Lindner, P.; Zemb, Th.,Eds.;Elsevier Science: New York, 1991; pp33-60.

35 Pan, A. C., Rappl, T. J.; Chandler, D.; Balsara, N. P. *J. Phys. Chem. B* 2006, ***110***, 3692-369

36 Liu, J., Cooper, S.J., Nicholson, C.E., *Langmuir*, 2007, publication pending.

Chapter 6

6.1 Introduction

In this chapter, details of work on some interesting effects that have been observed in crystallizing systems from emulsions. In particular, using the emulsion droplets as a template, could the formation of macroporous single crystals of glycine, along with other more complex morphologies be achieved? Also highlighted are the effects of phase inverting emulsions on nucleation rates, and the non-classical behaviour of crystallisation on both heating and cooling in these emulsion systems stabilised by non-ionic surfactants.

6.2 Literature Review

6.2.1 Growing Crystals From Solution In Emulsions

Turnbull and Hillig (1956) [1] proposed the use of emulsions to study crystallising systems, as they provided a method of partitioning a solution so that statistically only a few of the droplets would be subject to heterogeneous nucleation by dust particles and the like. This method can be widely applied to any solution or liquid provided that the surfactant used does not induce crystallisation of the solute or liquid. The very nature of emulsions includes phenomena such as percolation, Ostwald ripening, and phase inversion, which has led to a novel approach of mixing solutions to induce crystallisation. Not only can the emulsion droplets be used as 'micro-reactors' for processes such as polymerisation[2], they can be used as delivery systems for controlled amounts of solute to be mixed within a droplet and as a result of limited crystallisable material being available, well defined crystal sizes are achievable[3-5].

Recent uses of crystallisation within microemulsions have been of great interest in the production of quantum dots[2, 6-39]. Crystallising semiconducting materials in a

size that affects their band gap results in highly fluorescent particles that can be surface functionalised and used as tracers, or labels in biological systems.

Crystallisation within emulsions can be used to limit the amount of crystallisable material, and hence allow direct control of the size of the resulting particles. This method will work provided the crystals do not break the emulsion or continue growing by collision and subsequent merging with other droplets within the emulsion. Even if size control is not achieved, though, interesting effects can occur. For instance, Mann et al[40] produced co-aligned crystals of calcium phosphate forming a self assembled array similar to that found in abalone nacre and mollusc shells by using the surfactant calcium bis(2-ethylhexyl)phosphate and a high supersaturation level (pH = 9, [Ca]:[PO4] = 1.66) resulting in surfactant-coated nanorods that stacked side-on to produce a linear superstructure.

6.2.2 Crystallisation To Produce Porous Materials Using Solid Templates.

Use of templates to grow crystals around them is a simple way of producing new composite materials with different properties from that of the crystal alone. Introduction of polymeric or silica spheres followed by their subsequent removal and annealing will result in the formation of a porous material. The advantages of a porous material over a solid are easy to consider, reduced density thus weight, but if the crystalline structure is unaltered the chemical behaviour of the material will remain similar to the bulk. It is also desirable to engineer porous materials for their characteristics that differ from the bulk, such as optical properties, catalysts with high surface areas, or scaffolds for use as bone mimics.

Nature has long been able to tailor and control crystal growth to produce astounding materials[41], see Figure 6.1. Many attempts to copy this methodology and reproduce these materials in a lab from a bottom-up approach have yielded similar materials on a small scale and can be seen from the work of Meldrum and Mann[42-53],.

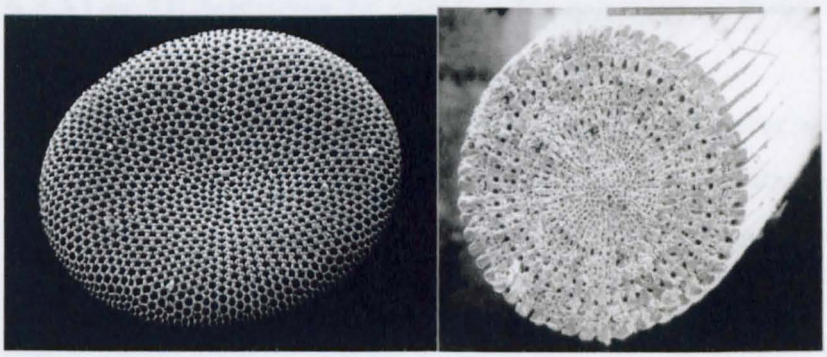

Figure 6.1. Viewed through electron microscope, Left Diatom, Right Sea urchin spicule.

The research of Meldrum focuses upon the reproduction of these complex calcium carbonate single crystalline materials by following the same mechanistic approach to crystallisation as found in the natural organisms. By using a confined volume of a templating material, firstly the amorphous precursor is deposited within the pores of a gel matrix or polymer cast of the original sea urchin spicule. Once the amorphous form of calcium carbonate has been deposited, it then undergoes transformation in the solid state to form a single crystal with the highly complex morphology reflecting the architecture of the template, see Figure 5.2. From these experiments, it is possible to mimic nature's control over the resulting shape of a given single crystal. However it is not yet as simple as nature itself, for the moulding material has to be removed by chemical or thermal methods.

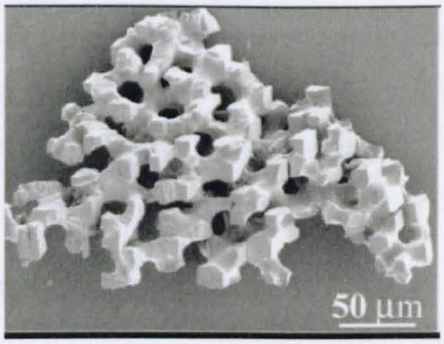

Figure 6.2 Porous single crystal of calcite, grown around a polymer cast of a sea urchin spicule, reproduced with kind permission from Dr F Meldrum's web pages.

6.2.3 Use Of Additives To Control Morphology & Polymorphic Form

Formations of ordered crystalline arrays similar to those found in dental enamel have been achieved by Mann et al.[54]. In this case the use of the ionic surfactant AOT in a calcium phosphate solution provides the structure directing ability to produce co-aligned crystalline fibres of hydroxyapetite, which are 750 nm in length. Other minerals crystallised within AOT reverse micelles, such as $BaSO_4$, result in other complex morphologies, such as filaments consisting of co-aligned fibers[55]. Cone-shaped aggregates were also possible provided microemulsions with a low $w_0 = [H_2O]/[AOT]$ value were used. This shows that it need not be a rigid template that needs to be present to result in single crystals with complex or unusual morphologies.

Use of specific proteins, or sections of proteins, extracted from biological systems that are known to have an effect upon the production of bioskeletons and crystalline self assembly, have been used to generate modified crystalline morphologies from solution crystallisation[56-58]. Another method of using additives to control crystal growth is when the promoting or inhibiting species is applied to specific areas of the crystal surface[59]. The resulting overgrowth of crystalline material can be patterned according to the substrate[59].

Indeed it need not just be a biologically extracted molecule that will act as a morphological modifier. Many examples of using tailored additives to control the resulting morphology of a crystal have been published.[60-62]

6.2.4 Porous Polymers Using Emulsions

Emulsions can also be used to form novel polymeric materials with a porous structure simply by using a monomer solution as the continuous phase and activating polymerisation in the presence of a dispersed aqueous phase. Using a high internal phase emulsion (HIPE), a highly porous polymer material is

achieved. Control over the droplet size is achieved by additives that stabilise the emulsion or cause greater droplet-droplet interactions to increase the porosity of the resulting material.

6.2.5 Solvent Effects On Crystal Morphology

If the crystalline structure that forms depends upon strong molecular interactions, then the solvent or pH of a solution may have a marked effect on the resulting crystal morphology.

The α- and γ- polymorphs of glycine consist of hydrogen-bonded pairs, whereas the β-polymorph does not. Glycine solutions will also generate different polymorphs depending upon the pH of the solution from which they are grown. At high and low pH, it is the γ-polymorph that will dominate, whereas at pH ~ 7 the α-polymorph will crystallise. The mechanism of molecular self poisoning that causes this effect in this system is discussed in great detail by Davey et al[63]

Using a polar solvent, such as ethanol, will disrupt the hydrogen bonding in the α- and γ- polymorphs of glycine entirely, resulting in the formation of β-glycine. The reason that many of the surfactants used in this work also produce the β-polymorph is probably that the carboxylic acid polar head groups interact with the glycine and as such the hydrogen-bonded pairs will not form to generate the α- or γ-polymorphs. Thus, this use of solvent polarity and the resulting interaction with the 'molecular building blocks' of a crystalline structure provides a method of producing a less thermodynamically stable polymorph, under conditions that would normally yield a more stable one.

Sulfathiazole also forms two types of 'molecular building block'. In this case, both are dimers but of different orientation, and so depending upon the solvent used, formation of these dimers may be assisted or disrupted resulting in different polymorphs of the sulfathiazole.[64]

Succinic acid is another classic example of a crystal exhibiting morphological changes due to solvent effects. In this instance[41], the growth of the (110) surface is promoted when in polar solvents, due to the interactions possible with the carboxylic acid groups on this face.

6.3 Context

6.3.1 Crystallisation On Heating & Cooling.

Switching nucleation on by temperature control is not a novel concept, simply common sense and thermodynamics. By cooling a solution or a melt the supersaturation can be increased, providing a greater driving force towards crystallisation to relieve this supersaturation. Indeed on cooling it is expected that the induction time (=1/nucleation rate) will fall as shown in Figures 6.3 and 6.4 for the majority of solute systems whose solubility increases with temperature.

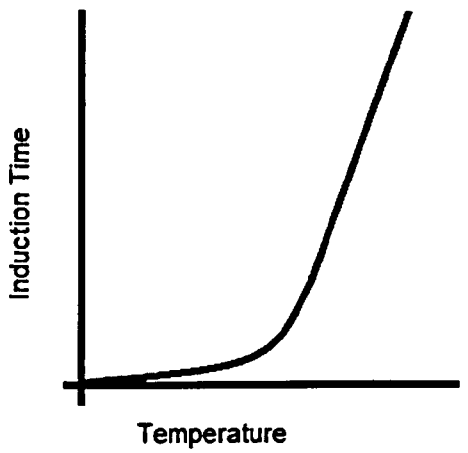

Figure 6.3 shows the typical induction time behaviour with temperature provided there are no other effects on the system.

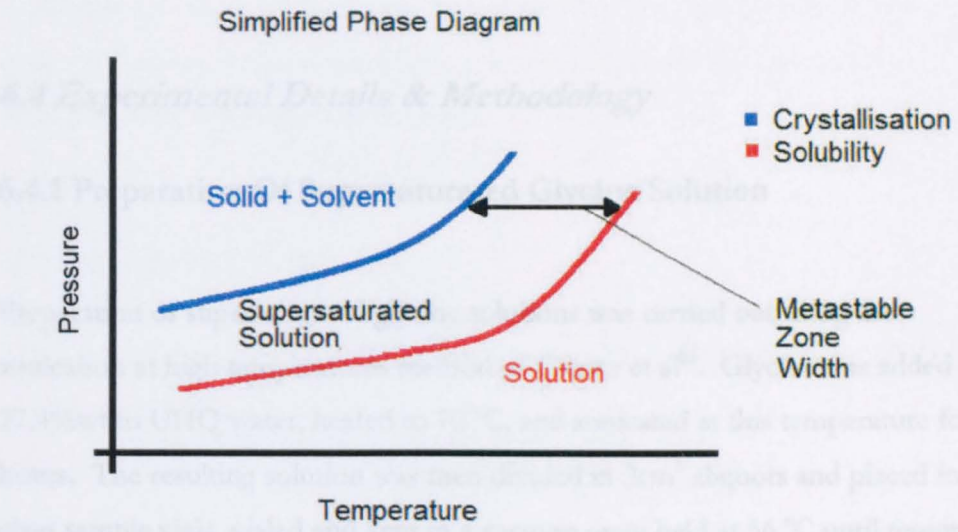

Figure 6.4. Illustrating the region of the phase diagram where the metastable supersaturated solution can exist below the solubility curve, along with the subsequent inevitable effect of crystallisation occurring upon further cooling.

Because the Crystallisation will typically occur via heterogeneous nucleation, this 'textbook" behaviour relies upon there being an approximately constant contact angle between the nucleating agent and critical nucleus of the crystallising material. If we remove this condition, though, we can achieve atypical Crystallisation rate behaviour with temperature. In particular, by using a non-ionic surfactant as the nucleating agent adsorbed at the emulsion droplet interface, and inducing phase inversion from a water-in-oil emulsion at higher temperatures to an oil-in-water emulsion at lower temperatures, we achieve a system in which the contact angle between the surfactant and critical nucleus can vary substantially. This is the system we will investigate in this chapter.

The aims of this chapter are; to show how using a polar oil, octanoic acid, in an oil-in-water emulsion formulation can lead to unusual crystal morphologies for a solute crystallizing in the continuous phase. Also, to demonstrate how a phase inverting system can produce non-classical Crystallisation rate behaviour and how this leads to the new concept of tuneable angle nucleating agents to provide unique control over Crystallisation rates.

6.4 Experimental Details & Methodology

6.4.1 Preparation Of Supersaturated Glycine Solution

Preparation of supersaturated glycine solutions was carried out using the sonication at high temperatures method of Garetz et al[66]. Glycine was added at 27.4%wt to UHQ water, heated to 70 °C, and sonicated at this temperature for 3 hours. The resulting solution was then divided in $2cm^3$ aliquots and placed in glass sample vials, sealed and kept in a vacuum oven held at 56 °C until required to add into an emulsion mixture. These samples were stable for up to a week under these conditions. To avoid cross contamination with any nuclei generated upon pipetting the glycine solution a new vial was used for each emulsion.

6.4.2 Emulsion Preparation

To generate an emulsion the surfactant or surfactant mixture was prepared and then dissolved in the required oil fraction. To ensure consistency and to be sure no gas bubbles were present this was done by sonication at 70 °C for 20 minutes. This emulsion base mixture was also stored in the vacuum oven at 56 °C so that when mixed the temperature of the resulting emulsion was not sufficiently low to induce crystallisation. Emulsions were mixed for 30 seconds on a vortex mixer at 2500rpm. Particular compositions are highlighted in the relevant sections below.

6.4.3 Observation Of Crystallisation

The resulting crystallisation of the Glycine based emulsions was observed using optical microscopy since in all cases the droplets under inspection are >1μm in diameter. Crystallisation was induced by lowering the temperature of the emulsion on the Linkam coldstage to 20 °C for the porous crystals, and to the

desired temperature for induction time measurements. Subsequent X-ray diffraction using the same samples on the D8 WAXS diffractometer was sufficient for polymorph confirmation.

6.5 Results & Discussion

6.5.1 Initial Studies To Determine Polymorph Crystallising With A Particular Surfactant

To determine the polymorphic form of glycine crystallised in the presence of various surfactants, a series of emulsions were made, all containing 0.10 g of surfactant and 0.80 g of decane. To this was added 0.20 g of glycine solution (24.7% wt), and the emulsion mixed on a vortex mixer at 2500 rpm for 1 minute. The emulsions were then left to crystallise, and any crystalline material was removed, placed on a silica slide and analysed on the D8 WAXS diffractometer as described in chapter 3.

The characteristic peaks expected for the different polymorphs of glycine are shown in Table 6.1 below.

Table 6.1 Typical growth conditions, appearance and characteristic X-ray diffraction peaks for the 3 polymorphs of glycine.

Polymorph	X-ray Diffraction Peaks /2θ °	Typical conditions for growth	Characteristics
α	19, 21, 30	Evaporation or cooling from aqueous solution	Elongated in the *c*-axis, most readily produced from aqueous solution at pH~7
β	18, 24, 28	Slow cooling of ethanolic solution	Fine needles transforms to α in air/aqueous environment
γ	15, 22, 25	Acidified solutions (typically with acetic acid)	Most thermodynamically stable at room temperature

It was found that the surfactants used to formulate emulsions have a direct effect upon the polymorph obtained, see Table 6.2.

Table 6.2 showing the polymorph of glycine obtained in o/w emulsions stabilised using a range of surfactant additives.

Surfactant	Polymorph
AOT	γ
Tween20	β
Tween80	β
Span20	β
Span80	β
Tween60	β
Span60	β
Brij30	β
Brij35	β
Brij72	β
Brij 92	β
Tergitol	β

6.5.2 Control Of Crystal Size

The crystals grown within w/o emulsion droplets stabilised with a Span 80/Tween 80 9:1 by weight blend are subject to nucleation at the surfactant/aqueous interface, resulting in spherical agglomerates of crystalline material limited to the dimensions of the droplet from which they have been crystallised, see Figure 6.5.

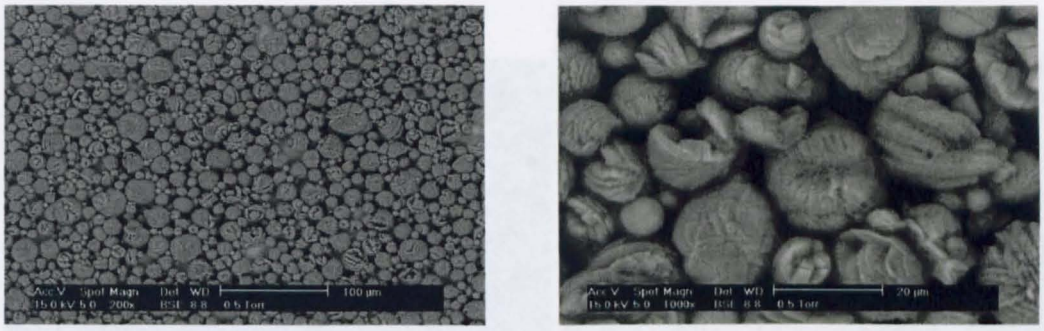

Figure 6.5. ESEM images of the β-polymorph of glycine crystallised within emulsion droplets.

6.5.3 Crystallisation Of Glycine From An Octanoic Acid-In-Water Emulsion

We wished to determine what would happen if glycine was crystallised from an octanoic acid-in-water emulsion. The choice of octanoic acid as the oil phase was not purely random. Previous work by Cooper[65] showed that this oil phase showed a strong affinity for certain crystal faces of L-asparagine, so much so that growth in particular directions can be inhibited. Preliminary studies by Jamieson[24] showed that the effect of octanoic acid upon glycine crystals was somewhat different. In particular, the octanoic acid can adhere strongly to the growing glycine crystal to produce inclusions in the glycine crystals. This behaviour required investigating more thoroughly.

The emulsion composition used to achieve the macroporous platelet-type β-glycine crystals was as follows. The surfactant mixture was comprised of 8:1 by weight of Span 20/Brij 30, and this formed 9% by weight of the total emulsion mixture. This was combined with 60% wt octanoic acid and the remaining 31% wt aqueous phase consisted of a 21.5% wt glycine solution. By cooling the emulsion from 25 to 20°C sufficient supersaturation was achieved to induce nucleation of the β-glycine. Figure 6.6 below shows the typical macroporous morphology obtained. The inclusion of the oil droplets can be observed particularly clearly by close inspection of the edges of the growing crystal, see the arrowed sections in Figure 6.6 a) below.

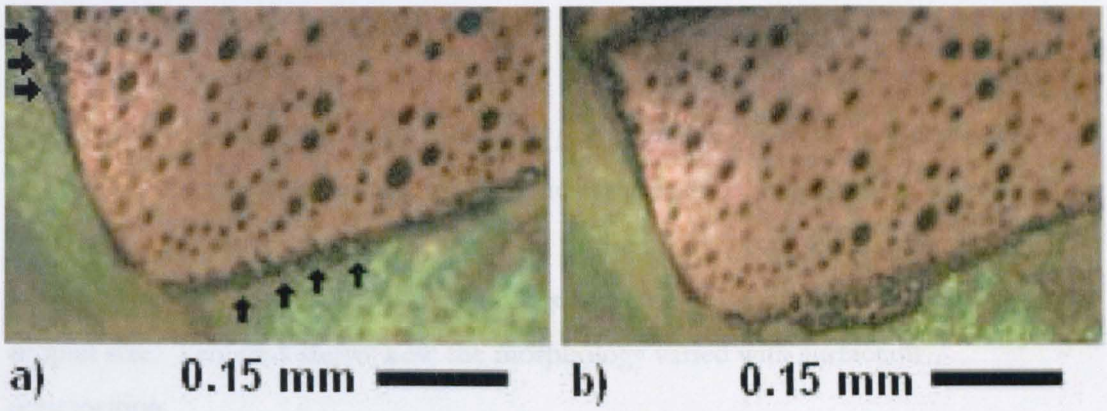

Figure 6.6 Porous single crystal of β-glycine growing from a 60 wt % octanoic acid-in-water emulsion stabilized with 9 wt % of 8:1 Span 20/Brij 30 viewed under crossed polarisers and with a red tint plate to aid crystal distinction. (a) Image taken 23 min after Crystallisation commenced. Note the highly curved growth fronts (arrowed) due to the adhesion of octanoic acid droplets. Many of these droplets become included in the crystal during subsequent growth, as shown in image (b), which was taken 80 s after image (a).

It was found that the highly curved growth fronts develop in time to completely surround the oil droplets, without causing droplet displacement or deformation. The ability of the octanoic acid droplets to adhere to the growing glycine crystals is a consequence of their high surface activity, and the ability of the carboxylic acid head groups to strongly adsorb onto the crystalline structure of the growth faces exposed in the β-polymorph.

The precise conditions to achieve complete droplet encapsulation and individual crystals were found by variation of the surfactant system used and the oil fraction of the emulsion. It was also found that a fenestrated morphology, see Figure 6.8b, could be obtained from the octanoic acid emulsions stabilized with 8:1 Tween 20/Brij 30. This morphology developed from crystals in which oil droplets were partially included, with crystal growth then continuing on either side of the droplets only to produce co-aligned dendrites. These crystals continued to grow laterally to result in joining of these dendrites to form the fenestrated structure as seen in Figure 6.8b. The reduced porosity of these crystals compared to their platelet-type counterparts formed using the Span 20 surfactant is due to

their rapid initial growth in the *b*-direction resulting in fewer droplets becoming included in the growing crystals.

Some combinations of Tween20 and Brij30 gave a greater proportion of this intergrown fenestrated structure, whereas increased Span 20 content would yield more of the platelet-type crystals. Variation of the oil fraction used affected the overall stability of the resulting emulsion but had little effect on the emulsion droplet size. Table 6.3 shows how the morphology varied with surfactant composition.

Table 6.3 Morphology achieved by different surfactant mixtures, all kept at 9%wt of the overall emulsion mixture composition.

% wt Brij 30	% wt Tween 20	% wt Span 20	Morphology
11	89	0	Highly fenestrated, co-aligned growth. Good inclusion of oil droplets over entire sample
44	56	0	Highly fenestrated, co-aligned growth. Begin to see some needles with no complete droplet inclusion, but growth around droplets is evident.
89	11	0	Poor inclusion of oil droplets, co-aligned growth, 50% needles with no inclusion
11	0	89	Good porous single platelet-type crystals. Droplets included. Some intergrowth and secondary nucleation observed.
44	0	56	Best single porous crystals. Latter stages of growth also give some co-aligned fenestrated crystals
89	0	11	Poor inclusion of oil droplets, co-aligned growth, platelet and needles produced.
11	22	67	Reduced emulsion stability, increased number of needles rather than fenestrated growth
22	22	56	Emulsion droplet polydispersity increased, reduced production of porous platelet-type crystals.

The nucleating ability of the non-ionic surfactants, Span 20 and Tween 20, resulted in the crystallisation of the β-polymorph exclusively, whereas formation of the α-polymorph would be expected in the absence of any other nucleating

promoting species. This can be seen from the X-ray diffraction signals that were obtained at 18 ° and 20 °. The aqueous mediated transformation of the β to α-polymorphs was also not observed, even after standing for several days. This shows that the strong surfactant and oil-crystal interactions result in the formation of a protective barrier to this dissolution and transformation mechanism.

The factors controlling the formation of these macroporous crystals relate quite specifically to the emulsion composition. By changing the oil phase to decane, no droplet adhesion is achieved. Acidification to pH 5.5 by addition of HCl does not result in the adhesion of oil droplets, and the surfactant still promotes nucleation of the β-polymorph. Further acidification to pH~3 resulted in the inclusion of 1 or 2 droplets in large μm size needle-like crystals; however this appeared to be simply a consequence of rapid crystalline growth of those particular needles and was not representative of the whole sample. Once again the formation of β rather than γ-glycine crystals illustrated the strong nucleating ability of the Span 20 surfactant.

In these o/w emulsions, the glycine nucleation is induced at the droplet interface by the non-ionic surfactants. Evidence for this includes the observation that crystals can sometimes be seen growing rapidly from this interface, and the fact that the β –phase occurs, rather than the expected α-phase. The latter finding is consistent with previous studies on glycine Crystallisation in w/o emulsions stabilized with non-ionic surfactants[4]. Indeed, even though the Span 20 is a weaker β -phase nucleator than Tween 20, it is still sufficient to hinder the Crystallisation of the γ- and α-polymorphs. By doping Span 20 emulsions with the cosurfactants AOT and α-aminohexadecanoic acid that promote the γ- and α-polymorphs, respectively, no observation of any polymorph other than β was observed. In fact, to achieve significant amounts of α-phase crystals from Span 20 emulsions containing 13.9 % wt aqueous glycine solutions, it was necessary to add 5% of acetic acid to the mixture.

The glycine crystals produced by this method of oil droplet adhesion are single crystalline in nature, as single birefringence colours were observed using polarising optical microscopy, see previous Figure 6.6. This was also confirmed by subsequent x-ray spectra taken over several points of a single platelet. Note here, though, that the divergence of the dendrite branches often led to a series of closely-spaced diffraction spots emanating from diffraction from the same crystallographic plane, see figure 6.7, rather than the single isolated diffraction spots that were seen for the single crystal platelets,.

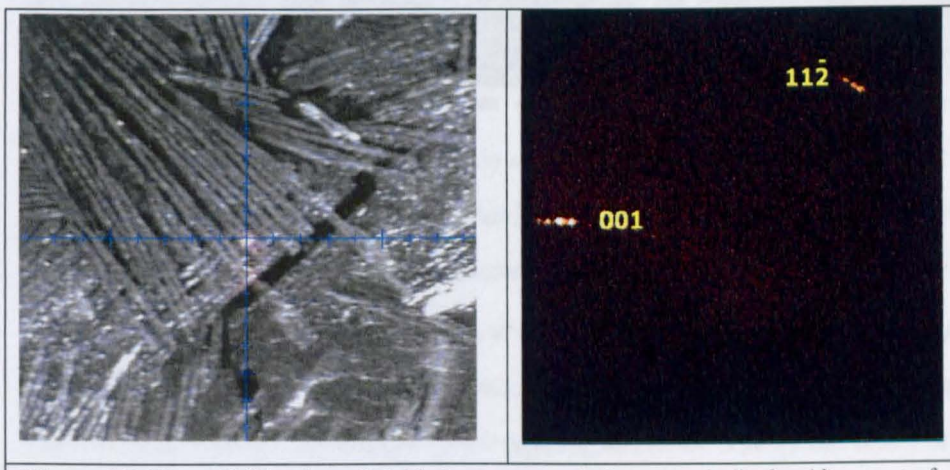

Figure 6.7 X-ray Diffraction of highly inter-woven glycine crystals. Left: Alignment of the beam over an intersecting part of the crystal. Right The resulting diffraction pattern on the area detector, with corresponding peaks labelled.

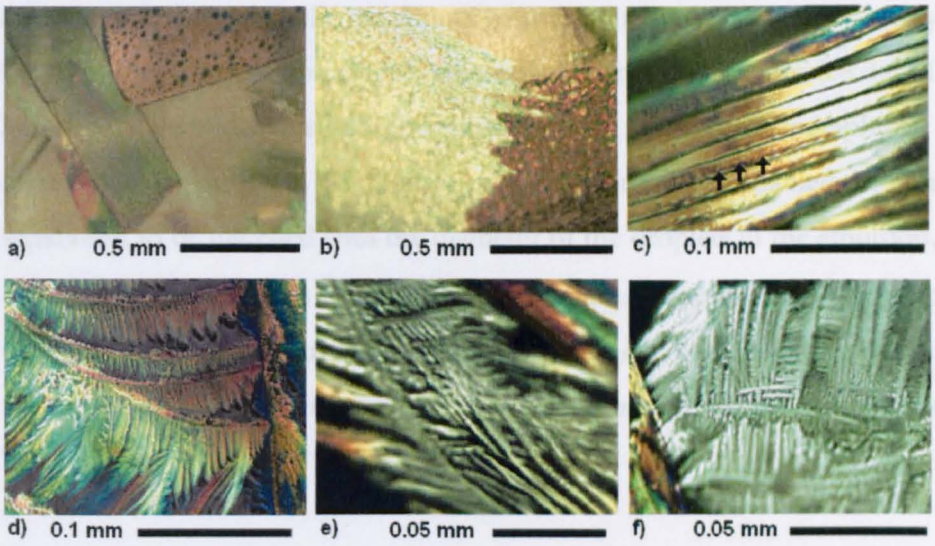

Figure 6.8 showing morphologies produced by octanoic acid in aqueous glycine emulsions a) Large macroporous platelets using a 8:1 Span20/Brij30 mix, b) co-aligned dendritic growth with intergrowth resulting in a fenestrated structure, produced by using a 8:1 Tween20/Brij30 surfactant mix, c) co-aligned dendrites without intergrowth. The droplet diameter ~2.5μm (arrowed) is equal to the spacing between dendrites, d)-f) highly complex woven morphologies where dendritic crystals have intergrown from opposing directions. The crystals shown in c) to f) were grown from octanoic acid emulsions stabilised with 50 wt % for the 8:1 Span 20/Brij 30 mix.

6.5.4 Reduced Droplet Diameter

On increasing the total surfactant concentration to 50 wt % for the 8:1 Span 20/Brij 30 mix, stable emulsions with smaller octanoic acid droplet sizes of 2-5 μm were obtained. These systems produced a more extreme dendritic morphology for β-glycine, see Figure 6.8 c-f.

Growth of these crystals was very rapid, with crystallisation complete within a matter of a minute or two. Typical growth rates for the different morphologies produced for β-glycine are shown in Table 6.4. Initially fine needles of β-glycine nucleated and grew very rapidly along what was determined to be the

crystallographic *b*-direction in these 50wt% surfactant blend emulsions. Once this initial spur had formed, the off-shoots grew from this parent needle-like crystal, thus forming the dendritic crystals so clearly illustrated in Figures 6.8 d-f. This latter growth was discovered to be predominantly in the crystallographic *a*-direction, see Figure 6.9. Close inspection of these crystals enabled the dendrite separation to be matched with the diameter of the droplets in the emulsion, i.e. between 2-5 μm. As can be seen from the included droplets arrowed in Figure 6.8 c, the adhesion and inclusion of the octanoic acid oil droplets are still directing the crystal growth. From this observation, a mechanism for droplet inclusion may be proposed.

Table 6.4 Growth rates of the crystalline morphologies obtained from octanoic acid emulsions

Crystallising system	**Crystalline morphology**	**Growth rate in b direction /μm s^{-1}**	**Growth rate in a direction /μm s^{-1}**
Octanoic acid emulsion	Platelets	3	0.8
Octanoic acid emulsion	Dendrites	62	46
Glycine solution and surfactant mixture	Platelets	0.42	0.65
Glycine solution and surfactant mixture	Needles	16.5	0.11
Glycine solution	Platelets (if formed)	0.004	0.00003
Glycine solution	Needles	25	2
Decane emulsion	Spherical aggregates	35	n/a

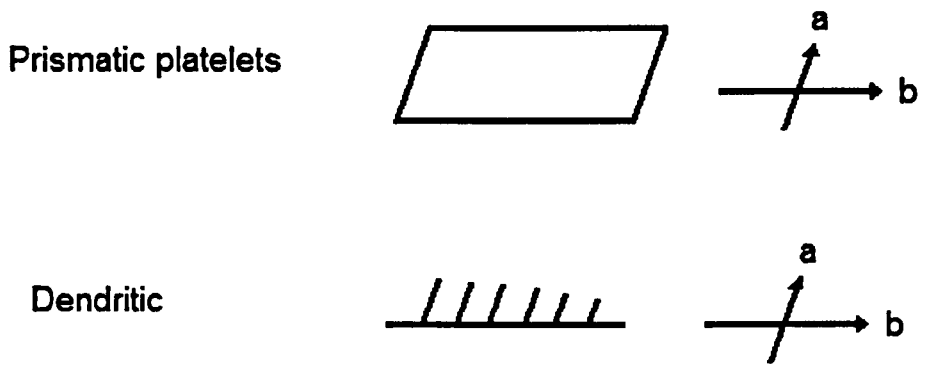

Figure 6.9. Directions of growth assigned to the platelet and dendritic-type β-glycine crystalline growth observed for the octanoic acid o/w emulsions.

Once again, this highly dendritic morphology is unexpected for the low glycine supersaturations in use in these o/w emulsions, and is indicative of the interfacial activity and adhesion properties of the octanoic acid oil phase onto the growing glycine crystals. The increased surfactant concentration required to stabilise these smaller droplets results in a reduced presence of the octanoic acid at the interface, and as such, the resulting number of droplets included into the growing crystal is reduced.

The formation of dendritic morphologies is usually attributed to a concentration gradient at the face of the growing crystal. In our case, though, it is due to the adhesion of the oil droplets rather than any localised fluctuations in the solution concentration. To show that this was the case, once again the oil phase was changed to decane, which does not adhere to the glycine crystals, and as a result no dendritic growth or droplet inclusion was observed; β-polymorph needles simply grew from the emulsion.

The two main factors influencing the growth of these complex crystalline architectures are as follows. Firstly the interfacial activity of the octanoic acid oil phase must be high enough such that strong crystal-oil interactions are possible through hydrogen bonding of the oil's carboxylic acid group to the corresponding

face of the glycine crystal, resulting in incorporation (full or partial) of the oil droplet rather than further glycine molecules into the crystal structure. The surfactants used must be able to allow this interfacial activity, and as such a blend of Span 20 or Tween 20 with the Brij 30 surfactant is required to result in droplet adhesion, whereas a pure Brij 30 stabilised emulsion will yield simple needle-like β-glycine crystals without any morphological modification or droplet inclusion.

The second important factor is that the droplet adhesion must occur on the fastest growing faces for inclusion and morphology modification to occur. As highlighted in Chapter 2, morphological modification occurs when growth is impeded on the fastest growing faces of a crystal. This is readily seen in the macroporous crystals by the change in crystal morphology from the typical β-phase needles elongated in the fast-growing *b*-direction to a more plate-like morphology as the Crystallisation and droplet adhesion proceeds. In contrast, selective adsorption on a slower growing face will merely produce a more asymmetric morphology without droplet inclusion, as in the case of the prismatic-to-needle morphology change observed for L-asparagine monohydrate in octanoic acid o/w emulsions. [65]

Figure 6.10 shows a schematic diagram indicating the mechanism of formation of the macroporous and dendritic β-glycine crystals achieved through emulsion droplet adhesion.

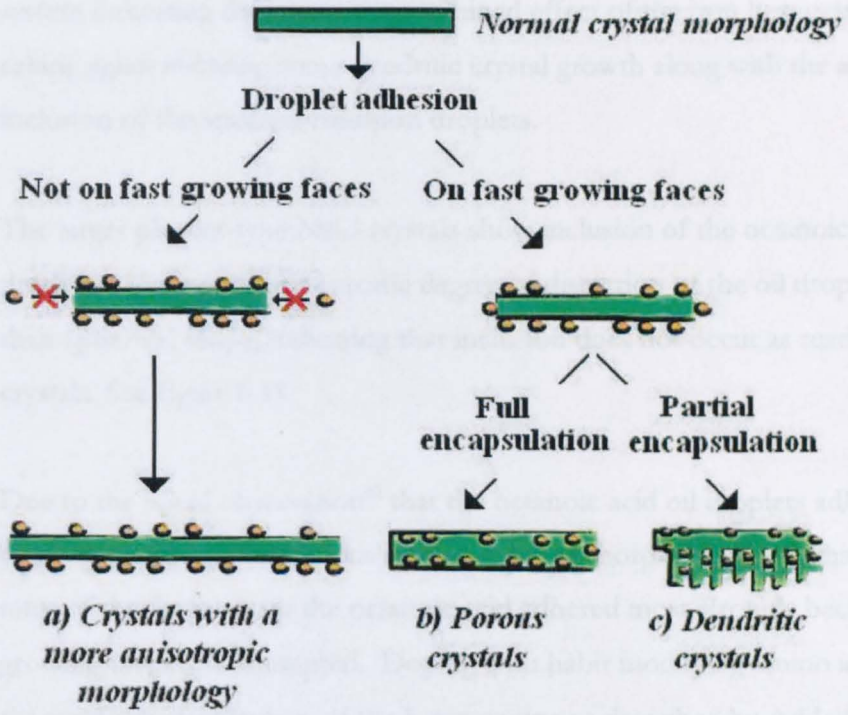

Figure 6.10. Development of Porous and Dendritic Crystals through Emulsion Droplet Adhesion

6.5.5 Other Porous Crystals

Preliminary studies on sodium chloride Crystallisation were conducted from octanoic acid o/w emulsions to determine whether similar complex architectures could be obtained. The choice of sodium chloride was to determine if this method of oil droplet inclusion was specific to amino acids, or if it could be more widely applied to other crystalline species such as ionic salts. To form the NaCl o/w emulsions, a surfactant mixture of 8:1 by weight of Span 20/Brij 30 was used as 9% wt of the total emulsion mixture. This was added to 60 wt % of octanoic acid and 31% wt of an aqueous phase with 42% wt NaCl. Crystallisation was induced by cooling the emulsion from 25 to 20°C. Both the porous single crystals and dendritic crystals are achieved using this system, see Figure 6.11, which is analogous to the one used to obtain the macroporous β-glycine single crystals. For the NaCl crystals, both morphologies are achieved from the same emulsion

system indicating that there is a combined effect of the iron hexacyanate anti-caking agent inducing some dendritic crystal growth along with the adhesion and inclusion of the smallest emulsion droplets.

The larger platelet-type NaCl crystals show inclusion of the octanoic acid oil droplets. However there is some degree of distortion of the oil droplets from their spherical shape, indicating that inclusion does not occur as readily for NaCl crystals. See figure 6.11

Due to the initial observation[65] that the octanoic acid oil droplets adhered strongly to L-asparagine, investigations into altering the morphology such that the growth rates of the faces where the octanoic acid adhered most strongly became fast growing faces was attempted. Doping with habit modifying amino acids to alter the resulting morphology of the L-asparagine as described by Addadi et al[60, 61] was attempted. Production of porous L-asparagine crystals was not possible even when the habit was modified by another amino acid (serine) to increase the platelet type growth. This suggests that systems that did successfully crystallise around the oil droplets were those that had high water solubility so that crystal growth rates were fast.

Attempts were also made to crystallise citric acid in a similar fashion since its high solubility made it an ideal candidate for use with this method. Citric acid is notorious, however, for crystallising in many different morphologies and in this instance the necessary large single crystallites did not form readily enough to result in full droplet inclusion, see Figure 6.11d.

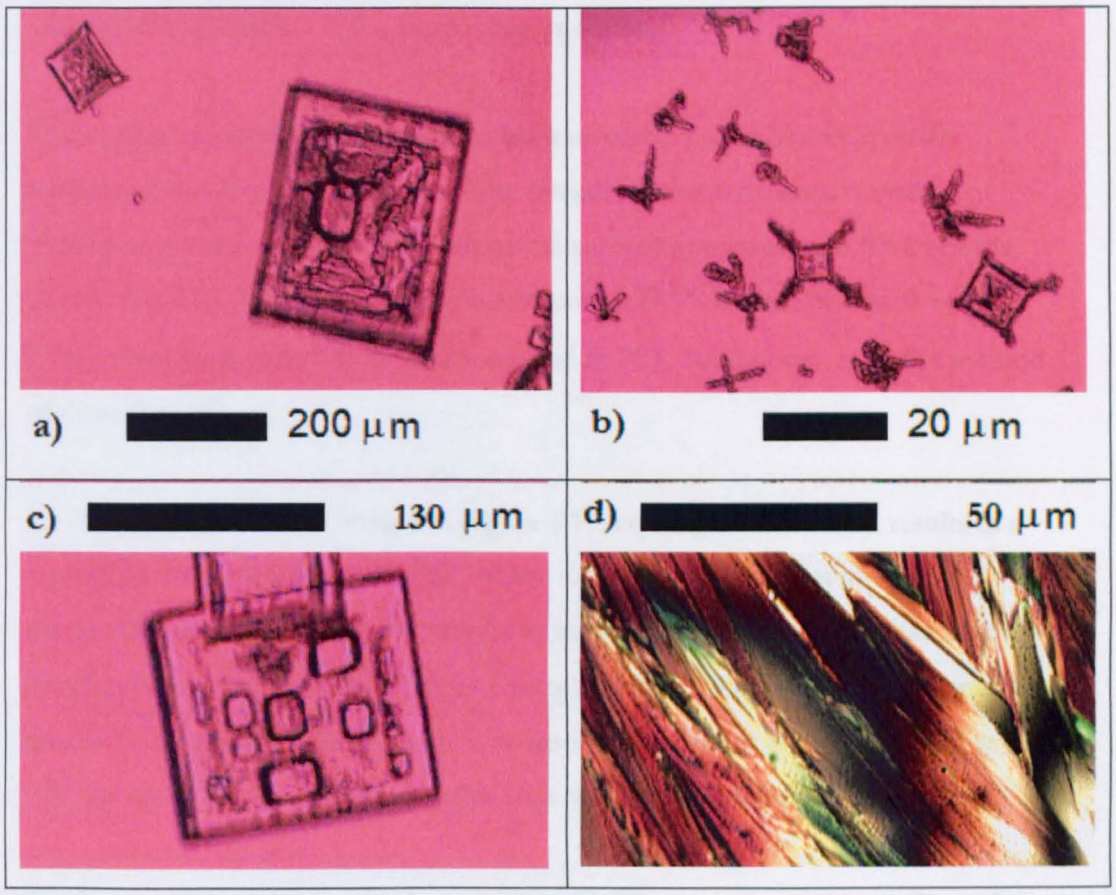

Figure 6.11 a-c) Sodium chloride crystals with modified morphology, d) Citric Acid with oil droplet inclusions.

6.5.6 Crystallisation On Heating In Span 80 W/O Emulsions

The rate of crystallisation of glycine in w/o emulsions stabilised with Span80 could be made to increase with increasing temperature. This is again contrary to the 'textbook' observation that the nucleation rate should decrease on heating. This ability of water in oil (w/o) emulsions stabilized with non-ionic surfactants to undergo a phase inversion to oil in water (o/w) emulsions on cooling is well-known. By exploiting this effect and, by using surfactants that promote nucleation, it was found that highly anomalous Crystallisation behaviour can be achieved. In particular, Crystallisation can be inhibited at the phase inversion

temperature (PIT), allowing systems held at, or slightly above, this temperature to undergo Crystallisation either on heating or cooling.

The system employed for the initial studies used the Tween20 and Span20 surfactants blended in a 5:95 ratio. The overall emulsion mixture consisted of 90%wt of the decane fraction, 5%wt of the surfactant mixture and 5%wt of the glycine solution. The glycine solution comprised 28.5%wt glycine dissolved in UHQ water (resistivity 18mΩ cm) sonicated at 70°C for 2 hours, as in the method of Garetz et al[66].

As can be seen from the images in Figure 6.10, cooling this emulsion results in a mottled texture forming at the PIT, where the ultra low oil-water interfacial tension characteristic of the PIT results in transient structures rather than discrete droplets being observed. Holding at a temperature below this PIT for ~1 minute results in complete inversion to an o/w emulsion. Systems can also be held at this PIT for up to 3 hours and kept in this state without crystallisation occurring.

Further cooling of this inverted emulsion, which is now of o/w type, will result in nucleation and crystallisation of the glycine at around 5 °C in ~1 minute only. The β-glycine polymorph is always crystallised, as expected by the nucleation promotion properties of the Span20/Tween20 surfactants. The β-glycine grows into the expected *b*-axis needle-like crystals. The polymorph was identified by x-ray diffraction of the sample using the D8 WAXS setup as described in chapter 3.

An unusual observation is that on re-heating the emulsion slowly through the PIT, so that the w/o emulsion is regenerated, is that further heating to 24 °C and holding for 5 to 10 minutes results in further glycine crystallisation occurring within the regenerated water droplets, see Figure 6.12 d, and Figure 6.13. This is highly unexpected as the supersaturation has been relieved both by the prior crystallisation in the o/w phase at lower temperatures and the subsequent heating, and as such the driving force towards further nucleation is significantly reduced.

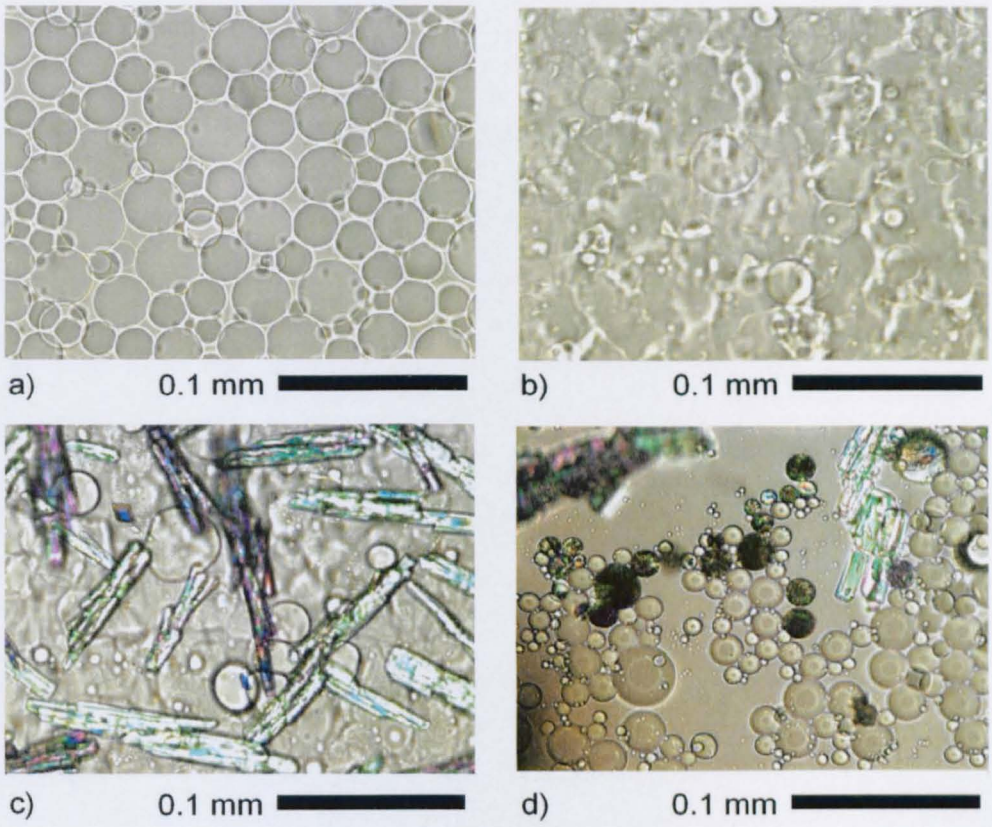

Figure 6.12. Optical micrographs through crossed polarisers of 27.4 wt % glycine solutions in Tween 20:Span 20 (5:95) 90 wt % decane emulsions: (a) w/o emulsion at T = 24 °C; (b) on cooling at 1 °C min^{-1}, the system starts to invert at T = 7 °C. (c) On further cooling to 5 °C, glycine crystals grow in the o/w emulsion, and (d) on heating at 1 °C min^{-1}, the system reinverts, and glycine begins to crystallizes in the w/o droplets on holding at 24 °C.

Pull to open

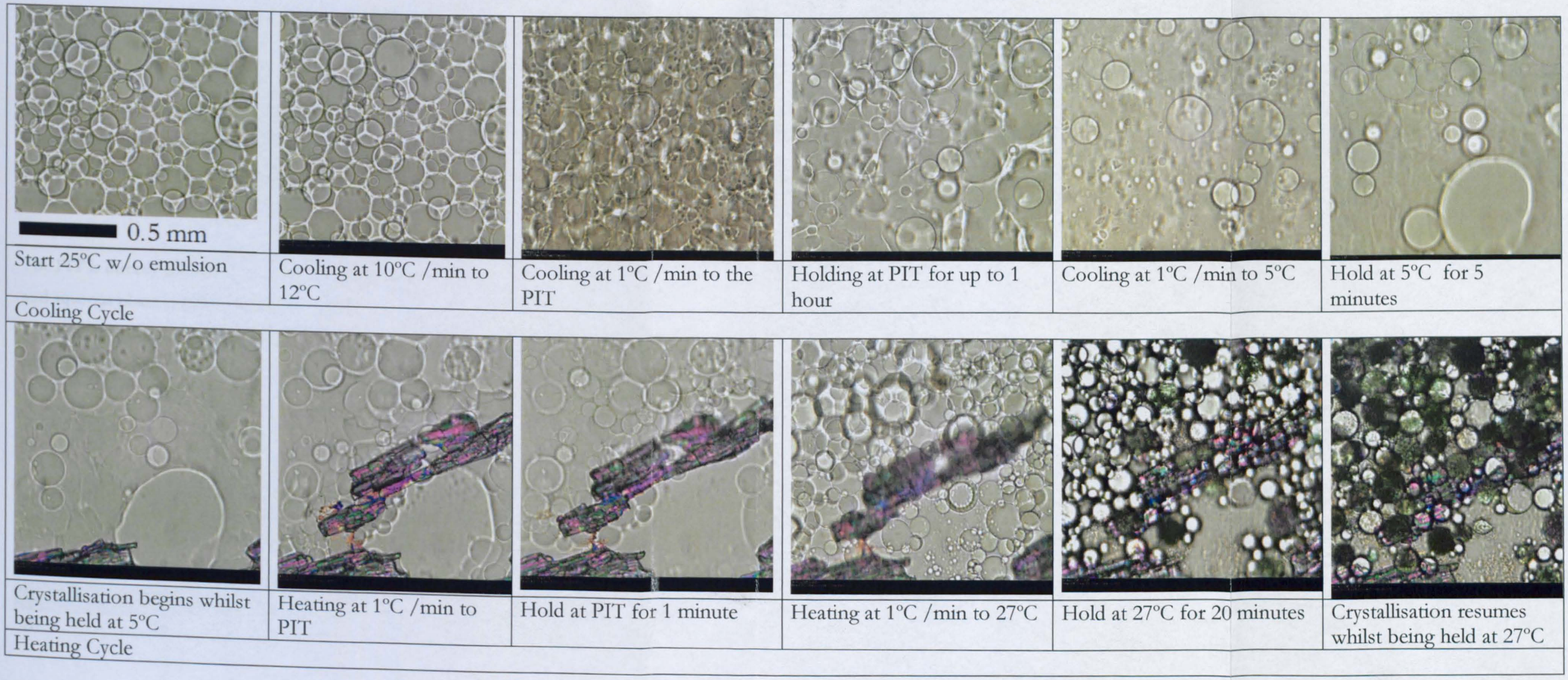

Figure 6.13 Stages of crystal growth on cooling and heating cycle of *27.4 wt % glycine solutions in Tween 20:Span 20 (5:95) 90 wt % decane emulsions, taken from optical micrographs through crossed polarizers. Scale applies to all images in the series.*

Another crucially important observation is that at, or just above, the PIT nucleation is not observed for up to 3 hours, despite the increase in supersaturation on cooling the emulsified solution from ambient to this temperature.

These observations are not just specific to this particular emulsion blend. Comparable observations were made for emulsions consisting of Tween20 / Span20 ratios of 1:99 and 10:90 by weight, decane fractions of 0.7 and 0.6, and reduced glycine solution concentrations of 22.2% wt.

The PIT is directly related to the blend of surfactants used, provided that the oil and aqueous phase remain constant. Therefore, by variation of the % Tween20 in the surfactant blend, the PIT and also the length of time that this state could be maintained was altered, as can be seen in Table 6.5.

Table 6.5 Surfactant blend used and the resulting PIT

%Tween20	%Span20	HLB	PIT/°C	Time stable at PIT/min
1	99	8.6	8	40 to 180
5	95	9.0	10	~20
10	90	9.4	12	< 2

This variation in the PIT occurs due to the HLB value of Tween20 being greater than that of Span20, so upon increasing the % of Tween20 in the blend there is a corresponding rise in the HLB value of the surfactant blend. As the HLB value increases, the PIT decreases.

Oil fractions of >0.6 were used for these studies, since for oil fractions below this value the resulting emulsion was very viscous and did not clearly show the phase inversion. Indeed, the higher the oil fraction used, the easier the crystallisation and phase inversion process was to observe simply due to the reduced droplet

density when viewed under the microscope. Another advantage of using higher oil fractions was that when the emulsion was heated to re-invert back to a w/o emulsion, the reformation of the water droplets was facilitated by smaller amounts of water to emulsify. Oil fractions of <0.7 did not yield a true emulsion on re-inversion from o/w to w/o, and often the previous transformation from w/o to o/w was catastrophic, i.e. non-reversible.

6.5.7 Crystallisation Inhibition At The PIT – Minimal Interfacial Nucleation Temperature (MIN)

The lack of observed crystallisation at the PIT can be correlated to the induction time for nucleation, τ. This induction time is simply a sum of two main time periods:

- the nucleation time and
- the time required for crystal growth of the nuclei to detectable dimensions.

For a rate-limiting nucleation step, $\tau = N/J$, where J is the nucleation rate and N is the number of particles per unit volume required for detection of the solid phase, which can be taken as a constant for a given detection technique.

In these systems, since crystal growth occurs rapidly for both the w/o and o/w case (for instance the time taken for complete crystallisation to occur within an aqueous droplet is less than 2 seconds), it can be assumed that the induction time gives a reasonable measure of 1/nucleation rate.

By cooling an emulsion to a given temperature and holding at this temperature until crystallisation is observed, an induction time for that crystallisation is established. Subsequent repeating of these experiments at different temperatures resulted in the data set shown below in Figure 6.14. It can be seen that at, and

slightly above, the PIT there is a large increase in the induction time. The associated large error bars either side of the PIT occur because of the large gradient of the curve in these regions. A slight fluctuation in temperature or variation in composition between samples will then result in a significantly different nucleating ability and so larger error bars will occur in this region.

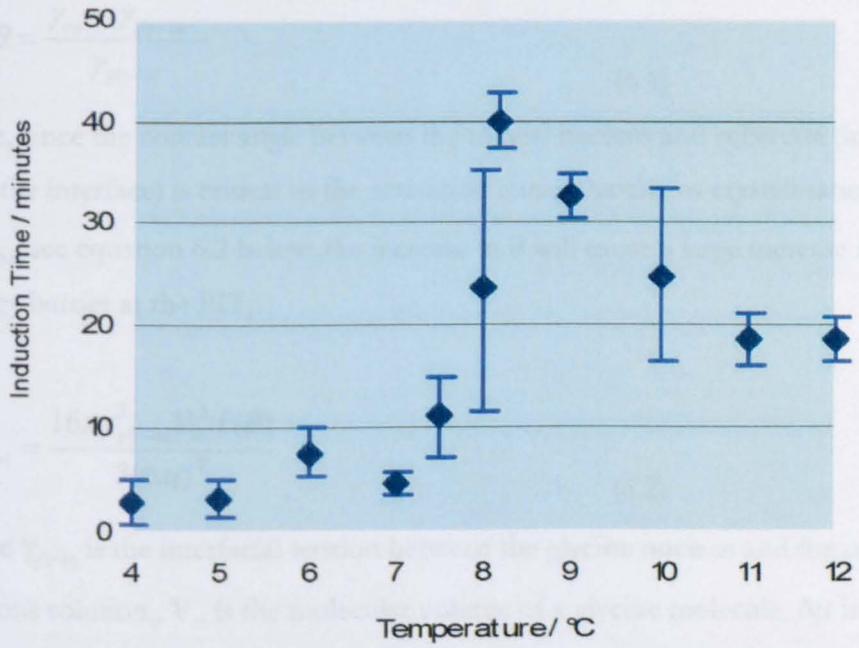

Figure 6.14 Graph of Crystallisation induction time, τ, versus temperature for 27.4 wt % glycine solutions in Tween 20:Span 20 (1:99) 90 wt % decane emulsions, showing the maximum in induction time at/ near the PIT. Indeed, even at 24 °C, τ is below the value at the PIT, despite the 16 °C temperature increase. For emulsions with an increased proportion (5 or 10%) of the Tween 20 nucleator, the induction times are reduced; however, a maximum induction time is still always observed at/ near the PIT.

These findings were highly unexpected. An extremely rapid rise in the nucleation rate, J, and hence rapid reduction in τ, is expected on cooling glycine solutions, owing to the associated increase in supersaturation, $\Delta\mu$, the driving force for crystallisation.[67] In fact, classical nucleation theory predicts a huge increase in nucleation rate upon reducing temperature for this system, by a factor of $\sim 10^{20}$ between 24 and 8°C[68] This predicted value is achieved using a θ value of 61°,

consistent with the observed nucleation rate at 24 °C, together with values of $\gamma_{gly\text{-}aq}$ = 35 mN m^{-1} [69] and γ_{ow} = 22 mN m^{-1}.

From Young's equation, see equation 6.1, it can be surmised that at the PIT the ultra low interfacial tension, γ_{ow}, occurring at this point will result in an increase in the interfacial contact angle, θ, between the interface and the glycine nucleus.

$$\cos\theta = \frac{\gamma_{ow} - \gamma_{gly-surf}}{\gamma_{gly-aq}} \qquad (6.1)$$

Then, since the contact angle between the critical nucleus and substrate (in this case the interface) is critical to the activation energy barrier to crystallisation, $\Delta G^*_{het,}$ see equation 6.2 below, the increase in θ will cause a large increase in this energy barrier at the PIT,

$$\Delta G^*_{het} = \frac{16\pi\gamma^3_{gly-aq}V_m^2 f(\theta)}{3(\Delta\mu)^2} \qquad (6.2)$$

where $\gamma_{gly\text{-}aq}$ is the interfacial tension between the glycine nucleus and the parent aqueous solution,, V_m is the molecular volume of a glycine molecule, Δμ is the supersaturation, f(θ) is a function of the contact angle between this nucleus and the interface of the droplet.

As the value of ΔG^*_{het} is increased at the PIT, the nucleation rate *J* will decrease exponentially according to equation 6.3:

$$J \propto \exp\left(\frac{-\Delta G^*_{het}}{kT}\right) \qquad (6.3)$$

By using classical nucleation theory and inputting values of $\gamma_{gly\text{-}aq}$ = 35 mN m^{-1} [69] and γ_{ow} = 22 mN m^{-1} at 24°C,[63] the contact angle can be estimated[70] to increase from ~61 to 97°; this explains the highly anomalous Crystallisation kinetics observed.

Another kinetic effect occurring at/close to the PIT is the transitory nature of the droplets formed. Since the interfacial tension is so low, droplets can form and disperse very rapidly at very little energy cost to the system and as such there is no stable interface for nucleation to occur upon. This will also limit the formation of a critical nucleus if the timescale for its formation is greater than the time for which the transient interface is present.

Above the PIT, θ is decreasing, sufficiently so in this case to outweigh any increase in supersaturation. Hence induction times decrease above the PIT. Immediately below the PIT, there is a rapid reduction in the induction time observed due to the increase in γ_{ow} and hence decrease in θ, and also the increase in supersaturation on cooling. So, the expected maximum in the induction time is always at, or just slightly above the PIT.

The crystals that eventually develop at/close to the PIT have an unusual morphology, consisting of spherical needle aggregates with some elongated crystal offshoots, see Figure 6.15. So this morphology is a unique combination of those observed above and below the PIT.

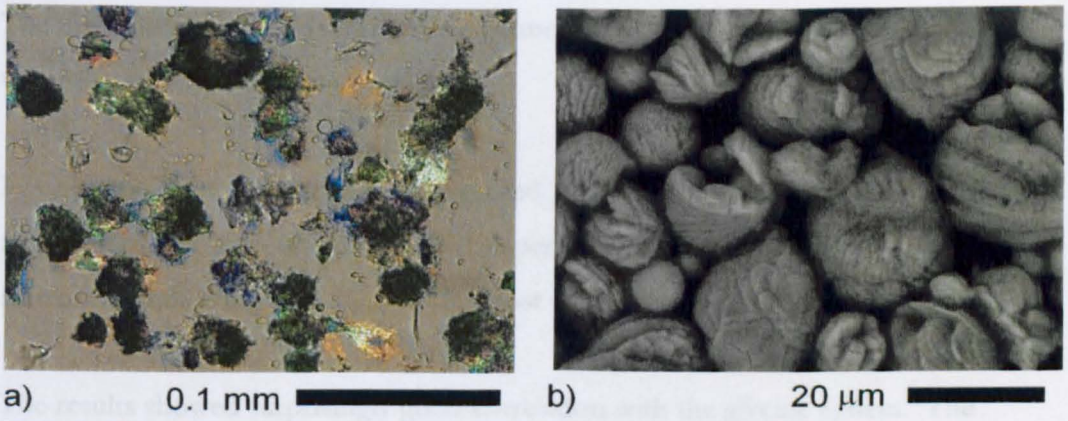

Figure 6.15 (a) Scanning electron micrographs showing (a) the unusual morphology of glycine crystals grown at the phase inversion for a Tween 20:Span 20 (1:99) system, and (b) the spherical aggregate morphology grown at higher temperatures from the w/o emulsions.

6.5.7 Extension Of The MIN Theory To Other Systems.

Investigations were pursued as to whether this anomalous Crystallisation rate behaviour could be observed in an aqueous L-asparagine system. This system was chosen because L-asparagine monohydrate has a single polymorph that was not templated by the Tween 20/ Span 20 surfactant system used. Then by adding different interfacial nucleators, we hoped to control both the resulting crystal morphology, in and the nucleation rate. Consequently a variety of morphology controlling additives were tested to determine whether Crystallisation rate inhibition would occur at the PIT if the additives nucleated the asparagine at the droplet interface.

L-asparagine has a solubility 10 times lower than glycine, so extremely high supersaturations of 400 to 900% were used to compare the minimal interfacial nucleation at the PIT theory on an equal weight of solute basis. A range of additives were tested as follows. The additives were first dissolved in chloroform at a concentration of 1% weight and then 20 µl of this solution was spread on top of a 400% supersaturated L-asparagine aqueous solution at 25 °C to see if the additives promoted L-asparagine monohydrate nucleation. These solutions were left at room temperature and the appearance of crystalline material was awaited. The most promising nucleation-inducing molecules were octadecanoic acid, tricontanoic acid, and hexadecylamine.

From these, three emulsions were prepared. Octadecanoic acid was then chosen for further study since the nucleation properties appeared unhindered by emulsion formation, indicating that this was the most interfacially-active additive.

The results showed surprisingly good correlation with the glycine system. The phase inversion temperature was now elevated slightly to ~14°C and the maximum induction times occurred at and slightly above this temperature, see Figure 6.16. The supersaturation of L-asparagine monohydrate in these systems was 600% at 25 °C.

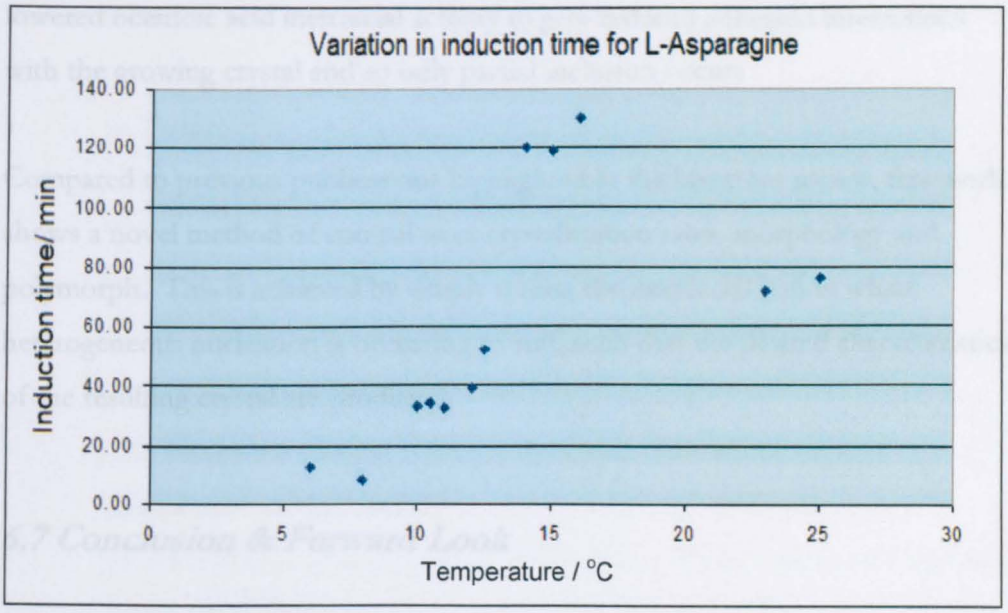

Figure 6.16. Induction time for L-Asparagine phase-inverting emulsions with added nucleating agent, octadecanoic acid.

As can be seen from these data, a carefully selected additive can induce crystallisation of a desired morphology, whilst the control of the nucleation rate is achieved by the varying oil-water interfacial tension of the phase-inverting emulsion.

6.6 Summary Discussion

Porous and dendritic, intricate morphology crystals of glycine can be obtained by the novel and simple method of emulsion droplet adhesion. This is achieved by using a polar oil as the dispersed phase that interacts strongly with the crystallising material. It was then found that porous single crystals could be produced with the pore diameters (~10-25 μm) corresponding to the emulsion droplet diameters. The glycine crystals produced by this method of oil droplet adhesion are single crystalline in nature, by observation of the birefringence colours using polarising optical microscopy, and confirmed by subsequent x-ray diffraction taken over several points of a single platelet. A complex dendritic morphology could also be achieved by using higher surfactant concentrations of 50 wt%. This results in a

lowered octanoic acid interfacial activity to give reduced adhesion interactions with the growing crystal and so only partial inclusion occurs

Compared to previous publications highlighted in the literature review, this work shows a novel method of control over crystallisation rates, morphology and polymorph. This is achieved by simply tuning the interfacial region where heterogeneous nucleation is occurring to suit, such that the desired characteristics of the resulting crystal are produced.

6.7 Conclusion & Forward Look

In conclusion, this emulsion droplet adhesion methodology may provide a simple, controllable route for production of porous and high surface area, intricate morphology single crystals of many other materials, providing suitable surface-active nucleating agents and strongly adhering co-surfactants can be found.

The phenomenon of minimal interfacial nucleation in phase-inverting systems is demonstrated for the first time for the case of glycine and L-asparagine monohydrate crystallisation. This work shows that the minimal interfacial nucleation temperature is expected to be at, or just above, the PIT. The morphology of crystals grown at/near the PIT is also an unusual combination of those observed at and below the PIT. This methodology provides considerable control over nucleation rates and may offer a paradigm shift in controlled Crystallisation strategies through the use of tuneable contact-angle nucleators.

References

1 W. B. Hillig and D. Turnbull, *Journal of Chemical Physics*, 1956, ***24***, 914.

2 J. Eastoe and B. Warne, *Current Opinion in Colloid & Interface Science*, 1996, ***1***, 800.

3 R. J. Davey and T. Hirai, *Journal of Crystal Growth*, 1997, ***171***, 318.

4 K. Allen, R. J. Davey, E. Ferrari, C. Towler, G. J. Tiddy, M. O. Jones, and R. G. Pritchard, *Crystal Growth & Design*, 2002, ***2***, 523.

5 J. A. Thomas, L. Seton, R. J. Davey, and C. E. DeWolf, *Chemical Communications*, 2002, 1072.

6 J. Eastoe and A. R. Cox, *Colloids and Surfaces a-Physicochemical and Engineering Aspects*, 1995, ***101***, 63.

7 J. Eastoe, S. Stebbing, J. Dalton, and R. K. Heenan, *Colloids and Surfaces a-Physicochemical and Engineering Aspects*, 1996, ***119***, 123.

8 W. F. C. Sager, *Current Opinion in Colloid & Interface Science*, 1998, ***3***, 276.

9 G. D. Rees, R. Evans-Gowing, S. J. Hammond, and B. H. Robinson, *Langmuir*, 1999, ***15***, 1993.

10 A. Agostiano, M. Catalano, M. L. Curri, M. Della Monica, L. Manna, and L. Vasanelli, *Micron*, 2000, ***31***, 253.

11 M. L. Curri, A. Agostiano, L. Manna, M. Della Monica, M. Catalano, L. Chiavarone, V. Spagnolo, and M. Lugara, *Journal of Physical Chemistry B*, 2000, ***104***, 8391.

12 M. Lade, H. Mays, J. Schmidt, R. Willumeit, and R. Schomacker, *Colloids and Surfaces a-Physicochemical and Engineering Aspects*, 2000, ***163***, 3.

13 P. Calandra, A. Longo, and V. T. Liveri, *Colloid and Polymer Science*, 2001, ***279***, 1112.

14 J. Zhang, L. D. Sun, C. Qian, C. S. Liao, and C. H. Yan, *Chinese Science Bulletin*, 2001, ***46***, 1873.

15 M. Summers, J. Eastoe, and S. Davis, *Langmuir*, 2002, ***18***, 5023.

16 S. Xu, H. C. Zhou, J. Xu, and Y. D. Li, *Langmuir*, 2002, ***18***, 10503.

17 G. Hota, S. Jain, and K. C. Khilar, *Colloids and Surfaces a-Physicochemical and Engineering Aspects*, 2004, ***232***, 119.

18 J. Xu and Y. D. Li, *Journal of Colloid and Interface Science*, 2003, ***259***, 275.

19 G. N. Karanikolos, P. Alexandridis, G. Itskos, A. Petrou, and T. J. Mountziaris, *Langmuir*, 2004, ***20***, 550.

20 C. Q. Xu, Z. C. Zhang, H. L. Wang, and Q. Ye, *Materials Science and Engineering B-Solid State Materials for Advanced Technology*, 2003, ***104***, 5.

21 C. L. Kitchens, M. C. McLeod, and C. B. Roberts, *Journal of Physical Chemistry B*, 2003, ***107***, 11331.

22 J. Perez-Conde and A. K. Bhattacharjee, *Physical Review B*, 2003, ***67***, art. no.

23 J. D. Holmes, D. M. Lyons, and K. J. Ziegler, *Chemistry-a European Journal*, 2003, ***9***, 2144.

24 R. A. M. Hikmet, D. V. Talapin, and H. Weller, *Journal of Applied Physics*, 2003, ***93***, 3509.

25 B. Wang, F. Gao, B. He, D. B. Zhang, H. M. Cheng, J. M. Ma, and L. M. Qi, *Acta Physico-Chimica Sinica*, 2003, ***19***, 21.

26 M. Rajamathi and R. Seshadri, *Current Opinion in Solid State & Materials Science*, 2002, ***6***, 337.

27 Y. F. Chen and Z. Rosenzweig, *Nano Letters*, 2002, ***2***, 1299.

28 H. F. Gao, Y. Q. Zhao, S. K. Fu, B. Li, and M. Q. Li, *Colloid and Polymer Science*, 2002, ***280***, 653.

29 H. Ohde, M. Ohde, F. Bailey, H. Kim, and C. M. Wai, *Nano Letters*, 2002, ***2***, 721.

30 B. A. Simmons, S. C. Li, V. T. John, G. L. McPherson, A. Bose, W. L. Zhou, and J. B. He, *Nano Letters*, 2002, ***2***, 263.

31 W. Wang and S. A. Asher, *Journal of the American Chemical Society*, 2001, ***123***, 12528.

32 B. Liu, H. P. Li, C. H. Chew, W. X. Que, Y. L. Lam, C. H. Kam, L. M. Gan, and G. Q. Xu, *Materials Letters*, 2001, ***51***, 461.

33 L. D. Sun, X. F. Fu, C. Qian, C. S. Liao, and C. H. Yan, *Chemical Journal of Chinese Universities-Chinese*, 2001, ***22***, 879.

34 J. P. Cason, M. E. Miller, J. B. Thompson, and C. B. Roberts, *Journal of Physical Chemistry B*, 2001, ***105***, 2297.

35 B. Liu, G. Q. Xu, L. M. Gan, C. H. Chew, W. S. Li, and Z. X. Shen, *Journal of Applied Physics*, 2001, ***89***, 1059.

36 E. C. Hao, H. P. Sun, Z. Zhou, J. Q. Liu, B. Yang, and J. C. Shen, *Chemistry of Materials*, 1999, ***11***, 3096.

37 R. P. Bagwe, B. K. Mishra, and K. C. Khliar, *Journal of Dispersion Science and Technology*, 1999, ***20***, 1569.

38 A. Manna, B. D. Kulkarni, K. Bandyopadhyay, and K. Vijayamohanan, *Chemistry of Materials*, 1997, ***9***, 3032.

39 S. Y. Chang, L. Liu, and S. A. Asher, *Journal of the American Chemical Society*, 1994, ***116***, 6739.

40 S. Sadasivan, D. Khushalani, and S. Mann, *Chemistry of Materials*, 2005, ***17***, 2765.

41 L. Addadi, D. Joester, F. Nudelman, and S. Weiner, *Chemistry-a European Journal*, 2006, ***12***, 981.

42 W. B. Yue, A. N. Kulak, and F. C. Meldrum, *Journal of Materials Chemistry*, 2006, ***16***, 408.

43 R. J. Park and F. C. Meldrum, *Journal of Materials Chemistry*, 2004, ***14***, 2291.

44 E. Loste, R. J. Park, J. Warren, and F. C. Meldrum, *Advanced Functional Materials*, 2004, ***14***, 1211.

45 F. C. Meldrum, *International Materials Reviews*, 2003, ***48***, 187.

46 E. Loste and F. C. Meldrum, *Chemical Communications*, 2001, 901.

47 R. Seshadri and F. C. Meldrum, *Advanced Materials*, 2000, ***12***, 1149.

48 F. C. Meldrum and R. Seshadri, *Chemical Communications*, 2000, ***29***.

49 S. Mann, *Advanced Materials*, 1996, ***8***, 183.

50 S. Mann and G. A. Ozin, *Nature*, 1996, ***382***, 313.

51 S. Mann, *Journal of Materials Chemistry*, 1995, ***5***, 935.

52 B. R. Heywood and S. Mann, *Advanced Materials*, 1994, ***6***, 9.

53 S. Mann, *Nature*, 1991, ***349***, 285.

54 C. E. Fowler, M. Li, S. Mann, and H. C. Margolis, *Journal of Materials Chemistry*, 2005, ***15***, 3317.

55 J. D. Hopwood and S. Mann, *Chemistry of Materials*, 1997, ***9***, 1819.

56 L. Addadi, A. Berman, J. Moradianoldak, and S. Weiner, *Abstracts of Papers of the American Chemical Society*, 1989, ***197***, 115.

57 L. Addadi, A. Berman, J. Moradianoldak, and S. Weiner, *Croatica Chemica Acta*, 1990, ***63***, 539.

58 L. Addadi and S. Weiner, *Angewandte Chemie-International Edition in English*, 1992, ***31***, 153.

59 N. B. J. Hetherington, A. N. Kulak, K. Sheard, and F. C. Meldrum, *Langmuir*, 2006, ***22***, 1955.

60 Z. Berkovitchyellin, L. Addadi, M. Idelson, M. Lahav, and L. Leiserowitz, *Angewandte Chemie-International Edition in English*, 1982, ***21***, 631.

61 L. Addadi, Z. Yellin, I. Weissbuch, M. Lahav, and L. Leiserowitz, *Molecular Crystals and Liquid Crystals*, 1983, ***96***, 1.

62 L. Addadi and S. Weiner, *Molecular Crystals and Liquid Crystals*, 1986, ***134***, 305.

63 C. S. Towler, R. J. Davey, R. W. Lancaster, and C. J. Price, *Journal of the American Chemical Society*, 2004, ***126***, 13347.

64 M. Parmar, *BACG Annual Conference*, Heriot-Watt University, 2006.

65 S. J. Cooper, *Crystengcomm*, 2001, art. no.

66 Garetz, B. A.; Matic, J.; Myerson, A. S. *Phys. Rev. Letts.* 2002, ***89***, Art. No. 175501.

67 $\Delta\mu = kT \ln \frac{c}{c_{sat}}$, where c and c_{sat} are the actual and saturation solute concentrations, respectively.

68 A θ value of 61°, consistent with the observed nucleation rate at 24 °C, is used for this calculation, together with values of $\gamma_{gly\text{-}aq}$ = 35 mN m-1 6 and γ_{ow} = 22 mN m^{-1}. However, irrespective of the precise value used, a dramatic increase in nucleation rate is always predicted.

69 The $\gamma_{gly\text{-}aq}$ value has not been determined. However, a value of 40 mN m^{-1} has been given for glycine in aqueous ethanol solutions. See: Walton, A. G. Formation and Properties of Precipitates; Wiley and Sons: New York, 1967. The greater solubility of glycine in water compared to that in ethanol is expected to provide an interfacial tension value lower than this.

70 This calculation results in a rather low value of $\gamma_{gly\text{-}surf}$ = 5 mN m^{-1}, which may reflect the inability of classical heterogeneous nucleation theory to model interfacial Crystallisation in emulsions.

Chapter 7

7.1 Conclusion Of This Work

The work published herein has shown a novel method of exploration of the early stages of heterogeneous nucleation using emulsions as vessels of confinement. It has been demonstrated that with careful choice of surfactant and co-surfactant additives that the resulting crystalline material may be controlled. The ability to choose polymorph, morphology, inclusions into single crystals and variation of the rate of nucleation have all been demonstrated.

7.2 Review Of Thesis Aims & Objectives

The aims of this thesis were to expand and add to the growing knowledge and models of the initial stages of crystallisation, particularly the nucleation step.

During the course of this investigation the effect of interfacial curvature on the epitaxial match between substrate and crystal nucleus has been shown to be of vital importance, and the extent of this effect ties in with classical nucleation theory predictions for the convex nucleus achieved when using w/o emulsions. This is a step forward from previous investigations carried out under Langmuir monolayers and carries on from previous work in the field, considering the convex nucleus grown on o/w emulsion droplets.

Extending this convex nucleus to the very limit of curvature where a critical nucleus is unable to form due to insufficient crystallisable material has led to the first direct measurement of the critical nucleus size for water, and has extended classical nucleation theory to account for the effects observed when considering minute crystals confined by microemulsions.

The effects of an interface upon a crystalline nucleus have to date remained largely unexploited, particularly when considering the degree of control over the resulting crystalline material that is achievable. The ability to exploit the ability of interfacially active additives to achieve an unstable polymorph and modify the morphology of the resulting crystals has been demonstrated. Further advances resulting in droplet adhesion and inclusion into a single crystal have yielded a novel method of achieving complex single crystalline architectures without the need for a solid template. This takes a step closer to mimicking the single crystalline materials formed by nature, and understanding the method by which such materials could be formed.

The effects of a highly unstable nucleating interfacial region achieved at the PIT have not been previously investigated, and it has been shown that highly anomalous nucleation inhibition is possible under these conditions. This may provide a method of tuning nucleation rates, allowing unprecedented control over systems at high supersaturations.

7.3 Suggestions Of Further Work

The work carried out in this thesis provides a brief introduction to the area of using surface and interfacial techniques to control crystallisation. There is much scope for extension and further investigation into all of the phenomena described herein.

The crystallisation behaviour of ice in w/o emulsions described in chapters 4 and 5, have provided an excellent test bed for the application of classical nucleation theory to systems with increased interfacial curvature. Furthermore, the first direct measurement of the critical nucleus has been possible for the case of ice. This work could be extended to systems where the crystallising material was a solute in the aqueous phase.

Polymorph selection using carefully chosen interfacially-active additives results in the growth of a chosen form of a crystal, which can be different to those normally generated in the bulk phase. This is shown in this work by the non-ionic Span and Tween surfactants inducing nucleation of the less stable β-polymorph of glycine. Although it is true that seeding at the correct amounts will yield a good result in terms of crystal size and polymorph, this method is not completely fail safe and can result in an inability to generate a desired polymorph should conversion of the seeding material change to a more stable one. A classic example of this was that of the pharmaceutical anti-AIDS drug, Ritanovir. By using a heterogeneous nucleating additive that does not contaminate the bulk crystalline material, this drawback of self-seeding was effectively avoided.

The strong relationship between the interfacial tension and the resulting nucleation rate has shown that unprecedented control over crystallisation rates can be achieved in systems with an interfacial tension that varies widely with temperature. In particular, the strategy of using phase-inverting emulsions stabilized with non-ionic surfactants to induce interfacial nucleation provides a relatively simple, tuneable method of controlling nucleation rates over a wide temperature range, particularly since the PIT and maximum oil-water interfacial tension values are readily varied by using different oil and surfactant blends. This strategy may provide a generic method of controlling emulsion nucleation rates, provided the inhibition mechanism is operative on doping the systems with co-surfactants that direct the nucleation to the required polymorph and morphology.[1-3] In this manner, it is hoped that all the non-classical crystallisation rate behaviours shown in figure 7.1 b)-d) might be achievable.

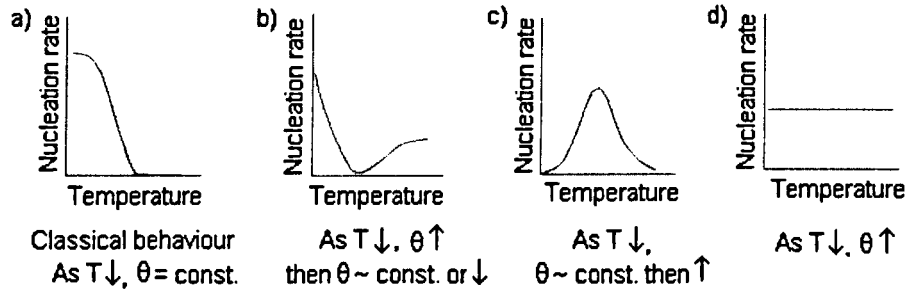

Figure 7.1 shows the possible variations of nucleation rate behaviour achievable using a system where the interfacial contact angle varies with temperature.

Furthermore, the intriguing recent finding[4] that water-oil interfacial tensions can decrease to ~0 mN m^{-1} on cooling in the presence of ionic surfactants, provided the oil undergoes surface freezing, suggests that tuneable nucleation rates may also be possible using these systems. Such systems may be advantageous in that no phase inversion occurs, so the crystals would always be growing in the continuous aqueous phase, albeit with hopefully highly modified crystallisation rates.
The ability to tune and control the nucleation step of crystallisation is of the utmost importance, as this provides a mechanistic approach to tuning of crystal size, and a method of keeping supersaturated solutions from crystallising, even at relatively high levels of supersaturation. Nucleation rate control is expected to produce batch crystals of a well-defined size, where by having a fast nucleation step for a limited time, the many nuclei generated at the same instant will all grow at equal rates resulting in many crystals of a given size. Conversely, by generating only a few nuclei and then effectively 'switching off' nucleation, these few nuclei will grow to a much larger size since that is then the only way to relieve the supersaturation of the system.

The octanoic acid emulsion droplet adhesion studies detailed in Chapter 5 showed that unusual macroporous single crystals and dendritic morphologies of β-glycine crystals and sodium chloride could be produced. Preliminary studies to investigate the application of forming macroporous crystals by this method to produce a porous collagen scaffold have been undertaken. Despite the initial

difficulty due to the increased viscosity of the emulsions produced, a collagen network was formed from a liquid crystalline phase, and can be seen in figure 6.2.

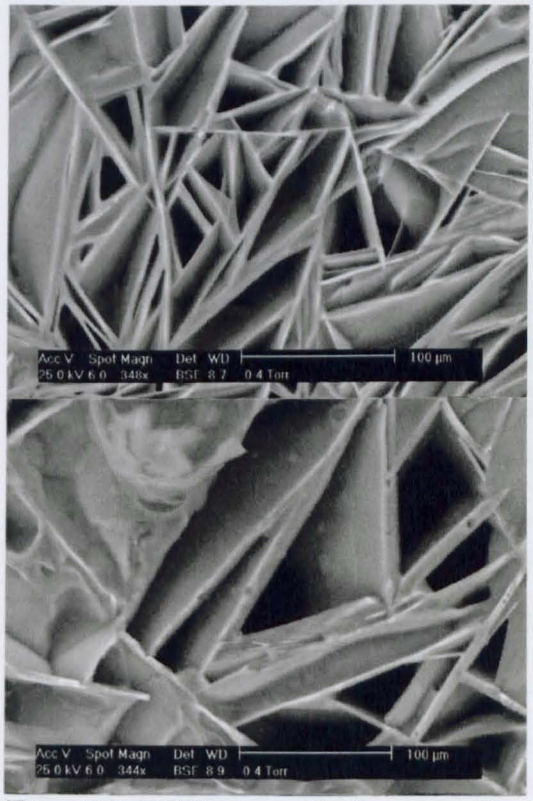

Figure 7.2 ESEM image of collagen crystallised from the octanoic acid emulsion of 8:1 Span 20/Brij 30, used as 50%wt of the total emulsion mixture, combined with 30 wt % octanoic acid, and 20%wt collagen solution.

Extension of this preliminary study to include the deposition of hydroxyapetite could result in a new method for the production of synthetic bone scaffolds. Benefits of this approach could be that large pores (~ 50 µm) are introduced, suitable for subsequent bone cell uptake, and the high surface area of the porous collagen may provide numerous sites for enhanced hydroxyapetite deposition.

I have recently become intrigued by the work of the optical tweezers laboratory at RAL. This provides a method of manipulating emulsion droplets into any shape or configuration desired, enabling ordered arrays to be formed. Should this be combined with the crystallisation techniques described in Chapter 6, this may provide the extra element of control required to form ordered macro-porous

materials. This would be an ideal scenario for the production of optical materials that require an ordered close-packed array of pores within a single crystal. As yet, the ability to create an array of more than 10 droplets is not possible with a single laser[5]. However with improved evanescent wave techniques as many as 30 silica spheres have been held recently in an organised cluster[6]. This means that if the difference in refractive index is great enough, there is now no reason for preventing this technique from being applied to emulsion droplets.

Emulsions are not the sole method of liquid-liquid confinement available. As can be seen in biological systems, phospho-lipid vesicles provide a means of confinement, and still allow transport of selected materials across the membrane. This may provide another avenue for future research where crystal growth may be induced by transport of material into or out of the aqueous phase, giving an alternative means of inducing nucleation where a surface active species is not practical, yet well-defined crystal sizes and polymorphs are desired.

References

1 Davey, R. J.; Hilton, A. M.; Garside, J. *Chemical Engineering Research & Design* 1997, ***75***, 245-251.

2 Allen, K.; Davey, R. J.; Ferrari, E.; Towler, C.; Tiddy, G. J.; Jones, M. O.; Pritchard, R. G. *Crystal Growth & Design* 2002, ***2***, 523-527.

3 Yano, J.; Furedi-Milhofer, H.; Wachtel, E.; Garti, N. *Langmuir* 2000, ***16***, 10005-10014.

4 Wilkinson, K. M.; Lei, Q. F.; Bain, C. D. *Soft Matter* 2006, ***2***, 66-76.

5 Ward, A. D.; Berry, M. G.; Mellor, C. D.; Bain, C. D. *Chemical Communications* 2006, 4515-4517.

6 Mellor, C. D.; Bain, C. D. *Chemphyschem* 2006, ***7***, 329-332.

Appendix 1

A1.0 Introduction

The notes contained in this appendix are a reproduction of a 4th year undergraduate lecture course given at Durham University in 2002, based upon the work of Cooper[1] For the main work contained in this thesis the assumed level of background knowledge into nucleation theory is given here.

A1.0.1 Classical Nucleation Theory

Consider a water vapour cooled so that the vapour is supersaturated with respect to liquid water.

- Initial stage of condensation requires the aggregation of water molecules to form a tiny droplet, or nucleus that then grows by additional vapour molecules impinging upon it.
- However, the Gibbs-Thomson equation indicates that this nucleus, and others like it, will have a vapour pressure many times that of bulk liquid.
- The vapour will not be supersaturated with respect to these nuclei and so these nuclei will tend to evaporate.
- The water vapour is in a metastable state, due to the existence of the energy barrier to the formation of the new phase.

So how does the new phase form?
In any thermodynamic system, statistical fluctuations about the normal state occur. Consequently, the new phase will be able to form provided a positive free energy fluctuation occurs that is equal to, or larger than, the magnitude of this energy barrier.

Homogeneous nucleation refers to nucleation of a species within a single component phase.

Heterogeneous nucleation refers to nucleation of a species upon a foreign substrate.

Crystal growth theories are concerned with the growth of the crystal nuclei to macroscopic dimensions.

A1.1 Classical Homogeneous Nucleation Theory

(see e.g. Gibbs, Volmer, Becker and Döering, Frenkel)

In nucleation, only aggregates of a size greater than a critical value will be stable and grow to become the condensed phase; aggregates of this size are termed **critical nuclei.**

In classical nucleation theory, the rate of nucleation, J, is considered to result from a two step process:

1. the formation of a near equilibrium concentration, n(i*), of critical nuclei and
2. the impingement at a rate, W*, of the condensable species upon these nuclei, which causes them to become essentially free-growing and thus eventually bulk, condensed phase.

Thus: $J = W^* n(i^*)$. (A1)

A1.1.1 Determination of $n(i^*)$, the equilibrium concentration of critical nuclei

$$n(i^*) = n \exp\left[\frac{-\Delta G^*}{kT}\right] \qquad \text{(A2)}$$

A1.1.2 Determination of ΔG^*, the Gibbs free energy of formation of the critical nucleus

The free energy of formation, ΔGi, of a cluster from i monomers in the vapour is:

$$\Delta G_i = -i(\Delta\mu) + \sum_n \gamma_n A_n \qquad \text{(A3)}$$

For a spherical cluster, Equation. (A3) becomes:

$$\Delta G_i = -\frac{4\pi r^3}{3v_c}(\Delta\mu) + 4\pi r^2\gamma \qquad \text{(A4)}$$

where: r is the radius of cluster and v_c is the molecular volume of the cluster.

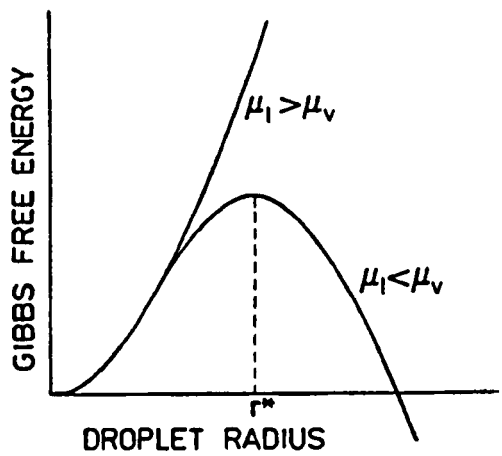

A graph of ΔGi against r shows a maximum at $r = r^*$, the radius of the critical nucleus, so that differentiating ΔGi with respect to r and equating to zero, i.e.:

$$\frac{d\Delta G_i}{dr} = -\frac{4\pi r^2}{v_c}\Delta\mu + 8\pi r\gamma = 0$$

gives:

$$r^* = \frac{2\gamma v_c}{\Delta\mu} \qquad \text{(A5)}$$

i.e. the Gibbs-Thompson equation.

Substituting Eq. (A5) into (A4) gives the Gibbs free energy of formation of the critical nucleus in terms of the supersaturation as:

$$\Delta G^* = \frac{16\pi\gamma^3 v_c^2}{3\Delta\mu^2} \qquad \text{(A6)}$$

or in surface free energy terms as:

$$\Delta G^* = \frac{1}{3}A\gamma \qquad \text{(A7)}$$

Equation (A7) is universal, as shown below.

The Gibbs free energy of formation of the critical nucleus for a crystal is given by:

$$\Delta G^* = -\frac{V_c^*}{v_c}\Delta\mu + \sum_n A_n\gamma_n \qquad \text{(A8)}$$

where: V_c = volume of the crystalline critical nucleus. The volume of any crystal can be considered as the sum of the volumes of pyramids constructed on the crystal faces with a common apex in an arbitrary point (the Wulff point) within the crystal, hence:

$$V_c^* = \frac{1}{3}\sum_n h_n A_n \qquad \text{(A9)}$$

where h_n are the heights of the pyramids and A_n are the surface areas of the corresponding crystal faces. Substituting for V_c^* and h_n in Equation. (A7) using Equations. (A9) and the Gibbs-Thompson equation gives:

$$\Delta G^* = -\frac{2\sum_n A_n \gamma_n}{3} + \sum_n A_n \gamma_n = \frac{1}{3}\sum_n A_n \gamma_n$$

i.e. Eq. (A7) as before.

A1.1.3 Determination of W^*, the impingement rate

The impingement rate W^*, is given by:

$$W^* = R^* s^* \qquad \text{(A10)}$$

where: R^* = adsorption flux, i.e. the frequency with which condensing molecules reach unit area of the critical nucleus and s^* = surface area of the nucleus, i.e. $4\pi r^2$ for a spherical nucleus.

A1.1.4 Overall Classical Homogeneous Nucleation Rate

Combining Equations. (A1), (A2), and (A6), the homogeneous nucleation rate can be written as:

$$J = R^* s^* n \exp\left[-\frac{\Delta G^*}{kT}\right] \quad \text{or} \quad J = \Omega \exp\left[-\frac{\Delta G^*}{kT}\right] \qquad \text{(A11)}$$

where: Ω is known as the pre-exponential factor. Ω is not very dependent upon the supersaturation, compared with the exponential factor, and therefore one can consider Ω as nearly a constant. Typical values of Ω are ~10^{25} -10^{35} $cm^{-3}s^{-1}$.

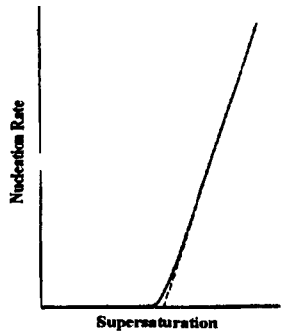

The form of Eq. (A11) is such that J remains negligibly small until the supersaturation reaches a critical value, the Ostwald metastable limit, at which point J suddenly and dramatically increases.

Hence, this critical supersaturation level can be arbitrarily set as the rate at which $\ln J = 0$, i.e. the rate is 1 nucleus $cm^{-3}sec^{-1}$ (or any other suitable experimentally detectable limit) with little loss of accuracy.

The main assumptions of classical nucleation theory are:

- equilibrium conditions and
- the validity of ascribing the macroscopic properties such as surface tension to the critical nucleus.

Hence classical nucleation theory is most applicable to systems at low to moderate supersaturations.

A1.2 Classical Heterogeneous Nucleation Theory

Nucleation occurs upon a foreign substrate, at a greater rate than homogeneous nucleation. Similarly to the homogeneous case, the heterogeneous nucleation rate, J_{het}, may be expressed by:

$$J_{het} = W^* n(i^*) \qquad \text{(analogous to A1)}$$

A1.2.1 Determination of $n(i^*)$, the equilibrium concentration of critical nuclei

$n(i^*)$ is given by:

$$n(i^*) = n_0 \exp\left[-\frac{\Delta G_{het}{}^*}{kT}\right] \qquad \text{(A12)}$$

where: n_0 is the adatom (adsorbed atom) concentration on the substrate and ΔG_{het}* is the Gibbs free energy of formation of the critical nucleus.

A1.2.2 Determination of ΔG*, the Gibbs free energy of formation of the critical nucleus

The value of ΔG_{het}* depends upon the shape of the critical nucleus upon the substrate.

Isotropic nuclei are cap-shaped, anisotropic nuclei may be disc-shaped or polygonal, depending upon the extent of anisotropy. There is also a statistical contribution to ΔG_{het}*, which is independent of the nucleus size or shape, that accounts for the distribution of the clusters and single adatoms among the adsorption sites of density n_s. This term, ΔG_{conf} is given by:

$$\Delta G_{conf} = -kT \ln(n_0 / n_s) \qquad \text{(A13)}$$

Including this ΔG_{conf} term in Eq. (A13) gives:

$$n(i^*) = n_s \exp\left[-\frac{\Delta G_{het}{}^*}{kT}\right] \qquad \text{(A14)}$$

where: ΔG_{het}* is the Gibbs free energy of formation of the critical nucleus, excluding the ΔG_{conf} contribution..

A1.2.3 Cap-shaped nuclei

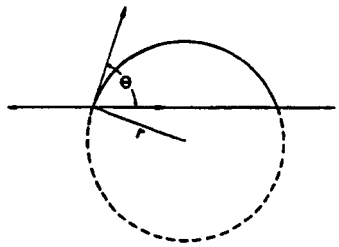

The contact angle, θ , may be determined by treating the interfacial tensions as forces and balancing them in the plane of the substrate, leading to Young's equation:

$$\cos\theta = \frac{\gamma_{sv} - \gamma_{sx}}{\gamma_{vx}} \quad . \qquad \text{(A15)}$$

Employing the classical technique of considering the cluster as bulk crystal with terms included to account for its surface, gives:

$$\Delta G_i = -\frac{4}{3v_c}\pi r^3 \Delta\mu\left(\frac{2-3\cos\theta+\cos^3\theta}{4}\right)+4\left(\frac{1-\cos\theta}{2}\right)\pi r^2\gamma_{vx}+\pi r^2\sin^2\theta(\gamma_{sx}-\gamma_{sv})$$

. . (A16)

Substituting for g_{sx}-g_{sx} using Young's Eq., this gives:

$$\Delta G_i = -\frac{4\pi r^3\Delta\mu}{3v_c}f(\theta)+4f(\theta)\pi r^2\gamma_{vx} \qquad \text{(A17)}$$

where: $f(\theta) = (2-3\cos\theta+\cos^3\theta)/4$. Maximising ΔGi with respect to r then leads to:

$$r^* = \frac{2\gamma v_c}{\Delta\mu} \qquad \text{(A18)}$$

i.e. the Gibbs-Thomson equation once more and

$$\Delta G_{het}^* = \frac{16\pi\gamma_{vx}^3 v_c^2}{3\Delta\mu^2}f(\theta) = \frac{\sum_x A_x\gamma_x}{3} = \Delta G_{hom}^* \frac{V_{het}^*}{V_{hom}^*} \quad . \text{(A19)}$$

where: ΔG_{hom} is the Gibbs free energy of formation for homogeneous nucleation of this system and V_{het}^* *and* V_{hom}^* are the volumes of the heterogeneous and corresponding homogeneous critical nuclei, respectively.

- For $\theta = 180°$, nucleation does not occur on the substrate and the homogeneous value of
  ΔG^* is obtained.
- If $\theta = 0°$, complete wetting occurs and this model then predicts no nucleation barrier. For $\theta = 0°$, though, the critical nucleus will be a 2-D monolayer disc and so Eq. (A19) will not be applicable for such cases of very strong adsorption of adatoms onto the substrate.

A1.2.4 Disc-shaped nuclei

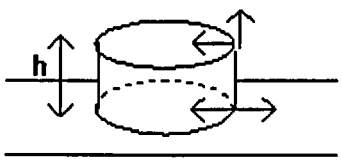

Such a disc shape may occur if either:

1. adatom adsorption on to the substrate is very strong, producing a monolayer 2D disc or
2. the nucleus is 3-dimensional and anisotropic.

The Gibbs free energy of formation for either shape will be:

$$\Delta G_i = -(\pi r^2 h \Delta\mu / v_e) + \pi r^2 (\gamma_{sn} + \gamma_2 - \gamma_{sv}) + 2\pi r h \gamma_1 \quad \text{(A20)}$$

For the monolayer disc, h is a constant equal to the height of the atom perpendicular to the substrate surface, whilst for the anisotropic, less strongly adsorbed nucleus, h will be determined according to the Gibbs-Wulff law.

A1.2.5 Monolayer discs

Maximising ΔGi with respect to r leads to:

$$r^* = \frac{\gamma_1}{(\Delta\mu / v_e) - [(\gamma_{sn} + \gamma_2 - \gamma_{sv})/h]} \quad \text{(A21)}$$

and

$$\Delta G_{het}^{*} = \frac{\pi h \gamma_1^{\,2}}{(\Delta\mu / v_c) - [(\gamma_{sv} + \gamma_2 - \gamma_{sv})/h]} = \pi r^{*} h \gamma_1 \quad . \quad \text{(A22)}$$

Notice that in this case, ΔG_{het}^{*} is equal to half the edge free energy terms, since the critical nucleus is a 2D, as opposed to a 3D, equilibrium shape. Any other 2D critical nucleus equilibrium shape will also have ΔG_{het}^{*} equal to half the edge free energy terms.

A1.2.6 Determination of W^{*}, the rate of impingement

The impingement of atoms onto the growing nucleus may occur by either:

- direct impingement of atoms from the vapour onto the nucleus surface (as in homogeneous nucleation) or
- adatom impingement by the surface diffusion of adatoms to the nucleus periphery.

For direct impingement, the rate, W_d^{*}, is the same expression as for the homogeneous nucleation case, i.e.:

$$W_d^{*} = R^{*} s^{*} \qquad \text{(i.e. Eq. A10)}$$

where: s^{*} = surface area of the critical nucleus.

For adatom impingement, the rate, W_s^{*}, is:

$$W_s^{*} = R^{*} l^{*} a_0 \exp\left[\frac{\Delta G_{des} - \Delta G_{sd}}{kT}\right]. \qquad \text{(A23)}$$

where: l^{*} = circumference of nucleus on substrate surface, a_0 = adatom jump distance, ΔG_{des}= free energy of activation for desorption and ΔG_{sd} = Gibbs free energy of activation for surface diffusion.

For nucleation from the vapour, the adatom impingement rate > direct impingement rate, hence the impingement rate is given by Eq. (A23). For

nucleation from solution/the melt, however, the reverse is often true, in which case the impingement rate will be given by Eq. (A10).

A1.2.7 Overall Classical Heterogeneous Nucleation Rate

Combining Eqs. (A1) and (A14), the classical heterogeneous nucleation rate becomes:

$$J_{het} = W^* n_s \exp\left[-\frac{\Delta G_{het}^*}{kT}\right] \quad \text{or} \quad J_{het} = \Omega_{het} \exp\left[-\frac{\Delta G_{het}^*}{kT}\right] \quad \text{(A24)}$$

where: W_{het} is the pre-exponential factor. As with the homogeneous nucleation case, W_{het} is also not very dependent upon the supersaturation.

Nucleation Process	Typical W_{het} values ($cm^{-2}s^{-1}$)
Condensation from the vapour	10^{17}
Crystallisation from sol.	10^{20}
Crystallisation from the melt	10^{22}

Set the critical supersaturation level for heterogeneous nucleation to the rate at which $\ln J_{het} = 0$, i.e. the rate is 1 nucleus $cm^{-2}sec^{-1}$.

A1.3 Epitaxy

The oriented growth of a crystalline material on a different material is termed epitaxy.

The epitaxial growth of thin films is the basis of the fabrication of numerous modern devices. Epitaxy is also important in biomineralisation, where growth of an inorganic mineral (such as $CaCO_3$) occurs on an organic matrix. The influence of the substrate can often be sufficient to induce the crystallisation of not only a specific orientation, but also a specific crystal polymorph.

A great variety of methods for epitaxial deposition of different materials have been invented. These include Chemical Vapour Deposition(CVD), Molecular Beam Epitaxy (MBE), Liquid Phase Epitaxy (LPE) and Atomic Layer Epitaxy (ALE) among others.

A1.3.1 Epitaxial theories

Heterogeneous nucleation theories consider whether a particular body will induce nucleation of another. Epitaxial theories consider the conditions under which a single overgrowth orientation minimises the interfacial energy of the system.

Epitaxial growth differs from normal crystal growth (i.e. the growth of a material upon the same material) in that the substrate and overgrowth crystals have different chemical potentials. This difference arises in two fundamental ways:

1. the substrate and overgrowth may differ in the nature and strength of their chemical bonds
2. the substrate and overgrowth may differ in their lattice structures.

The lattice mismatch (or misfit), m, between the substrate and overgrowth in a particular direction is defined as:

$$m = \frac{b - a}{a} \qquad \text{(A25)}$$

where: a and b are the lattice parameters of the substrate and overgrowth, respectively.

The chemical bonding between the substrate and overgrowth will determine the maximum interaction that can occur between the two, whilst the lattice mismatch will determine the spatial variation of the interaction.

Factors aiding epitaxy:

- strong substrate-overgrowth interaction

- small lattice mismatch
- high compressibility substrate/overgrowth

Different epitaxial theories have been developed to account for different overgrowth thicknesses and the manner in which any lattice mismatch is accommodated.

A1.3.2 Misfit accommodation

If the overgrowth-substrate interaction is sufficiently strong, an overgrowth monolayer may be constrained to match the crystal structure of the substrate completely, i.e. a coherent, or pseudomorphic, monolayer occurs. For this situation, the misfit is accommodated entirely by the homogeneous strain of the overgrowth. With either increased overgrowth-overgrowth bonding, or misfit, the coherent monolayer will become unstable, and misfit dislocations are then introduced to relieve this homogeneous strain. The misfit dislocations comprise regions of good fit between the substrate and overgrowth, producing the maximum substrate-overgrowth interaction and regions of bad fit, "the dislocation", in which this interaction is poor.

As the monolayer extends in height, the interaction between the substrate and subsequent overgrowth layers decreases, whilst the energy required to homogeneously strain the overgrowth into coherency remains practically constant per additional layer. Hence for any initially pseudomorphic monolayer, there will be a critical height at which the coherent structure becomes unstable and misfit dislocations are introduced to relieve the homogeneous strain, until eventually all this strain has disappeared and the misfit is accommodated entirely by misfit dislocations.

Finally, when the overgrowth-substrate interaction becomes so weak, compared to the overgrowth-overgrowth forces, each adatom will then be located at its usual

crystal lattice position. There is no strain whatsoever, and the misfit is accommodated entirely by a misfit vernier.

A1.3.3 Modes of epitaxial growth

The dependence of the chemical potential, m , of the overgrowth on its thickness, n, constitutes the main difference of the epitaxial growth from the usual crystal growth of a material, and leads to three well-known modes of epitaxial growth:

- Volmer-Weber mechanism of island growth
- Frank-van der Merwe mechanism or layer-by-layer growth
- Stranski-Krastonov mechanism, or layer-by-layer followed by formation of 3D islands.

A1.4 Crystal Growth

The mechanism of crystal growth is unambiguously determined by the structure of the crystal face.

A1.4.1 Classification of Crystal Faces

The equilibrium shape of crystals is bounded by the crystal faces with the lowest specific surface energies. Faces with the lowest surface tensions will typically be the most close-packed, be atomically flat, and have low Miller indices. A crystal face at a small angle to one of these low energy faces, however, will not be atomically flat; but will consist of terraces and steps. In fact, crystal faces can be divided into three groups.

F (flat) faces. These are parallel to at least two dense atomic rows.

S (stepped) faces. These are parallel to one dense atomic row.

K (kinked) faces. These are not parallel to any dense atomic rows.

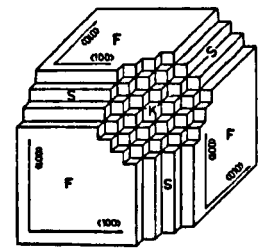

F faces are generally atomically flat. However, as temperature is increased and entropic factors become more important, F faces undergo a surface roughening transition at a critical temperature known as the roughening temperature, *Tr.*

The atomically rough crystal faces (i.e. S, K and F faces at temperatures above T_r) grow by a different mechanism to the atomically flat faces (F faces at temperatures below T_r).

A1.4.2 Classification of Crystal Surface Sites

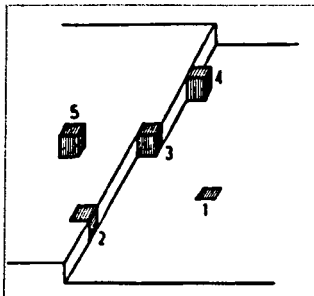

Position of atom	No. of saturated bonds
Within Face (1)	5
Within Step (2)	4
Within Kink (3)	3
Upon Step (4)	2
Upon face (5)	1

The detachment of these atoms will lead to a change in surface energy of the crystal for all but the atom at the kink position. At this position, the atom has 3 saturated bonds, and 3 unsaturated bonds.

In all crystals, the kink site has the following properties:

- It determines the equilibrium of an infinitely large crystal with the ambient phase.
- Its chemical potential is equal to the chemical potential of the crystal.
- Its desorption energy of the kink site is equal to the crystal enthalpy of evaporation.
- If a system is supersaturated, it will be favourable for an adatom arriving at the kink site to be incorporated into the crystal.

A1.4.3 Crystal growth mechanisms

A1.4.4 Continual growth mechanism for atomically rough faces

If a face is an S face, K face, or F face at a temperature above T_r, it is atomically rough and can grow continuously.

Growth rate is fast and is simply proportional to the flux of atoms from the parent phase, i.e. the growth is diffusion controlled. The rate of crystal growth is given by:

$$R = \lambda \Delta\mu \qquad \text{(A26)}$$

where: λ is the kinetic coefficient. Hence the growth rate depends linearly upon the supersaturation. The kinetic coefficient is proportional to the surface roughness (in terms of the probability of finding a kink site), and to the exponent of the activation energy, ΔU, for incorporation of a building unit into the lattice. Typical values of R are 10^{-4} - 10^{-1} cm sec^{-1}. Crystals that grow by the continual growth mechanism tend to have rounded morphologies. Atomically flat F faces (i.e. F faces at temperatures below T_r), however, cannot grow by this mechanism.

A1.4.5 Layer growth of flat faces

Consider an atomically flat crystal face belonging to perfect defectless crystal. A single adatom on such a face is bound more weakly than an adatom in a cluster of adatoms on the surface. Consequently, there is an energy barrier to the formation of each new crystal layer. This situation is the 2D analogue of homogeneous nucleation, and hence the rate of growth of this face will be determined by the frequency of the formation of 2D critical nuclei.

If the F crystal face is not perfect, and in particular if screw dislocations are present, then these screw dislocations represent a non-vanishing source of steps which alleviate the necessity of a 2D nucleation growth mechanism. Instead the rate of crystal growth is determined by the rate of the lateral movement of the steps.

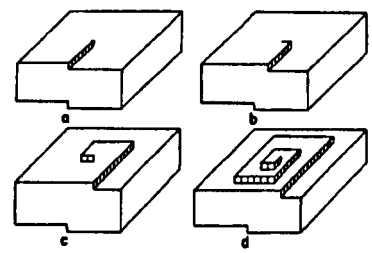

Growth of an atomically flat crystal face is surface controlled. Crystals grown under surface control are faceted (i.e. have well-developed crystal faces). Typical values of R for growth by a layer by layer are 10^{-9}-10^{-5} cm sec^{-1}.

A1.4.6 2D nucleation growth

The growth of a defectless, atomically smooth crystal face is a periodic process involving:

1. formation of a 2D nucleus (the rate determining step)
2. lateral spreading of this nucleus until the crystal face is completely covered. Further growth then requires the formation of a 2D nucleus again.

Similarly to the 3D nucleation case, the rate of 2D nucleation is given by:

$$R = \Omega_{2D} \exp(-\Delta G_{2D}^* / kT) \quad \text{(A27)}$$

where: Ω_{2D} is the pre-exponential factor for 2D nucleation and ΔG_{2D}^* is the Gibbs free energy for formation of the 2D critical nucleus. It can be shown that:

$$\Delta G_{2D}^* = \pi r^* h\gamma = \frac{\pi h v_e \gamma^2}{\Delta\mu} \quad \text{(A28)}$$

Thus R becomes:

$$R = \Omega_{2D} \exp\left(-\frac{\pi h v_e \gamma^2}{\Delta\mu kT}\right) \quad \text{(A29)}$$

The rate has a non-linear dependence on the supersaturation. Once more, the form of Eq. (A29) is such that growth will not proceed at a finite rate until a critical supersaturation is reached.

At high supersaturations, the face may grow by a multilayer mechanism due to the formation of multiple 2D nucleation sites. The exponential now becomes ($-\Delta G_{2D}^*/3kT$).

With increasing supersaturation, the 2D critical nucleus becomes increasingly small in size, so that only a few atoms are needed to form each critical nucleus. The density of 2D critical nuclei may then become so large that arriving atoms can be incorporated practically at any site. The surface becomes atomically rough so growth can now proceed continuously ($R \propto \Delta\mu$). This roughening of the crystal face, which occurs at very high supersaturations well below T_r is known as kinetic roughening, to distinguish it from the thermodynamic roughening transition that occurs at T_r.

A1.4.7 Screw dislocation growth

Experiments showed that growth of faceted crystals could occur at relative supersaturations, $\propto (P/P_0)$, as low as 0.01%, far below the critical supersaturation

limit for 2D nucleation growth. This indicated that a different growth mechanism must be operating.

Burton, Cabrera and Frank (BCF) developed the theory of screw dislocation crystal growth and found that:

$$R = C(\sigma^2 / \sigma_c)\tanh(\sigma_c / \sigma) \qquad \text{(A30)}$$

where: σ is the supersaturation parameter $\Delta\mu/kT$, σ_c is the characteristic supersaturation of the system and C is a rate constant. Two limiting cases can be distinguished:

At low supersaturations, $\sigma_c >> \sigma$, so $\tanh(\sigma_{c/s}) \rightarrow 1$, hence:

$$R = C(\sigma^2 / \sigma_c) \qquad \text{(A31)}$$

which is the BCF parabolic law.

At supersaturations sufficiently higher than σ_c, $\tanh(x \rightarrow 0) = x$, hence:

$$R = C\sigma \qquad \text{(A32)}$$

and the *BCF linear growth rate* is obtained.

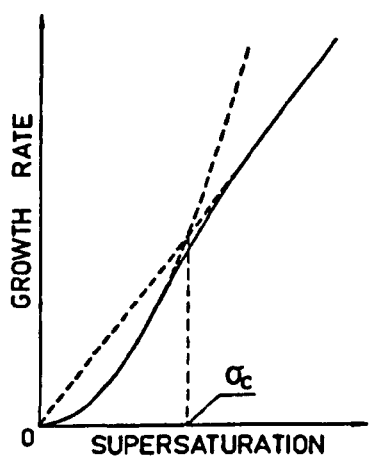

The parabolic law holds up to the characteristic supersaturation, σ_c beyond which a linear relationship is gradually established.
The density of kinks on the surface is then so high that the face becomes rough and so a continuous growth mechanism occurs.

A1.4.8 Growth regimes

- S and K faces always grow by the continual growth mechanism, so $R \propto \Delta\mu$.
- F faces will grow by this mechanism at temperatures above T_r or if the supersaturation is high, since the F faces are then atomically rough.
- At temperatures below T_r and at lower supersaturations, F faces grow by either the 2D nucleation or spiral growth mechanism and a non-linear growth rate is obtained.

Consequently, we can distinguish different growth regimes for an F crystal face as shown below.

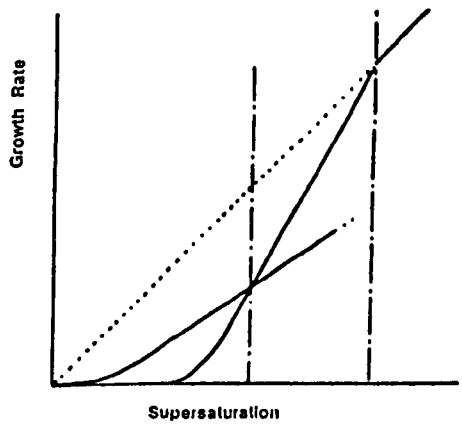

A1.4.9 Determination of roughening temperatures

Since an F face below and above T_r grows by entirely different mechanisms, it would be advantageous to know T_r. The parameter that will give an indication of T_r is ΔS_{trans}

- For $\Delta S_{trans}/R < 1.2$, the face is atomically rough for all $\Delta\mu$ values.
- For $\Delta S_{trans}/R > 3.3$, the face is atomically flat for all $\Delta\mu$ values.
- For $1.2 < \Delta S_{trans}/R < 3.3$, the lower the $\Delta\mu$ value, the more likely the face is to be flat.

In addition, an expression for the transition temperature has been given as (Chui and Weeks 1978, Fischer and Weeks1983):

$$T_r \approx 2\gamma_{hkl} d^2_{hkl} / \pi k \quad (38)$$

where: γ_{hkl} is the surface tension of crystal face (*hkl*), and d_{hkl} is its interplanar spacing (Chui and Weeks 1978, Fischer and Weeks 1983).

A1.4.10 Morphological instability and constitutional supercooling

Consider a chance fluctuation that gives rise to a protrusion on the crystal interface. Under stable conditions, further growth of this protrusion will be unfavourable and so the interface will return to a smooth shape. Under unstable conditions, further growth of the protrusion will be favoured, and so the interface will become distorted. This is known as morphological instability.

Constitutional supercooling occurs when the supersaturation or supercooling increases with distance into the parent phase. Consequently, the rate of growth of any protrusion will be greater than the growth rate of the rest of the crystal interface and hence morphological instability occurs. Constitutional supercooling typically occurs at high supercoolings /supersaturations due to the liberated enthalpy of crystallisation raising the temperature of the interface, and hence reducing the supercooling there.

Typical morphologies that can occur under unstable conditions are those of snowflakes.

A1.5 Crystal morphology

The ability to influence the rate of crystal growth, and the resulting morphology can have important consequences, e.g.

- In oil recovery, crystallisation of barium sulphate crystals in the pipes reduces the oil flow-rate, hence impeding the growth rate of these crystals is highly desirable.
- In the semiconductor industry, layers of a particular morphology are often required.
- Biomineralisation relies on the ability of an organic matrix in the organism to promote the crystallisation of specific morphologies or polymorphs of inorganic minerals.

Equilibrium crystals and macroscopic crystals

The equilibrium form of a crystal is governed by:

$$\sum_{x} \gamma_x dA_x = 0 \quad . \qquad \text{(Gibbs-Wulff law, A32)}$$

However, the equilibrium shape is only likely to occur for sub-microscopic crystals. As a crystal grows, its surface area to volume ratio decreases so the difference in the surface energy of various crystal forms becomes less significant. Kinetic factors, such as the relative growth rates of individual crystal faces, will dominate.

A1.5.1 Predicting crystal morphologies

For surface controlled growth, Hartman and Bennema (1980) have shown that the growth rate, R, of a face increases with increasing attachment energy, E_{att}, i.e.

$$R \propto E_{att}. \qquad \text{(A33)}$$

The attachment energy is defined as the interaction energy per molecule between a slice (hkl) and the crystal face (hkl) so $E_{att} = \Sigma E_i$, where E_i = interaction energy per molecule of a slice of thickness, d_{hkl}, with the i_{th} under/overlying slice.

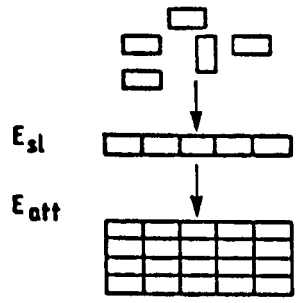

Crystal faces with the lowest E_{att} values will become dominant in the resulting crystal habit.

The surface tension represents to a first approximation (ignoring any entropic and surface reconstruction effects), the degree of unsaturation of bonds per unit area it may be seen that:

$$\gamma \approx -E_{att} / 2A_{hkl} \qquad \text{(A34)}$$

where: A_{hkl} = surface area of a molecule in the crystal face (hkl). Since $A_{hkl} = v/d_{hkl}$ Eq. (A34) becomes:

$$\gamma \approx -E_{att} d_{hkl} / 2v \qquad \text{(A35)}$$

i.e. $\gamma \propto E_{att} d_{hkl}$.

- Equilibrium form: faces with the lowest γ values dominate the crystal habit.
- Microscopic and macroscopic crystals grown under surface control, faces with the lowest E_{att} values dominate the resulting habit.
- For continuous growth (i.e. diffusion controlled growth), the crystal habits will tend to be rounded, as all crystal faces are rough and predicted to grow at the same rate.
- At very high supersaturations, morphological instability can occur and then dendritic, Hopper, cellular etc. growth forms may occur.

Reference:

1 Cooper S. J, PhD Thesis, Department of Chemistry, University of Bristol, 1995

2 Crystallisation Kinetics course, Durham University 2002, given by Cooper S J